

Lava Worlds: From Early Earth to Exoplanets

Keng-Hsien Chao^{a,1}, Rebecca deGraffenried^{a,1}, Mackenzie Lach^{a,1}, William Nelson^{a,1}, Kelly Truax^{a,1} and Eric Gaidos^{a,*}

^a*Department of Earth Sciences, University of Hawai'i at Mānoa, Honolulu, HI 96822 USA*

ARTICLE INFO

Keywords:

magma oceans
Moon
Io
exoplanets
planet formation
planetary atmospheres

ABSTRACT

The magma ocean concept was first conceived to explain the geology of the Moon, but hemispherical or global oceans of silicate melt could be a widespread "lava world" phase of rocky planet accretion, and could persist on planets on short-period orbits around other stars. The formation and crystallization of magma oceans could be a defining stage in the assembly of a core, origin of a crust, initiation of tectonics, and formation of an atmosphere. The last decade has seen significant advances in our understanding of this phenomenon through analysis of terrestrial and extraterrestrial samples, planetary missions, and astronomical observations of exoplanets. This review describes the energetic basis of magma oceans and lava worlds and the lava lake analogs available for study on Earth and Io. It provides an overview of evidence for magma oceans throughout the Solar System and considers the factors that control the rocks these magma oceans leave behind. It describes research on theoretical and observed exoplanets that could host extant magma oceans and summarizes efforts to detect and characterize them. It reviews modeling of the evolution of magma oceans as a result of crystallization and evaporation, the interaction with the underlying solid mantle, and the effects of planetary rotation. The review also considers theoretical investigations on the formation of an atmosphere in concert with the magma ocean and in response to irradiation from the host star, and possible end-states. Finally, it describes needs and gaps in our knowledge and points to future opportunities with new planetary missions and space telescopes to identify and better characterize lava worlds around nearby stars.

Contents

1 Introduction	2	4 Lava Worlds in the Early Solar System	11
2 Energetics of Lava Worlds	3	4.1 The Moon	11
2.1 Sources of Heat	3	4.2 Earth	12
2.1.1 Gravitational Energy	3	4.3 Mars	13
2.1.2 Stellar Irradiation	3	4.4 Mercury	13
2.1.3 Aluminum-26	5	4.5 Venus	13
2.1.4 Tides	5	4.6 Vesta	13
2.1.5 Induction	6	4.7 Other Small Bodies	14
2.2 Transport of heat	6	4.8 An Inner Solar System Synthesis	14
2.2.1 Magma Ocean Heat Transport	7	5 The Exoplanet Perspective	14
2.2.2 Atmospheric Heat Transport	8	5.1 Methods of Detection and Characterization	15
2.3 Putting it together: Magma ocean lifetime	8	5.1.1 Transit Photometry	15
3 Lava lakes as Analogs in the Solar System	9	5.1.2 Doppler Radial Velocity	15
3.1 Why Study Lava Lakes?	9	5.1.3 Transit Spectroscopy	16
3.2 Lava Lakes on Earth	9	5.1.4 Phase curves	17
3.3 Lava Lakes on Io	10	5.1.5 Direct Detection	17
3.4 Scaling from Lava Lakes to Lava Worlds	10	5.1.6 Sensitivity and Biases	17
3.4.1 Laminar vs. turbulent flow regimes	10	5.2 The Diversity of Lava Worlds around Other Stars	17
3.4.2 Crystallization	10	5.2.1 Ultra-Short Period Planets	17
3.4.3 Degassing and vesicularity	11	5.2.2 Post-Giant Impact Planets	18
3.4.4 Surface dynamics and crust formation	11	5.2.3 Tidally-Heated Planets and Satellites	18
		5.3 Three Prominent Lava Worlds	18
		5.3.1 CoRoT-7b	18
		5.3.2 Kepler-78b	19
		5.3.3 55 Cancri e	19
		6 Dynamics and Stability of Magma Oceans	20
		6.1 Vertical Stability	20
		6.2 Effect of Rotation	21
		6.3 Interaction with the Mantle	23

*Corresponding author

✉ gaidos@hawaii.edu (E. Gaidos)

ORCID(s): 0000-0002-0329-7511 (K. Chao); 0000-0003-2885-1870 (R. deGraffenried); 0000-0002-4778-9219 (M. Lach); 0000-0001-7296-697X (W. Nelson); 0000-0002-1283-3064 (K. Truax); 0000-0002-5258-6846 (E. Gaidos)

¹These authors contributed equally to this work.

7	Atmospheres of Lava Worlds	23
7.1	The Role of an Atmosphere	23
7.2	Primordial Atmospheres	24
7.3	Evolution of Atmospheres on Lava Worlds	24
7.4	End-State Atmospheres	26
7.4.1	Thick H ₂ O-CO ₂ Atmospheres	26
7.4.2	Silicate Vapor Atmospheres	27
8	Summary and Future Directions	27
8.1	Significant Advances	27
8.2	Major Outstanding Questions and Key Needs	28
8.3	Future Solar System Missions	28
8.4	Beyond the Solar System	29
9	Bibliography	29

1. Introduction

At Earth's surface, silicates form minerals and rocks, but at depth in volcanic areas where the temperature exceeds the solidus, which is about 1300 K at 1 bar for an Earth-like composition (Sarafian et al., 2017), silicates are partially molten and readily flow. These conditions are not presently widespread at or near the surface of any Solar System body: Venus and the subsolar point of Mercury are at 735 K and 800 K, respectively. It is only in active volcanic regions on Earth and the Jovian satellite Io that silicate melts appear, and only transiently. Yet, geochemical studies of Earth and returned samples, remote sensing by spacecraft of the Moon and other planets, and models of planetary accretion from smaller planetesimals all suggest that the silicate mantles of many Solar System bodies began in a partially or completely molten state (Elkins-Tanton, 2012a). Recent surveys of exoplanets, i.e. planets orbiting other stars, have discovered a class of rocky planets similar in size to Earth on very close-in orbits around their host stars which experience irradiation orders of magnitude higher than the terrestrial value (Winn et al., 2018). These have no analogs in the Solar System, and their equilibrium temperature could reach or exceed 2000 K, at which point silicates are completely molten and begin evaporating. Close-in planets on eccentric orbits or with non-synchronous rotation rates will experience strong tides from the central star, and dissipation within the planets could lead to widespread melting and global volcanism (Jackson et al., 2008) analogous to but on a larger scale than Io (Park et al., 2019). Young stars may harbor newly accreted, magma ocean-hosting planets at the present time.

Planets with molten silicates at their surfaces have been termed "lava planets" (Léger et al., 2011) and the liquid melt bodies "magma oceans", "lava oceans", or "lava ponds". The geologic definition of lava is simply magma that is erupted to the surface, a local phenomenon. Because this review is concerned with hemispherical or global bodies of melt not specifically related to volcanism, we will refer to these melt volumes as magma pools, seas, or oceans, although for terrestrial examples in craters and calderas they will continue to be termed lava lakes. We reserve the term "lava planet" or "lava world" for rocky planets with surface temperatures

reaching the solidus either globally or at least over much of a hemisphere *or* where the global average heat flow is at least $\sim 1 \text{ W m}^{-2}$, typical of terrestrial volcanic regions, sufficient to maintain a subsurface temperature gradient of 700 K km^{-1} , and permissive of melt within $\sim 2 \text{ km}$ of the surface regardless of surface temperature. Planets, including early Earth, Mars, and present-day Venus, could have "basal" magma oceans at their core-mantle boundaries that are well insulated from the surface; although these are discussed in this review, we do not term these lava worlds. Likewise, larger Neptune-like planets with magma oceans under thick, low-molecular weight envelopes, could be widespread (Kite et al., 2019), but are not considered here. Additional discussion of terminology can be found in Solomatov (2015).

The presence or absence of a magma ocean could have been a deterministic branch point in the evolution of the Solar System's rocky planets, governing their geologic history and, by influencing the distribution of the planets' volatile elements, atmospheric composition and evolution, climate, and habitability (Elkins-Tanton, 2012a; Hamano et al., 2013; Armstrong et al., 2019). This presumably also holds for rocky exoplanets, which are expected to be more diverse in terms of mass, formation history, and composition. Exoplanets that are very close to their host star are, by current principal methods, less difficult to detect and characterize (i.e., measurements of mass, temperature, and atmosphere). They will be among the high priority targets for future space missions such as the *James Webb Space Telescope (JWST)*, Beichman and Greene, 2018). "Evaporating" planets with tails of escaping or recondensing dust are an opportunity to probe interior composition (Bodman et al., 2018b), complementary to other measurements such as comparing mass and radius to interior models.

This review is motivated by: (a) The successful completion of the prime mission of the *Transiting Exoplanet Survey Satellite (TESS)*, Ricker et al., 2014). *TESS* is designed to discover "super-Earth"-size planets on close-in orbits around bright, nearby stars; in the case of the most luminous host stars the planets could be lava worlds. These planets are amenable to mass measurements using the Doppler radial velocity method with a new generation of precision spectrographs. (b) The planned launch of *JWST* in 2021, which will usher in a new era of spectroscopy at infrared wavelengths where the emission from lava worlds peaks. With *JWST* it will be possible to measure the temperature of a planet and infer the re-distribution of heat by any atmosphere, as well as identify some atmospheric constituents such as CO₂. And (c) a suite of new laboratory instruments to analyze meteorites and returned samples, and recent and future missions to Mercury (*Messenger*, *Bepi-Columbo*) and Mars (*Curiosity*, *InSight*, *Perseverance*), planets which may have had magma oceans, as well as proposed missions to Venus and Io, which could have interior magma oceans at the present time.

We begin this review with the fundamentals, i.e., an overview of sources and transport of heat on and in lava worlds (Sec. 2). In Section 3 we discuss lava lakes of Earth and Io as "natural laboratories" for the diverse behavior of magma near or

at the surface, the parameters that may govern that behavior, and the scaling laws relevant to applying lessons to other (exo)planets. Next we summarize what we have learned about surface and interior magma oceans in the inner Solar System beginning with the first-established and best-studied example, the Moon (Sec. 4). We review the evidence for magma oceans on Earth, other planets, and asteroids, and their potential physical and chemical diversity. We move beyond the Solar System in Section 5 to review the contributions of the field of exoplanets to the study of lava worlds, beginning with a summary of relevant observational techniques followed by a discussion of the population of short-period lava world candidates that these have uncovered and characterized. CoRoT-7b, Kepler-78b, and 55 Cancri e are presented as comparatively well-studied examples. The theoretical diversity of lava world exoplanets is addressed, with attention given to several scenarios where planets or satellites with magma oceans might in the future be detected on wider orbits. In Sec. 6 we discuss the physical and dynamical principles that determine the dynamics and stability of magma as controlled by the relative density and buoyancy of melts and solids, as well as the effects of rotation on magma ocean circulation. In Sec. 7 we discuss the role of atmospheres on lava worlds, the likely initial conditions that may have accompanied primordial magma oceans, the processes that governed the evolution of those atmospheres, and their Mercury-like and Venus-like end-states. Finally, we close with a synthesis of our current understanding, highlight outstanding questions and gaps in our knowledge, and describe promising future directions of research.

2. Energetics of Lava Worlds

2.1. Sources of Heat

Different sources of heat can form and maintain a magma ocean or pond, depending on a planet's size, age, and distance from the star (Fig. 2). A magma ocean will be maintained indefinitely on a mantle with an Earth-like (peridotite) composition if the surface temperature exceeds $\approx 1300\text{K}$. In the absence of an atmosphere, this requires an energy flux of $1.5 \times 10^5 \text{ W m}^{-2}$, or >300 times the present global mean insolation of Earth, to balance radiative loss. For a Venus-like CO_2 "greenhouse" atmosphere, the energy requirement falls to $\approx 2300 \text{ W m}^{-2}$, and for an optically thick, steam proto-atmosphere like that which presumably accompanied accretion, it is only $\approx 300 \text{ W m}^{-2}$ (Hamano et al., 2013); 1.3 times current terrestrial globally-averaged insolation or 8×10^3 times Earth's current internal heat flow (see Section 7).

2.1.1. Gravitational Energy

Transient magma oceans can be formed during planetary accretion as gravitational energy gained by infalling planetesimals is converted into heat during impact. As a protoplanet grows, the energy liberated per unit mass becomes comparable to the heat of melting of silicates. The energy flux per unit area, averaged over the time scale over which

many accretionary impacts occur, is:

$$q_{\text{accretion}} = \left[\frac{GM_p}{R_p} + \frac{1}{2}v_\infty^2 \right] \frac{\dot{M}_p}{4\pi R_p^2}, \quad (1)$$

where G is the gravitational constant, M_p and R_p are the instantaneous mass and radius of the planet, and v_∞ is the approach velocity of the impacting bodies. For a rocky planet $R_p \propto M_p^\epsilon$, with $\epsilon = 0.25-0.33$ (Grasset et al., 2009), and the rate of energy release is at least $2.3 \times 10^4 M_p^{2-3\epsilon} \tau_{\text{Myr}}^{-1} \text{ W m}^{-2}$ where M_p is in Earth masses and τ_{Myr} is the planet's accretion time in Myr. The corresponding blackbody equilibrium temperature is $T_{\text{eq}} = 800 M_p^{(2-3\epsilon)/4} \tau_{\text{Myr}}^{-1/4} \text{ K}$. Since accretion is likely to form a substantial atmosphere of volatiles released by impacts, the temperature at the boundary between radiative and convective heat transport (Section 2.2), rather than the surface temperature, is near T_{eq} ; the surface temperature will be much higher. The temperature at the surface of an Earth-sized planet with a thick steam atmosphere can be maintained above the solidus if the energy flux exceeds 300 W m^{-2} (Hamano et al., 2013), the case if accretion is continuous and happens in less than 100 Myr, which also happens to be about the inferred time for Earth's accretion (Jacobson et al., 2014).

In the canonical scenario, the late stage of rocky planet accretion is not continuous but consists of a small number of "giant" impacts by Moon- to Mars-size objects (Morbidelli et al., 2012) which will release enough energy to melt a fraction or most of the silicate mantle, which could then re-crystallize, depending on the depth of melting and the presence or absence of an atmosphere (Reese et al., 2011; de Vries et al., 2016). The largest of these impacts onto the proto-Earth is the leading scenario for the Moon's formation, which would have also generated magma oceans on both bodies (Sec. 4). Importantly, impacts deposit energy at depth, driving vigorous convection and mixing in the magma ocean as heat escapes to the surface. Additional energy will be released if metals (particularly Fe) segregate from silicates and sink to a growing core (Rubie et al., 2007).

2.1.2. Stellar Irradiation

Once accretion is complete, the principal energy source will be radiation from the host star. If the energy is uniformly distributed over the planet's surface by rotation and advection (by an ocean or atmosphere, see Sec. 2.2), the time-averaged energy flux over a nearly circular orbit is (Williams and Pollard, 2002):

$$q_{\text{stellar}} = \frac{L_*(1-A)}{16\pi a^2} = \frac{L_*}{4} \left(\frac{\sqrt{\pi}}{4GM_*P_K} \right)^{2/3}, \quad (2)$$

where L_* and M_* are the stellar luminosity and mass, respectively, a is the orbital semi-major axis, A is the planet's Bond (phase- and spectral-averaged) albedo, and P_K is the Keplerian orbital period. If L_* and M_* are expressed in solar units and P_K is in days, then $q_{\text{stellar}} \approx 8.9 \times 10^5 (1-A)L_*M_*^{-2/3}P_K^{-4/3} \text{ W m}^{-2}$. If there is no re-distribution of

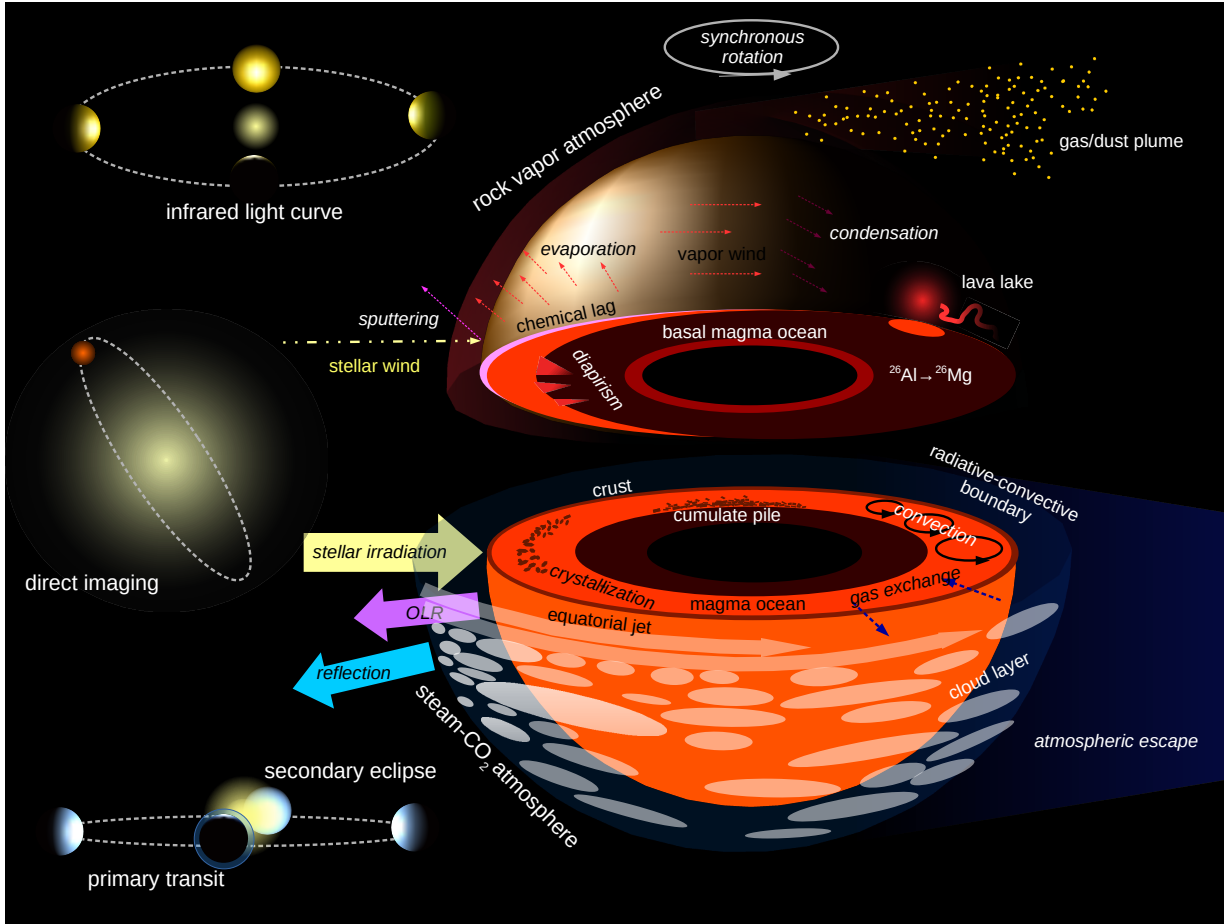


Figure 1: Schematic illustration of two “lava world” scenarios: a tidally-locked, synchronously rotating planet with one irradiated hemisphere, a hemispherical magma sea, and a thin rock vapor atmosphere (top); and a planet with a thick steam-CO₂ atmosphere and a global magma ocean (bottom). Components (normal font) and processes (italic labels) discussed in this review are represented, but not to scale or indicating the relative prominence. The left side figures illustrate methods of exoplanet detection/characterization discussed in Sec. 5.1. OLR = outgoing long-wavelength (infrared) radiation.

heat, i.e. no atmosphere, and the planet is locked by tides to synchronous rotation, then the local incident flux is maximum at the substellar point where it is four times that in Eqn. 2, and it varies with the cosine of the angle θ from that point to zero at the terminator (see Sec. 2.2). If A is low, the emissivity is near unity, and a stellar mass-luminosity relation for low-mass hydrogen-burning stars $L_* \propto M_*^{4.84}$ (Eker et al., 2015) is adopted, then $T_{\text{eq}} \approx 2000 M_*^{1.04} P_K^{-1/3}$ K for complete heat redistribution, and $T_{\text{eq}} \approx 2800 M_*^{1.04} P_K^{-1/3} (\cos \theta)^{1/4}$ K for no heat redistribution and synchronous rotation. The sensitivity to stellar mass means that, for a given orbital period, planets around stars with $M_* \gtrsim M_\odot$ can more readily host magma oceans, bearing in mind that the distribution of planets with orbital period also depends on stellar mass (e.g., Mulders et al., 2015).

Besides local stellar irradiance (time-averaged if the planet is non-synchronously rotating), the albedo and the efficacy of heat redistribution govern the temperature distribution on

an irradiated planet. The albedo of Solar System bodies varies from a few percent for primitive comets to nearly 80% for cloudy Venus (see Table 1 and Madden and Kaltenecker 2018). On an airless rocky body, the albedo will be determined by surface particle size distribution and composition, primarily the abundance of iron, which has a rich spectrum of transitions in the optical, and energetic particle bombardment or “space weathering” (Pieters and Noble, 2016). Carbon in the form of pure graphite has a moderate (≈ 0.25) reflectivity (Papoular and Papoular, 2014) but its actual reflectance in a planetary setting will depend on impurities. Since albedo is averaged over the spectrum of the star, it can vary significantly with the host star’s spectral type. For instance, aerosols scatter less at longer wavelengths and thus a planet with a hazy atmosphere would have a lower albedo around an M dwarf star.

Table 1
Bond Albedo of Planetary Surfaces

body or surface	value(s)	references
Moon	0.08-0.11	Buratti et al. (1996); Helfenstein et al. (1997)
Mercury	0.09-0.12	Mallama et al. (2017)
Venus	0.76	Haus et al. (2016)
Io	0.52	Simonelli et al. (2001)
Fresh basalt	~0.04	Spinetti et al. (2009)
H ₂ O-CO ₂ atmosphere	0.55-0.85	Pluriel et al. (2019) (model)

2.1.3. Aluminum-26

The decay of short-lived radionuclides (SLRs)², unstable isotopes with mean lives of kyrs to Myrs, in particular ²⁶Al (mean life of 1 Myr), was probably the principal internal heat source during the first few Myr of the Solar System. The presence of ²⁶Al is evidenced by a fraction of ²⁶Mg (the daughter isotope of ²⁶Al) in primitive meteorites that correlates with ²⁷Al. Regions of the inner Solar System from which we have samples had an initial (“time zero”) abundance of ²⁶Al relative to ²⁷Al of about 4.5×10^{-5} (Dauphas and Chaussidon, 2011). Its decay in a body of primitive chondritic composition would have released $6.7 \times 10^6 \text{ J kg}^{-1}$ (Moskovitz and Gaidos, 2011), significantly larger than the heat of fusion of the bulk rock ($\approx 2 \times 10^6 \text{ J kg}^{-1}$). In bodies larger than a few km, diffusion of this heat to the surface is slower than its release and melting would have occurred. This is thought to be the cause of the melting and differentiation of the parent bodies of the iron meteorites (Qin et al., 2008), pallasites, and achondrites, and, by extension, any body that accreted within ~ 2 Myr of time zero. Magnesium isotopes indicate that the accretion of the parent body of three related groups of meteorites – most likely from Vesta – occurred within 0.3 Myr of time zero, and that heat from the decay of ²⁶Al would have formed a magma ocean (Schiller et al., 2011, 2017) (see Sec. 4.6). There is evidence for other SLRs in the early Solar System, but their contribution to the heat budget would have been very minor (Huss et al., 2009).

²⁶Al was definitely present in the early Solar System, but neither its source nor its distribution within the protoplanetary disk are well established; both bear directly on expectations for the abundance of ²⁶Al in other planetary systems. ²⁶Al is endogenously produced by spallation reactions of high energy protons from the Sun with Mg atoms (Duprat and Tatischeff, 2007), and exogenously produced in intermediate- and high-mass stars and released into the interstellar medium by winds and supernova explosions and could have been incorporated into the Sun’s parent molecular cloud (Huss et al., 2009). High energy protons are produced by flares and shocks during coronal mass ejections; these are universal manifestations of magnetic activity on solar-type stars which is especially elevated when a star is younger and more rapidly rotating (Wright et al., 2011; Davenport et al.,

2019). On the other hand, an exogenous source of ²⁶Al in massive stars requires its formation, transport, and introduction into a protoplanetary disk within a few mean lives and the efficiency of this process could vary markedly from star to star (Gaidos et al., 2009; Lichtenberg et al., 2019). While the planets of the inner Solar System seem to have accreted in 10-100 Myr (Kleine et al., 2002), after the essentially complete decay of ²⁶Al, in other systems formation could have occurred more rapidly, i.e. close to the host star (Chiang and Laughlin, 2013; Chatterjee and Tan, 2014), especially around M dwarf stars where many planets on short-period orbits are found (Dressing and Charbonneau, 2015; Mulders et al., 2015; Gaidos et al., 2016). In these objects, intense heating by residual ²⁶Al could have readily sustained magma oceans for Myr (Fig. 2).

2.1.4. Tides

The dissipation of tidal deformation can be a much longer-lived internal heat source in planets. Tidal deformation can arise from non-synchronous rotation, non-zero orbital eccentricity, or non-zero obliquity (Driscoll and Barnes, 2015a). Heat production by these effects increases markedly with decreasing semi-major axis. For a synchronously rotating, homogeneous planet on a slightly eccentric orbit,

$$q_{\text{tide}} = \frac{84\pi^4 k_2 R_p^3 e^2}{QGP_K^4}, \quad (3)$$

where k_2 is the Love number and Q is the dissipation quality factor (Peale and Cassen, 1978). For rocky planets, the modified quality factor $Q' \equiv 3Q/(2k_2)$ is taken to be ≈ 100 (Clausen and Tilgner, 2015), but is expected to be weakly frequency dependent (Ray and Egbert, 2012), and could differ substantially for planet with magma oceans. For an Earth-size planet, $q_{\text{tide}} \sim 10 \text{ W m}^{-2} (e/0.1)^2 (P_K/10 \text{ day})^{-5}$. Thus, tidal dissipation in planets on moderately eccentric, close-in ($P < 10 \text{ day}$) orbits can drive widespread melting of their interiors (Fig. 2). One caveat is that this same dissipation circularizes the orbit, unless the eccentricity is continuously excited by a perturbing planet or stellar companion. Another is that Q depends on mantle rheology and will decrease as interior temperature approaches the solidus, e.g., Fig. 3 in Driscoll and Barnes (2015a). Tidal heating could be maximum at a certain distance from the star and be lower on interior/exterior orbits where the planets are hotter or cooler and thus less or more dissipative.

²To be distinguished from long-lived radionuclides (i.e., ⁴⁰K, ²³²Th, ²³⁵U, ²³⁸U) with mean lives of Gyr and total contributions of 10s to 100s of mW m⁻² to the heat flow from rocky Earth-like planets.

2.1.5. Induction

Induction heating, the ohmic dissipation of currents induced by the motion of a conducting body through a magnetic field, could be an important long-term heat source in a planetesimal or planet. The magnetic field is provided by the star, the motion can be a combination of rotation, orbital motion, or a stellar wind, and the conductor is either the metal core or a silicate mantle which becomes more conducting at high pressure and/or temperature (Soubiran and Militzer, 2018). Unipolar induction can take place if there is a complete electrical circuit that includes the planet, as is the case for Io's ionosphere and Jupiter (Goldreich and Lynden-Bell, 1969). If the planet is electrically isolated, induction heating can occur as dissipation of alternating eddy currents driven by oscillatory components of the magnetic field in the rest frame of the body due to, e.g., orbital motion through an inclined field or an eccentric orbit in an axisymmetric field. AC induction heating was first considered for the parent bodies of meteorites (Sonett et al., 1968), the Moon (Sonett et al., 1975) and Io (Colburn, 1980). The strength of a magnetic dipole field scales as a^{-3} , motivating models of this as a heat source in close-in planets around white dwarfs (Veras and Wolszczan, 2019), and M dwarf stars like TRAPPIST-1 (Kislyakova et al., 2017, 2018), as well as planetesimals close to young, magnetically active stars (Bromley and Kenyon, 2019).

An important aspect of this phenomenon is the skin depth δ , the characteristic scale over which eddy currents induced by a periodic field (here assumed to have an angular frequency equal to $2\pi/P_K$) cancel the imposed magnetic field:

$$\delta = \sqrt{\frac{P_K}{\pi \mu_0 \sigma}}, \quad (4)$$

where μ_0 is the magnetic permeability (close to the free space value) and σ is the electrical conductivity. Adopting $\sigma = 0.5 \Omega^{-1} \text{m}^{-1}$, appropriate for basaltic melts at low pressure (Gaillard and Marziano, 2005; Pommier et al., 2010), then $\delta \approx 200 P_K^{1/2} \text{km}$, where P_K is in days. Thus dissipation could occur throughout most or all of a surface magma ocean, but at high pressures and temperatures, especially within more massive planets, electrical conductivity increases by several orders of magnitude (Soubiran and Militzer, 2018) and the skin depth will be a few km.

The energy flux for eddy current dissipation in a uniform alternating field that induces a current density \mathbf{J} is given by the volume integral:

$$q_{\text{ind}} = \frac{1}{4\pi R_p^2} \int_V \frac{\vec{J} \cdot \vec{J}}{\sigma} dV. \quad (5)$$

If $\delta \ll R_p$, the dissipation can be approximated as occurring within a thin spherical shell of radius R_p (Nagel, 2018; Manser et al., 2019). For a planet on an orbit that is moderately inclined (i) to a stellar dipole magnetic field with sur-

face intensity B_* ,

$$q_{\text{ind}} = \frac{27\pi^{3/2} B_*^2 \cos^2 i}{4\mu_0^{5/2} G^2 \rho_*^2 P_K^{9/2}} \quad (6)$$

If P_K is in days and B is in Gauss, $q_{\text{ind}} \approx 3 \times 10^{-6} B^2 P_K^{-9/2} \text{W m}^{-2}$ and thus is negligible around slowly-rotating solar-type stars like the Sun ($B \sim 1 \text{Ga}$). It could, however, be appreciable for stars with stronger magnetic fields, i.e. close to rapidly rotating M dwarfs, young stars ($B \sim 500 \text{Ga}$, Vidotto et al., 2014; Kislyakova et al., 2018; Bromley and Kenyon, 2019), or white dwarfs ($B \sim 10^4 \text{Ga}$ Manser et al., 2019). Given the extreme period dependence, only planets with $P_K \lesssim 1$ day would have significant heat flow (Fig. 2). A higher-order field would produce an even more extreme period dependence. Remaining uncertainties in this scenario are whether this process can "bootstrap" from small amounts of existing melt, and the degree to which the planet's surface and interior would be shielded by any electrically conducting ionosphere.

2.2. Transport of heat

Vertical heat transport regulates the temperature profile and hence depth of a magma ocean, and lateral (meridional or longitudinal) heat transport regulates its extent. Both are usually manifested as internal circulation driven by buoyancy differences. Heat transport occurs by conduction, convection, advection, or radiation; convection is common in optically-thick regions of atmospheres (or above an irradiated surface), while in regions above the surface that are optically thin, net radiative transport from warmer lower layers upwards will flatten the temperature profile and suppress convection.

A dichotomy in the nature of heat transport will exist between "Mercury-like" planets with thin or nonexistent atmospheres and "Venus-like" planets with thick greenhouse atmospheres (Fig. 1). On the former, surface temperatures will be chiefly governed by local radiative balance³, and large gradients will exist between the sub-stellar point and terminator: $T_s \approx T_0(\cos \theta)^{1/4}$ for synchronous rotation, where T_0 is the sub-stellar point temperature and θ is the angle from that point, or between the equator and poles ($\bar{T}_s \approx T_0((\cos \theta)/\pi)^{1/4}$ for rapid asynchronous rotation, where θ is then the latitude). Associated density differences and buoyancy forces will govern the circulation and temperature structure in a magma ocean, and heat transport can be locally outward or inward.⁴

For "Venus-like" planets with an optically-thick atmosphere containing greenhouse gases like H_2O and CO_2 (Sec. 7)⁵, radiative balance occurs near the radiative-convective boundary in the atmosphere, typically at a pressure altitude

³Condensates, e.g. dust, in such an atmosphere can nevertheless influence this radiative balance.

⁴The consequences of strongly asymmetric surface temperature profiles for subsolidus convection in the planet's silicate mantle have been explored by van Summeren et al. (2011).

⁵In atmospheres hotter than 1000 K or 1500 K, alkali metals or Fe, respectively, will provide substantial opacity in the visible.

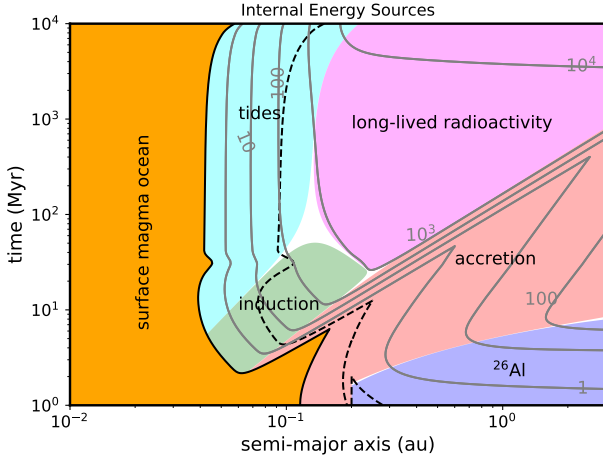


Figure 2: Approximate domains of dominant internal heat sources in an Earth-size planet orbiting a Sun-like star as a function of orbital semi-major axis and age. The orange zone is the area where the crust is <10 cm, i.e. a surface magma ocean, assuming efficient heat transport by an atmosphere but no greenhouse effect; the dashed line is the same boundary for a Venus-like 500 K greenhouse effect. In other parts of parameter space, gray contours indicate the thermal equilibrium thickness in meters of a crust. Since the crust can continuously founder, a surface magma could effectively exist over all but the upper right-hand region of this parameter space. Irradiation calculations use a model track from Dotter et al. (2008) and assume $A = 0.2$. Tidal heating assumes that orbital eccentricity is maintained at 0.05. A Solar System canonical initial ^{26}Al abundance is assumed. Long-lived radioactivity assumes an Earth-like inventory with an average mean life of 2.8 Gyr. Induction heating adopts the relationship between rotation period and magnetic field strength of Vidotto et al. (2014) and a solar-like Skumanich (1972) rotation history. Accretion assumes linear growth over 50 Myr at 1 AU and exponential decay of the growth rate as the protoplanetary disk is cleared with a 5 Myr time constant at 1 AU, and that the time constants scale with orbital period. In the absence of tidal heating that zone would be dominated either by induction heating (in younger planets) or long-lived radionuclides (in older planets).

of ~ 0.1 bar (Robinson and Catling, 2014), where the optical depth to space falls below unity. Above this altitude, radiation dominates and flattens the vertical temperature profile and the eddy diffusivity decreases with altitude, eventually reaching the molecular diffusion value at the homopause. Below this altitude, temperatures follow an adiabatic profile, and atmospheric circulation will impose a nearly uniform temperature distribution around the planet. In this case, the interior heat flow is everywhere outwards and set by internal sources of heat and cooling.

2.2.1. Magma Ocean Heat Transport

For the case of a hemispherical magma ocean of scale R_p on a tidally-locked, synchronously rotating ($P_{\text{rot}} = P_K$) planet, the boundary between the "Mercury-like" and "Venus-like" regimes of magma ocean heat transport is where $q_{\text{circ}} = q_{\text{int}}$, which for a hemispherical ocean of radius R_p on a tidally-

locked planet is:

$$q_{\text{circ}} = \frac{\rho c_p \delta_T (T_0 - T_l)}{\tau_T} \quad (7)$$

where δ_T and τ are the thermal boundary layer thickness and turnover time, respectively, and T_l is the lock-up temperature, where elevated viscosity prevents circulation, respectively (Kite et al., 2016). Assuming geostrophic flow over a hemispherical ocean of radius $\approx R_p$, then to a factor that is approximately unity:

$$q_{\text{circ}} \approx c_p \rho \alpha^{1/3} (\Delta T)^{4/3} \kappa_T^{2/3} g^{1/3} P_K^{1/3} L^{-2/3} \approx 20 \text{ W m}^{-2} (\Delta T / 100 \text{ K})^{4/3} M_p^{1/3} R_p^{-4/3} P_K^{-4/3}, \quad (8)$$

where M_p and R_p are in Earth units, P_K is in days, and α is the thermal expansion coefficient. Thus q_{circ} usually dominates over q_{int} (see Sec. 2.1), even for modest surface temperature gradients $\Delta T/R_p$. At least on airless planets, ocean circulation will be governed by the surface temperature gradient, but this heat transport is itself negligible compared to radiative terms ($> 10^5 \text{ W m}^{-2}$) and will not influence the surface temperature (Kite et al., 2016).

In the absence of surface temperature-driven circulation (i.e., near-uniform temperatures under a thick atmosphere), magma oceans will experience vigorous convection driven by the escape of interior heat, and the temperature profile will follow an adiabat:

$$\frac{\partial T}{\partial z} = \frac{\alpha' g T}{c'_p}, \quad (9)$$

where α' and c'_p are the thermal expansion coefficient and heat capacity, respectively, each modified to account for the volume change $\rho/\Delta\rho$ and latent heat L release associated with crystallization in a magma ocean, or condensation of solids in an atmosphere (Solomatov, 2015). The heat flow by conduction along such a gradient is $q_{\text{crit}} = k \alpha' g T / c'_p$, where k is the thermal conductivity. If $q > q_{\text{crit}}$ then convection occurs. For completely melted silicates with a basalt- or peridotite-like composition, $k \approx 2 \text{ W m}^{-1} \text{ K}^{-1}$, $\alpha \sim 10^{-4} \text{ K}^{-1}$ and $c_p \approx 2 \times 10^3 \text{ J kg}^{-1} \text{ K}^{-1}$ (Leshar and Spera, 2015) and with an Earth-like gravity, $q_{\text{crit}} \sim 1 \text{ mW m}^{-2}$. In a crystallizing magma ocean, $\alpha' / c'_p \approx \Delta\rho / (\rho L)$ (Solomatov, 2015) and again $q_{\text{crit}} \sim 1 \text{ mW m}^{-2}$. Thus q is usually $\gg q_{\text{crit}}$ (see Sec. 2.1) and, in the absence of other effects such as a temperature inversion or compositional gradient, convection will occur. The *style* of convection is characterized by the Grashof number, the ratio of convective to diffusive transport (Turcotte and Schubert, 2002):

$$Gr \approx \frac{g \rho \Delta \rho D^3}{\eta^2}, \quad (10)$$

where $\Delta\rho$ is the density change due to temperature differences or crystallization, D is the magma ocean depth, $\eta \sim 1 \text{ Pa-s}$ is the dynamic viscosity, $\rho = 2800 \text{ kg m}^{-3}$ (Leshar

and Spera, 2015) differences in mass density of a few percent, and D is in km, $\text{Gr} \sim 10^{15} D^3$.⁶ This regime of “hard” turbulence is characterized by large-scale circulation consisting of distinct hotter, ascending and cooler, descending plumes (Solomatov, 2015). It is only when the temperature is near the lock-up temperature that the crystallization fraction approaches the maximum packing crystal fraction (experimentally estimated to be $\approx 60\%$, Solomatov, 2015), and the viscosity soars does convection transition to disorganized “soft” turbulence.

On a rotating planet, flows can be rapid enough and the scales large enough that the Coriolis effects can be important, particularly since ultra-hot planets are likely to be synchronously rotating ($P \sim 1$ day). Two other dimensionless parameters capture this effect: the Ekman number, which is the ratio of viscous forces to Coriolis acceleration:

$$Ek = \frac{\eta P_{\text{rot}}}{4\pi\rho D^2 \sin\theta}, \quad (11)$$

and the local Rossby number⁷ at latitude θ , which is the ratio of the inertial forces to Coriolis acceleration:

$$Ro = \frac{P_{\text{rot}}}{4\pi\tau \sin\theta}. \quad (12)$$

Here, τ is a characteristic circulation time. For molten silicates, $\eta \sim 1$ Pa-s and $Ek \ll 1$ signifying that inertial/pressure forces balance centrifugal terms (the condition for geostrophic flow) and viscous forces are significant only in a thin “Ekman layer”. When $Ro \gg 1$ rotational effects are negligible. For rapidly rotating planets where $Ro < 1$ meridional flows are suppressed, and convective flow becomes more two-dimensional and less efficient (discussed further in Sec. 6).

2.2.2. Atmospheric Heat Transport

A substantial atmosphere can redistribute heat around the planet, i.e. from the illuminated substellar point to the poles and the night side. In astronomical systems where little is known about the details of the planet other than the assumption of synchronous rotation, heat transport is sometimes described as a dimensionless parameter C in terms that modify the radiation balance equation:

$$\sigma T^4 = (1 - A) q_{\text{stellar}}(\theta = 0) \left[(1 - C) \cos\theta \mathcal{H}(\pi/2 - \theta) + \frac{C}{4} \right], \quad (13)$$

where \mathcal{H} is the Heaviside step function. $C = 0$ represents no heat transport and $C = 1$ represents efficient heat transport and a uniform temperature distribution (e.g. Kreidberg and Loeb, 2016). Heat transport by the atmosphere across a temperature difference ΔT will scale as

$$q_{\text{atm}} \approx \frac{c_p \rho H v \Delta T}{R_p}, \quad (14)$$

⁶Alternatively, the flow can be characterized by the Rayleigh number $\text{Ra} = \text{Gr Pr}$, where the Prandtl number $\text{Pr} \gtrsim 10^3$.

⁷To be distinguished from the global Rossby number in which $\sin\theta$ is omitted.

where H is the atmosphere scale height and v is a characteristic meridional velocity, which, again assuming geostrophic flow, such that $v = P_{\text{rot}} \nabla p / (4\pi\rho \sin\theta)$, and ideal gas behavior,

$$q_{\text{atm}} \approx \frac{\gamma p P_{\text{rot}}}{2\pi(\gamma - 1)g \sin\theta} \left(\frac{R\Delta T}{\mu R_p} \right)^2 \sim 10^4 \text{ W m}^{-2} p_{\text{bar}} P_K \Delta T^2 R_p^{-2}, \quad (15)$$

where γ is the ratio of specific heats, R is the gas constant, and μ is the molecular weight, the numerical expression being for a CO_2 atmosphere. Comparing Eqn. 15 to Eqn. 2 shows that temperature gradients of < 100 K are sufficient to redistribute most heat around a magma ocean world. On a rapidly rotating planet, i.e. one that is tidally-locked to star on a short-period orbit (Sec. 5), with a low Rossby number, transport may take the form of eastward equatorial jets (“superrotation”) (Showman and Polvani, 2011).

2.3. Putting it together: Magma ocean lifetime

The characteristic cooling timescale of a magma ocean or pond will be the total latent heat of crystallization divided by the rate at which that energy can be lost to space:

$$\tau_{\text{MO}} = \frac{\rho D \mathcal{L}}{q}, \quad (16)$$

where ρ is the magma density, D the ocean depth, \mathcal{L} the latent heat of crystallization, and q the energy flux. There are three limiting cases; in the first, a stable crust or “lid” of thickness L forms and heat transfer is limited by heat transport through the lid. That time scale is $DL\rho\mathcal{L}/(k\Delta T \sim 2\text{Gyr}(L/100\text{km})(D/1000\text{km}))$, thus deep magma oceans can be stable for a significant fraction of a planetary system’s age (O’Rourke, 2020). (Lids thicker than ~ 100 km will experience subsolidus convection and not prolong crystallization.) In the second case, no stable lid forms but heat transfer is limited by a thick steam atmosphere to $q \approx 400 \text{ W m}^{-2}$ (Sec. 7) and the timescale will be $\sim 3 (D/100 \text{ km}) \text{ kyr}$. The third case is a planet with no or a thin atmosphere, with an exposed magma ocean radiating its energy to space at $\approx 1300 \text{ K}$, i.e. $q = 1.6 \times 10^5 \text{ W m}^{-2}$. Unless balanced by a heat source of equal magnitude (Sec. 2.1), a lava ocean cannot persist under such circumstance and crystallization occurs in decades. These timescales are also the relevant timescales for the entirety of a lava ocean to respond to changes in heat input, although surface boundary layers can respond far more rapidly (Kite et al., 2016). Under such conditions, heat loss is limited by heat transport within the lava ocean, by convection and/or crystal settling. Cooling and crystallization at the surface of a magma ocean will release latent heat and stabilize the magma column against convection. If individual crystals cannot settle quickly enough a surface mush layer will develop until the density difference causes overturn via a Rayleigh-Taylor instability (Michioka and Sumita, 2005; Culha et al., 2020). If crystals are more buoyant than the melt then a stable crust will develop, as happened on the Moon (Sec. 4).

Table 2

Extant or Recent Active Lava Lakes († = drained or solidified in 2018)

volcano	size [m]	temp [K]	η [Pa-s]	% crust	chemistry	references
Ambrym†	20/50	1350–1400	10^3	20–30	basaltic	Firth et al. (2016); Shreve et al. (2019)
Erebus	30	1250	5000	50	phonolitic	Birnbaum et al. (2020)
Erta 'Ale	34-100	1413	30	95	basaltic	Harris et al. (2005); Spampinato et al. (2008)
Kilauea†	250	1443	10^2	50–95	basaltic	Patrick et al. (2019)
Masaya	50	1500	630	30	basaltic	Aiuppa et al. (2018); Pering et al. (2019)
Mt. Michael	110	1262–1552	?	?	?	Gray et al. (2019)
Nyamuragira†	20–200	?	?	?	nephelinitic	Campion (2014); Coppola et al. (2016)
Nyiragongo	50–240	1370-1400	60-150	90	nephelinitic	Valade et al. (2018)
Villarica	30	1408	850	20–30	basalt/andesitic	Witter et al. (2004)

3. Lava lakes as Analogs in the Solar System

3.1. Why Study Lava Lakes?

Magma is a complex mixture of liquids, crystalline solids, and gases, and their properties, especially on large scales, are challenging to investigate in the laboratory or simulate numerically. With the possible exceptions of Io (Sec. 3.3) and Venus (Sec. 4.5) there are no longer magma oceans in the Solar System and the largest known bodies of magma at the surface of any Solar System body are lava lakes on Earth and (probably) Io. Lava lakes, particularly those on Earth (Table 2), have been studied extensively, and are useful analogs to understand fundamental processes such as convection, degassing, crystallization, and crust formation (Lev et al., 2019) that could be relevant to magma oceans. However, issues of scaling from lava lakes to lava worlds must be considered, and there are numerous caveats. An obvious difference between lava lakes and magma oceans is size; all terrestrial lava lakes are <500 m across (Lev et al., 2019), and the largest lava lake on Io is 200 km in size (Matson et al., 2006). Another is the geometry of the heat sources, i.e. advective heat transfer from below vs. stellar irradiation from above. Thus, it is important to consider how processes scale through dimensional analysis, i.e. dimensionless numbers that typically relate competing effects. It is also important to remember that the range of compositions and temperatures that are spanned by the lakes of the Solar System is probably limited compared to what is proposed or inferred for exoplanets. The general framework to begin tackling such scaling problems is beginning to be developed, but tying together multi-scale and multi-phase flow is at the forefront of modeling (e.g., Keller and Suckale, 2019).

3.2. Lava Lakes on Earth

Terrestrial lava lakes are our only opportunity at present to directly study the behavior of large bodies of magma. Lava lakes are categorized as either "active" lakes that form on top of a volcanic conduit and are constantly fed fresh magma (including gas) from depth, or "passive" lakes that form when lava travels from its initial eruption site and collects in a topographic depression then cools passively (e.g., Tilling, 1987). To compare with magma oceans which are expected to have some circulation (Sec. 2.2), we will only consider active lakes. In these, hotter, gas-rich magma erupts from a

conduit, then cools, de-gasses and descends back to the conduit. Most long-lived lava lakes on Earth have been subjects of extensive study (Table 2). Most of these lakes are basaltic or andesitic-basaltic in composition, though other compositions are represented.

Investigations of terrestrial lava lakes have measured gas emission to determine magma exchange rate (Lev et al., 2019) and the stability of the lake against draining away (Witham and Llewellyn, 2006). Many lava lake studies have described heat flow (Harris et al., 1999; Cipar et al., 2012; Coppola et al., 2016) and surface velocity (Peters et al., 2014; Valade et al., 2018; Pering et al., 2019). A few studies have also used analog models (Witham et al., 2006). These large and varied data on lake behavior have permitted the development and testing of sophisticated models of lake dynamics. Observations of surface motion have constrained models of convection (e.g., Harris, 2008; Birnbaum et al., 2020). Harris (2008) used observations of surface motion and heat flux at Erta 'Ale to develop a model of lava lake convection, including density changes due to both crystallization and temperature (but not vesiculation, see below). This model shows that convection can be driven by fractional density differences as small 0.2%.

Vesiculation (formation of gas bubbles) influences the dynamics of lava lakes via its lowering of bulk density. The effect of vesiculation on convection in Ray Lake (Erebus) was quantitatively addressed by Birnbaum et al. (2020). Their 2-d model, which combines the effects of cooling, crystallization, and vesiculation on density, exhibits two regimes of circulation: *diapirs* occur when there is a large density contrast between freshly supplied and recirculated lava. Pulsating plumes occur when the density difference is small between the older lake lava and newly supplied lava. Birnbaum et al. (2020) find that that the relative rate of gas loss to gas influx govern the density difference and hence the circulation regime. However, the Erebus lava lake is atypical in terms of its phonolitic composition and higher viscosity (10^4 Pa-sec, as compared to the typical 10^2 Pa-sec for basalts; (Sweeney et al., 2008)), and it remains to be shown how this model applies to other lakes.

A numerical study by Witham and Llewellyn (2006) demonstrates that the long-term stability of lava lakes is strongly dependent on the relative rates of gas supply and loss. Lakes that have large exsolved gas fractions are typically unsta-

ble and will collapse and drain away with system perturbations (e.g., the Pu'u O'o and Kilauea lava lakes; (Witham and Llewellyn, 2006)). Lev et al. (2019) synthesized data available on the main active lava lakes and found a strong relationship between lake surface velocity and the ratio of total gas flux to lava lake area. Additionally, they categorized lava lakes into two types of surface behavior - chaotic and organized. Surface behavior controls the relative rates of gas loss. Chaotic lakes tend to lose gas more efficiently, and organized lava lakes tend to develop crusts that trap gas, thus reducing gas loss.

3.3. Lava Lakes on Io

Jupiter's satellite Io was first recognized as volcanically active from data collected by the *Voyager 1* spacecraft (Morabito et al., 1979). Partial melting of the interior is caused by dissipation of tides on Io's orbit, the eccentricity of which is maintained by a Laplace resonance with the other Galilean satellites. Subsequent observations by *Galileo* showed that eruptions occur primarily from *paterae*, volcanic-tectonic depressions similar to calderas on Earth (e.g., Davies et al., 2001; Radebaugh et al., 2001). Resurfacing by lava is largely confined to these *paterae*, which are thought to host active lava lakes, with the rest of the satellite's surface being mostly covered by plume deposits (Lopes et al., 2004).

The largest and most well-studied of these *paterae* is Loki Patera. Despite accounting for only 0.07% of Io's surface, it accounts for 10-20% of Io's total heat output (Veeder et al., 1994; Matson et al., 2006). Loki was first hypothesized to contain a lava lake by Rathbun et al. (2002), but whether the *patera* actually contains a lake or is only resurfaced by lava flows is still debated (e.g., Davies, 2003; de Pater et al., 2004; Matson et al., 2006; Gregg and Lopes, 2008; de Kleer and de Pater, 2017; de Kleer et al., 2017; de Pater et al., 2017). Recent high-resolution ground-based observations in the infrared support the lava lake hypothesis (Conrad et al., 2015; de Pater et al., 2017). This illustrates the difficulty of interpreting the limited information provided by remote sensing (temperatures, fluxes, and morphology) and using it to test models, a problem that is vastly more exacerbated in the case of exoplanets, where at best, only fluxes and spectra from the unresolved planet are available (Sec. 5). The current model of Loki lava lake dynamics is one of foundering of denser crust, producing one or multiple resurfacing wave(s) of lava that propagate(s) across the *patera* (Rathbun et al., 2002; Matson et al., 2006; de Kleer and de Pater, 2017). This is analogous to multiple locations of down-welling in many terrestrial lava lakes (e.g., Patrick et al., 2017). The densification and foundering of the crust due to cooling and degassing might be accelerated by repeated extension and compression of the crust by the tidal stresses experience by Io on its eccentric orbit around Jupiter (Matson et al., 2006).

Io may distinguish itself as the only body in the Solar System for which there is at least indirect evidence – induction by Jupiter's field in the satellite's interior – of an interior magma ocean (Khurana et al., 2011). de Kleer et al. (2019) also describe orbital periodicity in volcanic activity

that could be a result of changes in magma conduits from tidal stresses. The magma ocean interpretation remains tentative, with Blöcker et al. (2018) showing that the changes in local magnetic field observed by the *Galileo* spacecraft could also be explained by plasma interactions with Io's atmosphere.

3.4. Scaling from Lava Lakes to Lava Worlds

3.4.1. Laminar vs. turbulent flow regimes

One to two orders of magnitude in scale separate magma oceans from the lava lakes of Io; another three orders of magnitude separate Io from the much more accessible terrestrial counterparts. This size difference translates into a difference in flow regime, as characterized by the Reynolds number

$$Re = \frac{\rho v L}{\eta} \quad (17)$$

where L and v are the characteristic size and velocity, respectively, of a convective eddy, and the transition from laminar to turbulent flow occurs at $Re \approx 200$ (Harris, 2008). Eddy sizes are typically $\lesssim 10$ m and for basaltic lava viscosities ($\sim 10^2$ Pa-sec) and $v \sim 0.1 - 1$ m sec $^{-1}$, convection in most lava lakes is laminar. However, eddy sizes will scale with the depth of magma oceans (many km) and Re values will fall well inside the turbulent regime (Solomatov, 2015). Higher temperatures, superliquidus or silica-poor (i.e. low polymerization) melts on lava worlds will have substantially lower viscosity (see Sec. 2.2), with yet higher Reynolds numbers and stronger turbulence (see Sec. 2.2). Turbulence affects heat transport but also mixing, i.e. mixing of crystallizing solids vs. gravitational settling of those solids into a cumulate pile (Solomatov, 2015). Convection in terrestrial lava lakes is clearly not representative of these processes in magma oceans. Investigations of the lava lakes of Io, which are substantially larger, and potentially much hotter (>1600 K) than basaltic magmas (Davies et al., 2001) and thus presumably less viscous, could partly bridge this gap.

3.4.2. Crystallization

Along with vesiculation, crystallization produces differences in density that drive circulation within magma bodies. In a magma with a crystalline component, the latent heat absorbed or released will buffer temperatures between the solidus and liquidus and reduce that variable's contribution to density. Crystals and as well as bubbles dramatically increase the viscosity of magmas; viscosity increases with crystal fraction and depends on crystal aspect ratio (Mader et al., 2013). These effects will persist in turbulent, well-mixed magmas (Costa et al., 2009). In low Re , crystal-rich magmas, crystals will settle collectively in down-welling plumes, initiating a process known as crystal-driven convection (Michioka and Sumita, 2005; Culha et al., 2020).

Crystallization will not be a factor in magma oceans that are at superliquidus temperatures, e.g., at the substellar point of highly-irradiated, tidally-locked planets on very short-period orbits (see Sec. 5). They will apply, however, to cooling, crystallizing magma oceans and to the regions of tidally planets close to the terminator, on the "shores" of a magma ocean

where temperatures are well below the liquidus, crystal fractions reach the “lock up” value of $\approx 60\%$ (Léger et al., 2011; Kite et al., 2016), a finite plastic yield strength becomes important (Pinkerton and Stevenson, 1992) and ultimately there is a transition to subsolidus-style convection.

3.4.3. Degassing and vesicularity

Bubbles will form and grow (vesiculation) in ascending magma as the ambient pressure falls below the saturation pressure for any dissolved volatile, e.g., H_2O , CO_2 , and SO_2 . Bubbles lower the bulk density and increase the buoyancy of the magma, potentially accelerating its ascent and further vesiculation. The degree to which the acceleration happens depends on the viscosity of the magma, which governs how strongly bubbles are retained; in high-viscosity rhyolitic melts bubbles are strongly coupled to the melt, and magma ascent and bubble growth accelerates (Cashman and Sparks, 2013). Bubbles more readily escape from low-viscosity basaltic melts and acceleration by vesiculation is less pronounced. The two scenarios will lead to vigorous upwelling through the magma column vs. a more passive style of convection, respectively. The dynamic of vesiculation in and gas escape from a magma column is predicted to produce a wide range in lava lake behavior (Witham and Llewellyn, 2006).

While vesiculation can be profoundly important for active lava lakes, it is unclear if it has any role in convecting magma oceans. Without in-gassing, the magma ocean will devolatilize and equilibrate with any atmosphere in a few convective turnover times. In-gassing could occur during melting of the underlying mantle in response to the evaporation of the ocean and advection of more volatile constituents to cooler regions of the planet (Kite et al., 2016). It could also occur if the planet is actively accreting gas from the protoplanetary disk (Olson and Sharp, 2019). Or volatiles might be trapped as bubbles in a crust and then recycled into the interior when the crust eventually founders (see Sec. 3.4.4 below). A very thick, Venus-like atmosphere (see Sec. 7.4.1) can suppress bubble formation, regardless of whether a source of volatiles is maintained.

3.4.4. Surface dynamics and crust formation

Wherever the equilibrium surface temperature is below the solidus, crystallization can occur in a thermal boundary layer at the surface, and these crystals can aggregate into a crust which will usually founder because of the higher density of solids. In some circumstances the crystals are less dense than the melt, such as the flotation crust of the Moon (see Sec. 4.1).

Otherwise, crust formation depends on the rate of radiative cooling of the surface and the convective turnover time (which together regulate the thickness of the boundary layer) and the (negative) buoyancy of the crust (which regulates foundering). In terrestrial lava lakes, the process is thought to occur as hotter, relatively buoyant lava erupts through the crust and floods it (Stovall et al., 2009). Bubbles can be trapped in the crust, increasing its buoyancy and

hence lifetime. On the other hand, vigorous vesiculation, that accelerates upwelling and, on larger scales, tides (Matson et al., 2006), can disrupt the boundary layer and inhibit crust formation.

4. Lava Worlds in the Early Solar System

As a consequence of energy liberated by accretion and short-lived radionuclide decay during planet formation (Sec. 2), magma oceans could have been widespread in the early Solar System (Table 3). The concept of a magma ocean was originally introduced to explain lunar geology as revealed by samples returned by the Apollo 11 mission (Wood et al., 1970). The Moon is both the best preserved and most accessible ancient surface, and the Lunar Magma Ocean (LMO) remains a touchstone against which other bodies are compared and models are tested (Warren, 1985), but the LMO is unlikely to be representative of diverse magma oceans in the past inner Solar System.

4.1. The Moon

While the generally accepted theory of lunar formation – one or more giant impacts (Hartmann and Davis, 1975; Cameron and Ward, 1976) – followed the idea of a LMO, the former is necessary for any LMO model because the exact formation scenario determines the initial extent of melting of the Moon. A scenario with a single giant impact of a Mars-sized impactor (dubbed “Theia”) successfully explains the Moon’s bulk composition, small iron core, and paucity of volatiles (Halliday, 2000). However, in its simplest form this scenario fails to explain the extreme chemical and isotopic similarity, particularly oxygen isotopes, between Earth and the Moon (Wiechert et al., 2001; Young et al., 2016; Greenwood et al., 2018). This is because models predict that the Moon should contain proportionally more material from Theia and be chemically distinct from Earth (Asphaug, 2014). One explanation is that Theia somehow accreted on the same orbit and from the same reservoir as Earth (Belbruno and Gott, 2005). Alternatively, the Moon could have accreted from the cumulative debris of many smaller impacts to which the impactors contributed much less (Rufu et al., 2017). At the other extreme, a single large impactor could have completely homogenized the two bodies (Canup, 2012). Or, a large, high angle impact completely vaporized the proto-Earth, forming a rapidly rotating ellipsoid of silicate gas (“synestia”) from which condensed Earth and smaller bodies that formed the Moon (Lock et al., 2018). Increasing numbers and precision of measurements might eventually resolve the question: Cano et al. (2020) report small but significant variation in lunar oxygen isotopes that suggest the Moon’s *interior* is different from Earth.

The original evidence for a LMO, i.e. a crystallizing global melt, are the petrological characteristics of the different suites of lunar crustal rocks, chiefly widespread anorthosite in the lunar highlands. Anorthosites are low-density volcanic rocks that are uncommon on Earth and typically found only in large igneous intrusions. However, they are widespread in the lunar crust, having been identified in lunar samples, lu-

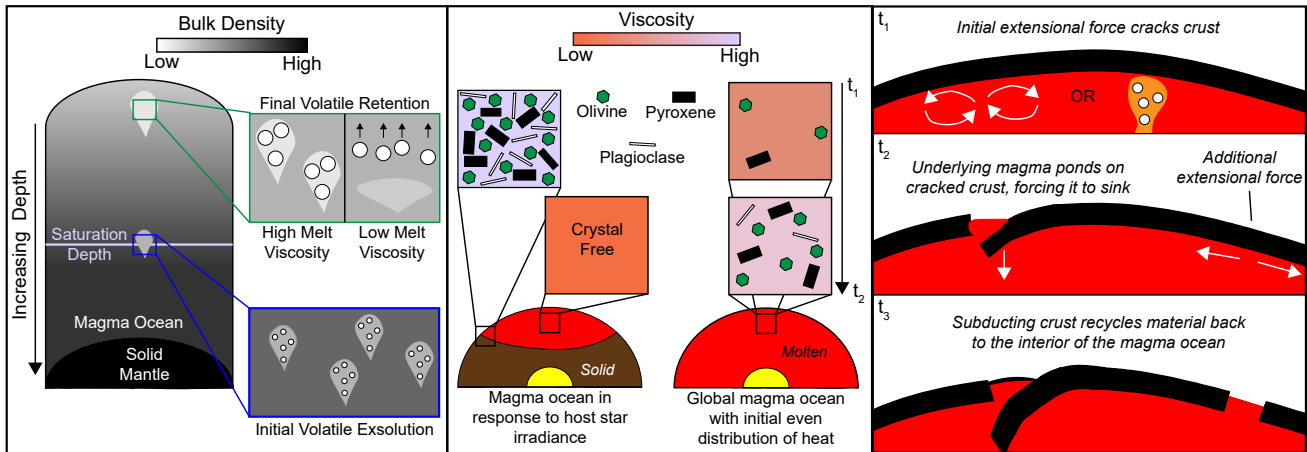


Figure 3: Schematic representation of processes in lava lakes and their potential role in the dynamics of magma oceans/seas. Left: Effect of vesiculation (bubble formation) and melt viscosity on the rise of a plume. Bubbles will initially accelerate the rise of a volatile-rich plume, but the outcome is also determined by whether the melt is viscous enough to retain bubbles. The gray scale indicates bulk density. Middle: Variations in bulk viscosity of a magma ocean depend on thermal evolution and crystallization. In a magma ocean maintained by stellar irradiance on an airless planet (left), crystallization will be minimal except at "shores" near the terminator. Crystallization in a cooling global magma ocean (right) will proceed through time, increasing bulk viscosity. Background colors in the boxes indicate bulk viscosity; other colors are used merely to distinguish components. Right: Foundering of the crust of a lava lake, as described by Stovall et al. (2009). Tension is applied to a dense, mature crust, e.g., by underlying convection currents or a rapidly ascending plume. The crust fails, and lava floods the broken crust, causing it to sink. This foundering can impose additional extensional stress in the crust and cause failure at other locations.

nar meteorites (Nagaoka et al., 2014), and by remote sensing (Yamamoto et al., 2012; Cheek et al., 2013). Shortly after the Apollo 11 mission, Smith et al. (1970) and Wood et al. (1970) proposed that lunar anorthosites were produced by accumulation of crystals into a buoyant crust on a LMO. For separation to occur, buoyancy forces must overcome viscous forces and this is favored in an anhydrous magma ocean that crystallizes at higher temperature and a lower viscosity. A volatile-depleted Moon is the expected outcome of the giant impact scenario, but this consistency with observations has been upset by accumulating evidence for lunar water (McCubbin et al., 2010; Hui et al., 2013) and has prompted more sophisticated approaches to reconciliation (Lin et al., 2017).

The oldest suite of rocks on the Moon, the ferrous iron-containing (ferroan) anorthosite suite and the magnesium-rich (magnesian) suite are characterized by a mixture of minerals that crystallized first or early from a primitive melt (Dymek et al., 1975; Papike et al., 1997). Younger rocks such as the KREEP basalts (see below) and the alkali suite anorthosites (Snyder et al., 1995) contain quartz and alkali feldspars implying that they crystallized from more evolved melts (Dowty et al., 1976; Snyder et al., 1995). This favours a progressively evolving source, as one would expect in a crystallizing magma ocean.

Progressive segregation of crystals from the melt would have driven chemical evolution in the LMO and "fingerprinted" lunar rocks. One such fingerprint is enrichment of potassium, rare earth elements, and phosphorous (KREEP) in younger lunar rocks such as mare basalts, the alkali suite anorthosites, and KREEP basalts (Rapp and Draper, 2018). The most evolved lunar rocks form from the final residual liquid before

complete crystallization, the "ur-KREEP" melt, (Warren and Wasson, 1979). Elements such as europium and strontium that are compatible in plagioclase are depleted from the melt (Walker et al., 1975; Papike et al., 1996). This is reflected in negative anomalies (depletion) of Eu and Sr in all lunar rocks that formed from melts that are younger than the anorthosite crust (Papike et al., 1996):

4.2. Earth

The energy released during the giant impact(s) that formed the Moon is also expected to have formed a terrestrial magma ocean (TMO). As in the case of the Moon, the extent of melting and degree of mixing between the bodies depends on the impact scenario (Nakajima and Stevenson, 2015). Unlike the Moon, plagioclase is not expected to crystallize early at higher pressures in the TMO and form a floatation crust (Elkins-Tanton, 2012b). Also unlike the Moon, plate tectonics and crustal recycling have destroyed the terrestrial rock record older than 4 Gyr, erasing any petrologic evidence for a TMO. Evidence for the TMO is therefore strictly geochemical. The mantle abundance of siderophile elements are elevated with respect to that predicted by chemical equilibrium between silicates and core-forming metallic iron at the surface (Ringwood, 1966). These elements become less siderophilic and there is better agreement with mantle abundances if equilibration happened at high pressure, i.e. at the base of a deep magma ocean where metallic iron may have temporarily pooled (Li and Agee, 1996; Righter and Drake, 1997). Some (but not all) of this excess, particularly in the highly siderophilic elements, could also be due to a late "veener" of siderophile-rich, chondritic material that never

equilibrated with the core (Kruijjer et al., 2015; Creech et al., 2016). This also must be reconciled with the isotopic evolution of Earth (Fischer-Gödde et al., 2020) and the isotopic similarity between Earth and Moon (see Sec. 4.1).

Another line of evidence for a TMO is the disparity in neodymium (Nd) isotopes between Earth and primitive chondritic meteorites. Boyet and Carlson (2005) reported that chondritic meteorites have a $^{142}\text{Nd}/^{144}\text{Nd}$ that is 20 ppm lower than the majority of terrestrial rocks. (See also Cipriani et al. (2011).) This requires either that Earth accreted from material with a non-chondritic $^{142}\text{Nd}/^{144}\text{Nd}$ that is not represented in meteorite collections, or that the isotopes were fractionated between reservoirs within the mantle, e.g. by global melting. The corollary is that there must be an unsampled reservoir in Earth's interior with $^{142}\text{Nd}/^{144}\text{Nd}$ that is sub-chondritic. Age constraints using multiple radiometric isotope systems indicate that this global differentiation event took place within 200 Myr of "time zero" of Solar System formation (Caro et al., 2005, 2006), bracketing estimates of the time of lunar formation.

4.3. Mars

Evidence for a Martian magma ocean and crustal differentiation has accumulated from analyses of SNC meteorites (McSween Jr, 1985). Radiometric dates point to a global differentiation event (and by inference, a magma ocean) within the first 50 Myr of "time zero" (Wood and Ashwal, 1982; Borg et al., 1997). Radiometric Nd ages suggest that the magma ocean had a protracted lifetime, perhaps due to a thick proto-atmosphere (Debaille et al., 2007). However, Bouvier et al. (2018) and Kruijjer et al. (2020) used the U-Pb and the Mn-Cr radioisotope systems, respectively, to infer that crystallization of any magma ocean was complete by about 20 Myr.

Recently, the idea of a magma ocean at the base of the Martian mantle has been suggested. Zeff and Williams (2019a) predicted that the residual liquids of melts produced by impacts on Mars would be denser than the surrounding mantle and would sink and accumulate at the core-mantle boundary. This explains the lack of an internally-generated magnetic field, as this hot layer would limit the escape of heat from the core that would otherwise drive a magnetodynamo. Melts become negatively buoyant because of the comparatively high Fe content of the martian mantle and the tendency of heavier Fe to remain in a melt (Taylor, 2013); this process might not operate in other, more iron-poor mantles in the inner Solar System.

4.4. Mercury

Evidence for a past Mercurian magma ocean is based on remote sensing, particularly by the recent *Messenger* mission (Solomon et al., 2007), as no meteorites have been tied to Mercury. Mercury has many unusual characteristics that point to a magma ocean formed under comparatively reducing (low oxygen fugacity or $f\text{O}_2$) conditions (Malavergne et al., 2010; Cartier, 2019). The crust of Mercury is iron-poor but sulphur-rich relative to other planets (Nittler et al.,

2011; Evans et al., 2012), which could reflect S-rich but Fe-poor magmas that would erupt during the late stages of crystallization of a low $f\text{O}_2$ magma ocean (Zolotov et al., 2013). A more volatile-rich crust would help explain Mercury's substantial phase of late-stage volcanism (Thomas et al., 2014). Under reducing conditions, carbon becomes more of a lithophile than a siderophile, and graphite can saturate in a magma ocean: Regions of unusually low albedo could represent exposures of a global graphite-rich flotation crust (Peplowski et al., 2016), and such a crust could have allowed a magma ocean to survive for longer than otherwise. In contrast, silicon becomes a siderophile at low $f\text{O}_2$, and dissolution of significant Si into the metallic core could partly explain Mercury's proportionally larger core (Cartier, 2019).

4.5. Venus

Despite its importance as Earth's "sister" planet, we have only cursory knowledge of the composition and geologic history of Venus due to the absence of samples and the presence of a thick atmosphere which blocks most remote sensing of its surface. The surface appears very young ($\lesssim 1$ Gyr) as a result of some global resurfacing event that destroyed most or all of any older crust (Phillips et al., 1992). Despite these gaps in our understanding of Venesian geology, the similarities in its interior structure to that of Earth (Aitta, 2012) and by inference, accretion history, suggest an early magma ocean phase. Of course, Venus has no Moon. It is also possible that a basal magma ocean has survived to the present time. O'Rourke (2020) shows that, should a basal magma ocean have formed, the absence of plate tectonics and reduced heat flow from the mantle would have allowed such a magma ocean to persist to the present. The thermal buffering provided by its ongoing crystallization would suppress heat flow from the core and prevent the operation of a magnetodynamo, explaining why Venus currently lacks a magnetic field.

4.6. Vesta

The large main belt asteroid Vesta is the only sub-planetary body widely agreed to have had a magma ocean. Vesta is thought to be the source of the Howardite-eucrite-diogenite (HED) suite of meteorites that are grouped by their similar oxygen isotopes and linked to the asteroid by spectral similarities (McCord et al., 1970; Binzel and Xu, 1993), and the existence of both an impact crater and a family of smaller, related asteroids ("vestoids") that could be debris from the impact and the intermediary source of HED meteorites (Binzel and Xu, 1993). This connection has been strengthened with observations by the *Dawn* mission (McSween Jr et al., 2013). There is direct, but model-based evidence for a magma ocean, i.e., petrogenesis of the HED suite by equilibrium crystallization followed by fractional crystallization of a chondritic parent melt (Righter and Drake, 1997). There is also indirect evidence, i.e., the existence of an iron core as supported by the depletion of moderately siderophile elements in the HEDs (Righter and Drake, 1997) and a paleomagnetic signatures of a magnetic field during crystallization (Fu et al., 2012).

Though the existence of a Vestan magma ocean is widely accepted, the extent of melting of the body is debated. Mandler and Elkins-Tanton (2013) argue that Vesta's primary plausible heat source – the decay of ^{26}Al (see Sec. 2.1) was efficiently retained by a conductive lid and as a consequence the interior was entirely molten. In contrast, Neumann et al. (2014) argue that ^{26}Al will partition (along with its stable counterpart ^{27}Al) into silicate melt and migrate toward the surface faster than the mean life of the isotope, thus reducing the effectiveness of heating and maintaining a shallow ocean for about 150 Myr (see also Moskovitz and Gaidos (2011)). They invoke another radioisotope – ^{60}Fe – to explain the convection in the core needed for a magnetodynamo, but the abundance of this isotope is now considered to have been much lower than previously thought (Tang and Dauphas, 2012), and there are alternative mechanisms to drive convection (Nimmo, 2009). Likewise, there is a range of potential scenarios for the crystallization of the magma ocean: Kawabata and Nagahara (2017) showed that the chemistry (i.e., Mg abundance) of the cumulate crust that is the source of the HED meteorites can be used to constrain the thickness of the conductive crust and the size and hence settling time of crystals.

4.7. Other Small Bodies

The canonical theory of planet formation includes a phase with many small bodies and it seems implausible that Vesta was the only such body with a magma ocean, although it might be the only one that has survived intact (c.f., Wilson and Keil, 2017). The meteorite collections contain hints that there may have been others. Several related achondritic meteorites, Northwest Africa (NWA) 7325, 8014 and 8486, contain abundant plagioclase, have enrichments in Eu and Sr like those seen in lunar anorthosites, and have a bulk chemistry consistent with that derived from melting of a pyroxene-rich anorthosite (Frossard et al., 2019), all suggesting they derive from a parent body which had a lunar-like anorthosite crust. However, the bulk element abundances rule out a lunar origin, and these meteorite are unrelated to any known meteorite groups. Potential counterparts to these enigmatic meteorites could be searched for among the Main Asteroid Belt (Reddy et al., 2015).

4.8. An Inner Solar System Synthesis

There is circumstantial evidence that magma oceans were widespread in the inner Solar System. Because the physical and chemical state of a magma ocean can profoundly influence the evolution of the interior, e.g. via overturn of the cumulate crust (Elkins-Tanton et al., 2003) and core formation (Rubie et al., 2007), as well as the composition of the atmosphere (Sec. 7), variation in those properties could underpin the diversity among inner Solar System bodies (Schaefer et al., 2018). Arguably the two most important parameters controlling magma ocean outcomes are (i) the size of the body, which regulates the supply of energy in accreting planetesimals (Eqn. 1) and governs the adiabatic temperature profile and hence the depth of the magma ocean (Eqn. 9) (Albarède and Blichert-Toft, 2007); and (ii) the oxygen

fugacity of the mantle, as that is related to the abundance of iron (as FeO) and the composition of gases that are released to the surface during partial melting (Kasting et al., 1993). Figure 4) plots the approximate locations of inner Solar System bodies in this two-parameter space.

Assuming that the inner rocky planets all accreted more or less from the same reservoir, the oxygen fugacity of a mantle was set by (a) the abundance of incorporated water (as a variable source of oxygen); and (b) the charge disproportionation of $3\text{Fe}^{2+} \rightarrow 2\text{Fe}^{3+} + \text{Fe}^0$ in silicate perovskite at high pressure (Bindi et al., 2020), and the sequestration of Fe^0 (metallic iron) into the core, leaving the mantle more oxidized (Armstrong et al., 2019). The latter is predicted to have occurred in Earth's deep mantle but not in that of Mars or the Moon due to lower pressures there, meaning that the mantles of these smaller bodies are more reduced (Deng et al., 2020). Sr and Eu abundances may be evidence for these reduced mantle, at least for the Moon. Under reducing conditions, i.e. one log unit below the iron-wüstite (IW) redox buffer, Eu^{3+} reduces to Eu^{2+} . Sr and Eu^{2+} are incompatible in major minerals common on the Moon. Depletion of Sr and Eu in lunar basalts suggests that the oxygen fugacity of formation was one log unit below the IW buffer (Papike et al., 1996). Such reducing conditions would have meant any carbon would have been primarily out-gassed as CO or COS rather than CO_2 (Renggli et al., 2017). In contrast, planets with comparatively oxidized mantles would be more likely to have CO_2 -containing atmospheres.

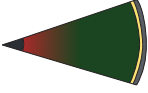
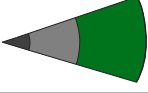


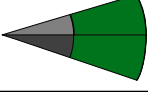
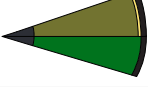
Thus, large planets which formed further from the Sun and which (it is assumed) accreted more water-rich material would have the most oxidized mantles, while close-in small planet would have the most reduced. Earth has the most oxidized mantle, with Mars as a close second, followed by Venus and tiny, highly reduced Mercury (Fig. 4). The amount of Fe left in the mantle would also influence the density of the residual melt as magma oceans began to crystallize, with mantles with high mantle Fe contents like Mars being more like to evolve residual liquids with densities that cause them to sink to the core-mantle boundary, forming a basal magma ocean (Sec. 6).

5. The Exoplanet Perspective

While magma oceans in the Solar System may not have persisted to the present day, with Venus (O'Rourke, 2020) and Io (Khurana et al., 2011) as possible exceptions, they almost certainly are present on some planets around other stars. In the past two decades more than 4000 candidate exoplanets have been discovered⁸. Among this diverse population are objects that are small enough to be primarily rocky and that exist in environments where they could host magma seas or oceans and could experience high rates of melting (Sec. 2.1). As instrumentation improves, methods of detection are refined, and more space- and ground-based facilities are developed (Table 4), the number of detected and characterized exoplanets continues to increase.

⁸<https://exoplanetarchive.ipac.caltech.edu/>

Table 3
Solar System Bodies with Suspected Past or Present Magma Oceans.

object	interior structure ^a	evidence	reference(s)
Moon		anorthosite flotation crust Fe-rich lavas KREEP enrichments Oxygen isotopes	Wood et al. (1970) Borg et al. (2019) Warren and Wasson (1979) Cano et al. (2020)
Earth		Nd isotopes siderophile abundances in mantle	Boyet and Carlson (2005); Cipriani et al. (2011) Li and Agee (1996); Righter and Drake (1997)
Mercury		carbon-rich crust sulfur rich basalts	Peplowski et al. (2016); Klima et al. (2018) Cartier (2019)
Venus		resurfacing/overturn absence of a dynamo	Smrekar et al. (2018) O'Rourke (2020)
Mars		petrology/geochemistry of SNC meteorites	McSween Jr (1985); Wood and Ashwal (1982) Borg et al. (1997)
Vesta		geochemistry of HED meteorites	Righter and Drake (1997)

^aRepresentative/proposed interior with lithologies shown approximately to scale. Key to colors: Yellow: late-stage, evolved-melt. Green: silicate mantle. Dark gray: solid metallic core. Light gray: liquid metallic core. Red/green gradient (on Moon): chemical gradient in mantle representative of cumulate overturn. Orange: existing melt. Black: crust. Top half-slices represent either an existing basal magma ocean (for Venus and Mars) or a past shallow magma ocean (for Vesta).

5.1. Methods of Detection and Characterization

5.1.1. Transit Photometry

Of the many methods used to detect and characterize exoplanets (Table 4), transit photometry has proven to be the most successful and most widely employed, with over three-quarters of currently known exoplanets discovered via this method, mostly by space-based telescopes and especially by *Kepler* (Table 5.1). The successor to *Kepler*, the Transiting Exoplanet Survey Satellite (*TESS*), is particularly well-suited to discovering Earth-size planets on short-period orbits around bright, nearby stars; planets such as these are candidate hosts of magma oceans. The transit method detects the small, repeated change in the apparent brightness of a star as an unresolved planet on a fortuitously highly-inclined orbit crosses the stellar disk (Deeg and Alonso, 2018). From these data, the planet's orbital period P_K can be estimated as well as planet radius:

$$R_p \approx R_* \sqrt{\delta} = 1 R_{\oplus} \frac{R_*}{R_{\odot}} \sqrt{\frac{\delta}{8.4 \times 10^{-5}}} \quad (18)$$

where R_* is the stellar radius and δ (the “transit depth”) is the fractional change in stellar brightness during the transit. Extreme photometric precision, only routinely achieved from space, is required to detect Earth-size planets around Sun-like stars (Eqn. 18). Although such planets can be detected around smaller M-type dwarf stars (Gillon et al., 2016; Dittmann et al., 2017), for a given P_K they will have lower T_{eq} and be less likely to host magma oceans (Eqn. 2). Even where detection and precise determination of δ is feasible, often it is limited knowledge of the host star properties that impact the precision/accuracy of determinations of planet radius and irradiance or T_{eq} (Berger et al., 2020).

5.1.2. Doppler Radial Velocity

The Doppler radial velocity (RV) method, while initially employed as a method to detect new planets, is now often used to validate planet candidates found by the transit method and determine their mass. A star's RV (motion along the line of sight) is measured by the Doppler shift in its spectrum; if the star hosts one or more planets, those can be revealed by detecting the periodic motion of the star around the systemic

Table 4
Exoplanet Observation Methods

method	parameters	notable surveys/missions	references
transit photometry	P, R_p	<i>CoRoT, Kepler, TESS</i>	Deeg and Alonso (2018); Baglin et al. (2006); Ricker et al. (2014); Koch et al. (2010)
Doppler RV	$P, M_p \sin i, e$	HIRES, HARPS, ESPRESSO, EXPRES	Fischer et al. (2016); Wright (2018); González Hernández et al. (2018); Petersburg et al. (2020)
transmission spectra	atmosphere	<i>Hubble, Spitzer, JWST</i>	Crossfield (2015); Kreidberg (2018); Deming et al. (2019)
secondary eclipse	T_{eq}, A	<i>Kepler, Spitzer, JWST</i>	Alonso (2018); Deming et al. (2019); Beichman and Greene (2018)
phase curves	day/nightside variations	<i>Kepler, Spitzer, JWST</i>	Koll and Abbot (2015); Deming et al. (2019); Parmentier and Crossfield (2018)
direct detection	emission, reflection	GPI, SPHERE, ELTs, LUVVOIR, <i>HabEx</i>	Bonati et al. (2019); Birkby (2018); Gaudi et al. (2018a,b);

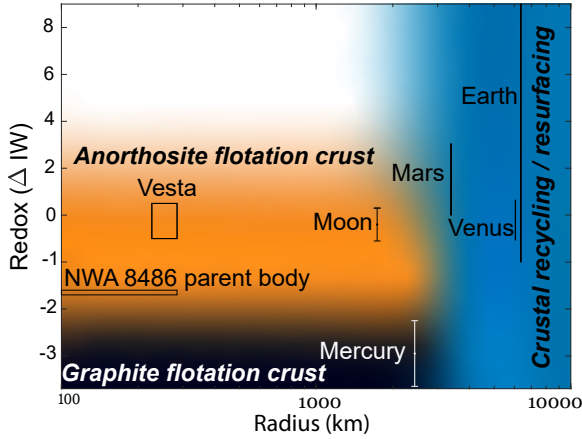


Figure 4: Plot of radius of vs. oxygen fugacity of different objects in the inner Solar System with suspected past or present magma oceans. Regions of parameter space for different magma ocean outcomes are labeled. Crustal recycling or resurfacing has only been observed on larger bodies. Graphite flotation crusts form only in mantles that are comparatively reducing with low H_2O abundance. Vesta is in red as it does not possess a flotation crust, despite an oxygen fugacity similar to that of the Moon.

center of mass or barycenter. In the case of a single planet, the planet mass M_p is related to the amplitude K of the RV signal by:

$$M_p \sin i = K (1 - e^2)^{1/2} \left(\frac{P_K M_*^2}{2\pi G} \right)^{1/3} \quad (19)$$

$$\approx \frac{K}{0.64 \text{ m s}^{-1}} \left(\frac{P_K}{1 \text{ day}} \right)^{-1/3} \left(\frac{M_*}{M_\odot} \right)^{2/3}$$

where i is the orbital inclination to the plane of the sky, M_* is stellar mass (assumed much larger than M_p), and e is the eccentricity (taken to be $\ll 1$). Since $\sin i < 1$ only the

minimum planet mass can be measured with RVs alone, but $\sin i \approx 1$ for transiting planets. For these planets, P and orbital phase are also precisely known, allowing more exact measurement of the remaining Keplerian orbital parameters; for circular orbits this is the single parameter K . Current RV precision is generally limited to about 1 m sec^{-1} . The goal of the rising generation of instrument projects is to achieve $\sim 0.1 \text{ m sec}^{-1}$, but stellar sources of noise (“jitter”) must be overcome (Fischer et al., 2016; Wright, 2018).

An RV-determined mass (Eqn. 19), combined with a transit-determined radius (Eqn. 18), yields a mean density and can be compared to models of planet interiors (Lopez, 2017; Dorn et al., 2017). Mass and radius can also be combined to calculate a surface gravity $g = GM_p/R_p^2$, a key parameter for models of planetary atmospheres (Ciardi et al., 2019). Radial velocities can also constrain eccentricity, which through tidal dissipation can drive melting on close-in planets (Sec. 2.1).

5.1.3. Transit Spectroscopy

If a transiting planet has an atmosphere, a very small fraction of the star light that reaches a distant observer will pass through the upper layers of that atmosphere. Condensates and gases in the atmosphere will absorb and/or scatter that light in a wavelength-dependent manner (Fig. 1), causing the planet’s transit-derived apparent radius to vary slightly with wavelength. Observations at multiple wavelengths, i.e. spectra, can be used to detect and constrain the structure of the atmosphere and identify constituents (Kreidberg, 2018). For lava worlds, this could include sulfur compounds such as SO_2 as evidence of widespread volcanism (Kaltenegger and Traub, 2009).

Transiting planets on near-circular orbits will also be periodically occulted by their host stars, and the light that is reflected and/or emitted from the spatially unresolved planet can be isolated by differencing observations during and outside of this “secondary eclipse” (Fig. 1). Since $R_p \ll a$

the planet's reflected signal is very small and, with the exception of Jupiter-size planets on ultra-short period orbits (Angerhausen et al., 2015; Mallonn et al., 2019), usually undetected. Due to the lower temperature of a planet compared to its star, smaller planets are only detected at infrared wavelengths where the planet radiates significantly and a signal could be detected, and if the observations are obtained from space. The infrared emission from the planet can be used to estimate its emitting temperature, a value expected to be close to T_{eq} (MacDonald et al., 2020), and by energy balance, albedo and heat re-distribution (Garhart et al., 2020). Lava worlds with high surface temperatures (not necessarily equal to T_{eq}) therefore lend themselves to this method. The infrared regime also contains many broad features produced by molecular absorption lines and thus the spectrum of this emission is a diagnostic of the composition and structure of any atmosphere. Sufficiently high-cadence observations during the ingress and egress portions of a secondary eclipse offer the opportunity to partly resolve spatial variation in emission over the planet, or "eclipse mapping" (Williams et al., 2006; Rauscher et al., 2018).

5.1.4. Phase curves

As a planet orbits its star, the phase angle for a distant observer varies periodically (Fig. 1). Measurement of the change in flux from the unresolved planet with phase provides information about the scattering properties of the surface or atmosphere (at optical wavelengths), or longitudinal variation in the temperature and atmospheric structure between the illuminated and dark sides of the planet (in the infrared). Infrared phase curves, in particular those from *Spitzer*, have been useful in measuring the day- and night-side temperature contrast on the planet, which is the efficiency of heat transport, i.e. by an atmosphere and rotation (Koll and Abbot, 2015, Sec. 2.2), which models suggest depends on the rotation and composition of the atmosphere (Zhang and Showman, 2017). determining if the emission is strongly peaked at the substellar point, as expected for an airless, tidally locked planet, or if there is a westward or eastward shift of this peak or "hotspot" due to heat transport and the thermal inertia of the atmosphere (Rauscher et al., 2018). Observations at multiple wavelengths probe longitudinal variations in albedo and cloud structure (Parmentier and Crossfield, 2018). To date, most studies to date have been on giant planets on short-period orbits (e.g., Zellem et al., 2014; Dang et al., 2018) with analyses attempted only a handful of rocky planet on ~ 1 -day orbits (Batalha et al., 2011; Sanchis-Ojeda et al., 2013; Hu et al., 2015; Demory et al., 2016; Angelo and Hu, 2017).

5.1.5. Direct Detection

Direct detection can identify and characterize planets on non-transiting orbits, separating their signal from the central star either spatially (in images) or by velocity (in spectra). This is usually considered most feasible at infrared wavelengths where the planet-to-star contrast is the most favorable. Direct imaging offers an unambiguous extraction of

the planet's signal, e.g. to obtain a spectrum. To date, this method has lent itself to the detection of young, super-giant planets in orbits of tens of AU (see review by Bowler, 2016). Direct imaging might eventually detect planets on wide orbits heated by a giant impact, or their tidally-heated satellites (see below). In contrast, direct spectroscopic detection identifies the Doppler-shifted signal of a spatially unresolved planet and its Keplerian variation via cross-correlation (Birkby, 2018). This could, in principle, be used to detect the emission from hot planets on close-in orbits. Some directly imaged planets might have satellites: Agol et al. (2015) have proposed a *spectroastrometric* separation of signals from a planet and its satellite using the wavelength-dependent shift of the image centroid.

5.1.6. Sensitivity and Biases

All methods of exoplanet detection and characterization have limited sensitivity and intrinsic biases which influence the observed distribution and characteristics of exoplanets. The transit method detects only those planets on highly-inclined orbits (within R_*/a of edge-on for circular orbits, or ~ 1 -10% of a randomly-oriented population). As a consequence of this geometric requirement and Kepler's Third Law, the transit method is biased towards planets on close-in planets which are more likely to transit and transit more often. Thus, it is well-suited to detecting highly-irradiated planets, as long as the cadence is sufficient to resolve the transit, which will be less than an hour. The Doppler RV method is also biased towards short period planets, since, for a given planet mass, the Doppler amplitude increases with decreasing orbital period (Eqn. 19). Since the mass of rocky planets scales roughly as R_p^4 while the transit depth scales as R_p^2 (Eqn. 18), the Doppler RV method is less sensitive to smaller planets. While transit photometry may be able to readily detect Earth-size planets on short-period orbits, their masses might remain uncertain until more precise instruments and better mitigation of stellar noise become available. Direct detection is highly biased towards giant planets, particularly in young systems (Crossfield et al., 2015) and it may contribute only in rare cases such as post-impact planets (Sec. 5.2.2).

5.2. The Diversity of Lava Worlds around Other Stars

5.2.1. Ultra-Short Period Planets

Highly-irradiated planets on ultra-short period orbits (USPs) include the most likely lava world candidates. The period cut-off for USPs is arbitrary and varies, but the convention is one day (e.g., Sahu et al., 2006; Sanchis-Ojeda et al., 2014; Winn et al., 2018; Dai et al., 2019), with Kepler-974c as the current record-holder at $P = 4.25$ hr (Ofir and Dreizler, 2013; Rappaport et al., 2013). Approximately 0.5% of Sun-like G-type stars host USPs and they appear slightly more common around cooler K-type stars (Sanchis-Ojeda et al., 2014). To date, nearly 80 USPs have been discovered by transit photometry; nearly all have radii less than $2R_{\oplus}$ (Winn et al., 2018) and are thus likely to be primarily rocky (Weiss

and Marcy, 2014). Indeed, most of those USPs with masses established by Doppler RV observations, are consistent with rocky composition with a few measurements (or limits) that suggest a thick atmosphere (Fig. 6) (Demory et al., 2011; Winn et al., 2011; Dai et al., 2017).

USPs orbit inside the observed inner edge of protoplanetary disks around T Tauri stars, thus these objects could not have arrived at their present location by migration through a disk. USPs tend to be the innermost planet in multi-planet systems, and the larger mutual inclinations and wider orbital spacing of these particular systems suggest that that USPs were scattered inwards by gravitational interaction with companion planets (Sanchis-Ojeda et al., 2013; Lee and Chiang, 2017; Dai et al., 2018; Winn et al., 2018; Petrovich et al., 2019). Some USPs could have possessed thicker atmospheres which were then removed by the intense radiation and particle fluxes from the host stars (Owen and Wu, 2013; Dai et al., 2017; Lopez, 2017) (see Sec. 7.3). While few USPs have measured masses or mean densities, lower limits for those of Kepler-947c have been estimated using the Roche criterion for disruption by the tides from the host star (Rappaport et al., 2013; Price and Rogers, 2020); these suggest an iron-rich interior. Three of the best-studied USPs are described and discussed in Sec. 5.3.

5.2.2. Post-Giant Impact Planets

The planets of the early inner Solar System probably hosted magma ocean phases sustained by heat from accretion of planetesimals and giant impactors (Secs. 2.1 and 4). Around very young stars, rocky planets are presumably in the same magma ocean phase; in principle these could be directly detected, especially soon after a giant impact (Stern, 1994; Miller-Ricci et al., 2009; Bonati et al., 2019; Lupu et al., 2014). Meng et al. (2014) have reported infrared variability in a young star consistent with the debris of such a collision. Identifying such planets and studying their emission will enhance our understanding of the corresponding era in the Solar System's history. Because of the heat capacity of a deep magma ocean produced by such an event, and the continuous foundering of any crust, planets will remain super-luminous in the infrared and possibly detectable for several million years (Bonati et al., 2019; Lupu et al., 2014). The potential for direct detection is strongly influenced by the insulating effects of the atmosphere, which throttles the loss of energy to space, increasing the magma ocean lifetime and making this phase statistically more likely to be observed, but at the same time rendering the planet less detectable in the infrared (Bonati et al., 2019). As the magma ocean cools, its emission spectrum is expected to evolve (Hamano et al., 2015). Any planet heated by a recent giant impact would presumably be accompanied by a tell-tale debris disk or dust cloud that could distinguish it from other scenarios (Meng et al., 2014).

5.2.3. Tidally-Heated Planets and Satellites

The Jovian satellite Io owes its intense volcanism to the tidal deformation it experiences on its eccentric orbit close

to Jupiter (see Sec. 3.3). Planets on close orbits around their host stars (or satellites around Jupiter-like planets) could experience significant internal heating, either due to the eccentricity of the orbit or non-synchronous rotation (Sec. 2.1). These “exo-Ios” would experience large-scaling melting and widespread volcanism (e.g., Jackson et al., 2008; Henning et al., 2009; Cassidy et al., 2009; Peters and Turner, 2013; Driscoll and Barnes, 2015b; Oza et al., 2019)). In systems of multiple planets (or satellites), mutual interactions could maintain eccentric orbits, interior heating, and thus lava oceans or volcanic activity for much of the stellar lifetime. These, in principle, may be observable (Henning et al., 2009; Peters and Turner, 2013; Oza et al., 2019). The persistence of measurable orbital eccentricity against orbital circularization by tidal dissipation in a system with known age, or the degree to which the orbit is excited by companion planets could constrain tidal dissipation in the planet and hence the modified quality factor $Q' = 3Q/(2k_2)$ (appearing in Eqn. 3). A low value compared to that typical of solid rocky planets ($Q' \sim 100$) could indicate a magma ocean (Barr et al., 2018). Henning et al. (2009) predict significant tidal heating for $P_K = 10 - 30$ days and $e \lesssim 0.1$; partial melting on a global scale occurs for $P_K < 2$ days from tidal heating alone. While tidal effects may increase equilibrium temperatures by only a few K (Henning et al., 2009), other manifestations such as volcanic hotspots or volcanic gases in the atmosphere could be detected (Henning et al., 2009; Kaltenegger and Traub, 2009). Tidally-heated “exomoons”, i.e. Io-like satellites of giant planets, might be detected by the orbital phase variation of their contribution to the combined infrared emission of the unresolved planet plus satellite (Peters and Turner, 2013; Forgan, 2017). However, detection will only be feasible in cases of large (i.e., Earth-size), hot (≈ 850 K) satellites around planets that are on wide orbits around relatively dim host stars, i.e., M dwarf stars (Peters and Turner, 2013).

5.3. Three Prominent Lava Worlds

5.3.1. CoRoT-7b

CoRoT-7b, a $1.68 \pm 0.09 R_{\oplus}$ “super-Earth” on a 20-hour orbit around a G-type star, was the first exoplanet identified as plausibly rocky (Léger et al., 2009). High stellar RV noise compared to the expected planet signal have hindered an accurate mass estimate, with values from $2.3 \pm 1.8 M_{\oplus}$ to $8 \pm 1.2 M_{\oplus}$ reported (Queloz, D. et al., 2009; Hatzes, A. P. et al., 2010; Ferraz-Mello, S. et al., 2011; Pont et al., 2011; Boisse, I. et al., 2011). This translates into uncertainty in bulk density, complicating models of interior composition. Leger et al. (2011) find that an Earth-like proportion of silicate mantle and metallic iron core is consistent with the median reported RV mass range ($6.9 \pm 1.2 M_{\oplus}$). A mass at the upper end of the range of measurements (e.g., Queloz, D. et al., 2009; Hatzes et al., 2011; Ferraz-Mello, S. et al., 2011) would require a comparatively larger Mercury-like core (Valencia et al., 2010; Wagner et al., 2012).

If CoRoT-7b is tidally locked and lacks an atmosphere, day-side temperatures could be as high as 2600 K, and the

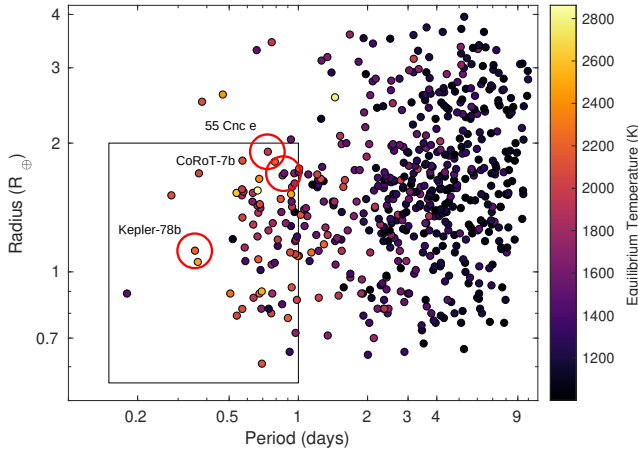


Figure 5: Orbital period versus radius of planets with periods less than 10 days and with equilibrium temperatures greater than 1000K. A box marks the domain of Ultra Short Period planets ($P_K < 1$ day) that are plausibly rocky. Some USPs around M dwarf stars may not be hot enough for melting ($T_{meq} < 1300$ K), while some planets on wider orbits around more luminous stars will be at least partially covered by a magma ocean. 55 Cnc e, Kepler-78b, and CoRoT-7b, discussed in detail in Sec. 5.3, are circled. Stellar and planetary data were downloaded from the NASA Exoplanet Archive December 2 2020. Equilibrium temperatures for some planets were not reported and were derived from stellar and orbital parameters as in, for instance, Sheets and Deming (2014), assuming a planet with albedo $\ll 1$ and efficient redistribution of heat.

planet would possess a hemispherical dayside magma ocean (Léger et al., 2009). Night-side temperatures will be far lower; assuming inefficient heat transport, no greenhouse effect, and a geothermal heat flux of 300 mW m^{-2} , Léger et al. (2009) predict night-side temperatures as low as 50 K. An atmosphere would serve to move heat from the day-side to the night-side and would serve to significantly diminish this dichotomy. Dissipation of tides raised by the host star in the planet may also induce a significant amount of heating on the nightside (Barnes et al., 2010). The depth of the magma ocean on CoRoT-7b depends inversely on its surface gravity, which controls the pressure at a given depth (Léger et al., 2011), as well as transport of heat by mantle subsolidus convection to the night side (Kite et al., 2016). The planet’s proximity to the host star is usually assumed to have led to the removal of any substantial atmosphere, but a larger planet radius based on a more accurate stellar radius from a parallax by the *Gaia* mission suggests a volatile-containing planet (Stassun et al., 2017; Dai et al., 2019). Regardless, CoRoT-7b could retain a thin atmosphere composed of out-gassed volatile compounds or more refractory elements sputtered from the surface. An exosphere composed of refractory elements might be expected to be trailing away from the parent star (Mura et al., 2011). To date, no absorption lines originating from an exosphere have been detected in CoRoT-7b’s transmission spectrum (Guenther, E. W. et al.,

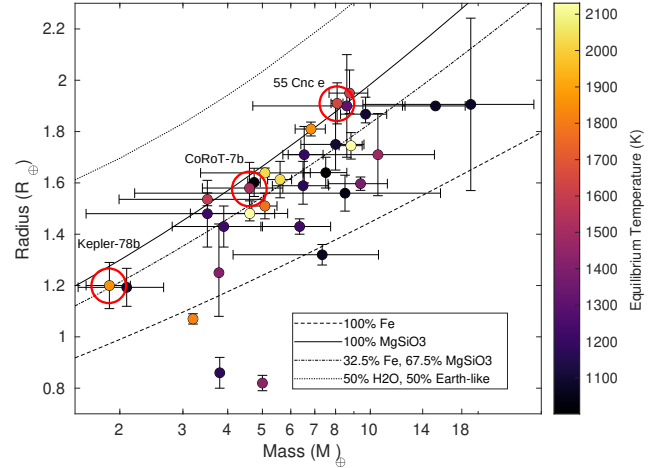


Figure 6: Earth- and super-Earth-size exoplanets with equilibrium temperatures > 1000 K for which both mass and radius have been measured. 55 Cnc e, Kepler-78b, and CoRoT-7b are circled in red. The masses and radii are from Dai et al. (2019) and the NASA Exoplanet Archive, with the latter up-to-date as of August 2 2020. Models of planet composition from Zeng et al. (2019) are plotted for pure iron, Earth-like (silicate mantle and iron core), pure silicate, and Earth-like planets overlain by a water envelope (50% by mass).

2011).

5.3.2. Kepler-78b

Kepler-78b is on an 8.5-hour orbit around a K-dwarf; with a radius of $1.2 \pm 0.09 R_{\oplus}$ and a mass of $1.69 \pm 0.41 M_{\oplus}$, it is likely to have an Earth-like interior (Howard et al., 2013; Pepe et al., 2013; Dai et al., 2019). Like CoRoT-7b, stellar activity has limited accurate Doppler RV measurement of its mass, but in this case detrending by Gaussian process regression has partially ameliorated these systematics (Grunblatt et al., 2015). Possible compositions range from Moon-like and iron-deficient to Mercury-like and iron-rich (Hatzes, 2014; Stassun et al., 2017).

Using *Kepler* photometry of the phase curve and secondary eclipse, Sanchis-Ojeda et al. (2013) has constrained the dayside T_{eq} and the reflected light (albedo) of Kepler-78b to 2300–3100 K and 0.4–0.6, respectively, although they note that the constraint on albedo are loose and allow for values outside this range. This is invariably hot enough for a surface lava-ocean (Pepe et al., 2013) and, while crude, is in agreement with Rouan et al. (2011), Batalha et al. (2011), and Sheets and Deming (2014), who have argued for a similarly high albedo for the magma ocean surface of another USP, Kepler-10b.

5.3.3. 55 Cancri e

55 Cnc e (also designated ρ Cnc e) is a $1.91 \pm 0.08 R_{\oplus}$ planet Demory et al. (2016) that is the innermost ($P_K = 18$ hr) of five known planets orbiting a bright, nearby K-type dwarf star. The star also has an M-dwarf companion at a projected separation of 1060 AU (Mugrauer et al., 2006). Perturba-

tions by this stellar companion could have misaligned the orbit of 55 Cnc e with respect to the host star's spin axis (Kaib et al., 2011), but a detection of this misalignment using the Rossiter-McLaughlin effect (Bourrier and Hébrard, 2014) has not been confirmed due to the predicted weak signal (López-Morales et al., 2014). It is possible that the entire planetary system was misaligned by the gravitational influence of the M dwarf companion; interactions among the planets and with the secondary star in the 55 Cnc system have potentially had consequences for the system's evolution (Hansen and Zink, 2015; Nelson et al., 2014; McArthur et al., 2004).

RV observations with multiple instruments point to a mass at or near $8.08 \pm 0.31 M_{\oplus}$ (e.g., Demory et al., 2011; Endl et al., 2012; Nelson et al., 2014; Demory et al., 2016). The bulk composition of the planet is controversial, since the nominal mass-radius is marginally ($\approx 2\sigma$) inconsistent with a purely silicate mantle-iron core composition (Fig. 6) and allows for a substantial atmosphere of volatiles (Winn et al., 2011; Demory et al., 2011; Gillon et al., 2012). More exotic compositions have been proposed, i.e., a rocky world enriched in refractory Ca and Al and lacking an iron core (Dorn et al., 2018) or one that is carbon-rich, with carbides replacing silicates, but with a metallic core (Madhusudhan et al., 2012). The latter scenario was motivated by a report that the parent star has a high C/O ratio (Delgado Mena et al., 2010), a claim that has since been disputed (Teske et al., 2013).

Observations of secondary eclipses in the infrared, i.e., by *Spitzer*, are an independent probe of any atmosphere. On the one hand, *Spitzer* found the night side of the planet to be around 1600K; if the planet is tidally locked, as expected, this suggests appreciable but relatively inefficient heat transport from the day side (at 2700 K) to the night side hemisphere by an atmosphere (Demory et al., 2016). Moreover, there is a ≈ 40 deg eastward shift in the location of peak emission on the dayside - the expected effect of a super-rotating atmosphere. Demory et al. (2016) propose two explanations: a thick atmosphere that transports heat from the dayside across the terminator but which condenses out on the cooler nightside, or an airless world with a low-viscosity magma ocean that convects heat to the nightside. A re-analysis of *Spitzer* phase curves supports heat transport by a thick atmosphere (Angelo et al., 2017).

Ideas on the most plausible composition of 55 Cnc e's atmosphere have evolved from H-, He-, or supercritical water-dominated compositions (Demory et al., 2011; Winn et al., 2011; Gillon et al., 2012) to those with higher molecular weight volatiles or even refractories that are evaporated or sputtering of refractory-rich compounds analogous to the exosphere of Mercury. The mixing ratio of hydrogen is controversial since it is expected to rapidly escape from a planet this close to its host star. Ehrenreich et al. (2012) did not detect a H exosphere while Tsiaras et al. (2016) report the detection of features in an infrared transmission spectrum consistent with HCN. Ridden-Harper et al. (2016) and Bourrier et al. (2018a) report tentative detections of Ca^+ and Na in the exosphere.

Especially intriguing is potential orbit-to-orbit variability in the depth of both the secondary eclipse and primary transit, in different spectral bands. Variability in the secondary eclipse depth at $4.5\mu\text{m}$ as measured by *Spitzer* suggests a transient source of infrared opacity in the atmosphere. Demory et al. (2015) propose volcanic plumes as one possible source; such plumes would raise the effective emitting altitude (unity optical depth) of the planet's atmosphere to where the temperature and infrared emission are lower, thus decreasing the depth of the secondary eclipse. Likewise, Tamburo et al. (2018) propose volcanic clouds of alumina, olivine, and pyroxene grains to explain variations in the scattered light from the planet detected in the optical. Sulis et al. (2019) limit the planet's geometric albedo to 0.47 (2σ), but this does not rule out atmospheres with clouds of mineral grains (e.g., Mayorga et al., 2019). A circumstellar dust torus similar to the one in the Io-Jupiter system could be an alternate source of the observed variable IR opacity (Demory et al., 2015). Observations of the primary transit in both the optical (Sulis et al., 2019) and infrared ($4.5\mu\text{m}$ band of *Spitzer*, Demory et al., 2015; Tamburo et al., 2018). show no significant variability, e.g. by volcanic plumes or a dust torus. Modulations in the host star's brightness in the far-ultraviolet have been detected (Bourrier et al., 2018b). 55 Cnc e may be close enough to its host star for magnetic interactions to occur, exerting influence on the stellar wind and causing a starspot that rotates with the planet over its 18-hr period (Winn et al., 2011; Sulis et al., 2019; Folsom et al., 2020). Bourrier et al. (2018a) propose that this interaction could result in a coronal rain of cooler gas, similar to what is observed in the Sun, and could explain the observed UV flux modulation.

6. Dynamics and Stability of Magma Oceans

6.1. Vertical Stability

Magma oceans that are cool globally or locally will eventually crystallize, and the (negative) buoyancy of the mineral grains with respect to the surrounding melt and the melt with respect to the underlying mantle at ambient conditions are important but poorly understood factors controlling the evolution and stability of magma oceans (Caracas et al., 2019). Buoyant minerals will tend to float to the surface of a magma ocean on a timescale governed by the melt viscosity and vigor of convection (Solomatov, 2015). Denser minerals will tend to sink and accumulate at the base of the ocean, where they could penetrate the solid mantle if there is sufficient density contrast. Where surface temperatures are sufficiently high, more volatile elements in the melt will evaporate, and can be either lost to space or condense at cooler regions of the planet's surface. These processes of physical segregation will drive chemical evolution in the melt, which in turn will influence any further crystallization and the fate of those grains. Independently, the effect of pressure at depth on the density of solids and liquids, described by equations of state (EOS), mean that both the mass of the planet and the depth of the ocean play important roles in the dynamics.

At low pressures, most solids are denser than their par-

ent liquids (with a few exceptions such as water ice, plagioclase in a silicate melt, and graphite in a reducing melt) and thus crystals will tend to sink. However, liquids tend to be more compressible than solid phases because the atoms in the former are mobile. This means at a sufficiently high pressure (or depth) the solids that are crystallizing from a liquid will be less dense, and will rise to a level where they attain neutral buoyancy (the *cross-over depth*). The difference in compressibility between liquids and solids arises from the difference in the coordination numbers of cations in liquids vs. crystalline solids. In silicates, this coordination number quantifies the number of cation-anion polyhedra in silicates and the degree of packing of the atoms; for a given composition, the higher the average coordination number, the greater the density. In liquids the average coordination number of cations (a continuous distribution) is typically slightly lower than its solid counterpart, which is why the liquid is less dense. The average coordination number increases continuously with pressure in a liquid (Solomatova and Caracas, 2019), whereas the cations in solid counterparts do not change their coordination numbers unless a phase transition occurs, and thus the liquid eventually becomes denser.

For example, in the single giant impact scenario of lunar formation, the Earth's mantle could have been completely molten to the core-mantle boundary at a pressure of 130 GPa (Solomatova and Caracas, 2019). Below a cross-over pressure depth of 115 GPa, the liquid melt is denser than the first crystallizing solids, i.e. bridgmanite, and crystals formed at that depth would be buoyant. All else being equal, on lower mass planets crystallization will produce a cumulate "pile" at the base of the magma ocean. In a deep enough magma ocean on a sufficiently massive planet, the cross-over depth occurs within the magma column, crystals accumulate in a layer at that depth, and physically separated and chemically distinct upper and lower magma oceans can form (Fig. 7). The lower ocean could become denser than any underlying mantle and leading to turnover and migration to the core-mantle boundary. This phenomenon motivated the hypothesis of a basal magma ocean in Earth (Labrosse et al., 2007)

As crystallization proceeds, the composition of the residual melt and hence the density evolves. In magma oceans with a Mg-Fe-silicate (mafic) composition, cooling and crystallization will first produce Mg-rich minerals with higher melting points, e.g. forsterite and enstatite. Thus the iron content of the residual melt increases and the density also increases due to the higher atomic weight of Fe compared to Mg. In the case of Earth, as bridgmanite forms, the increasing density of the melt causes the cross-over depth to occur at lower pressure (shallower), reaching 50 GPa when the magma ocean is 50% crystallized, at which point viscosity rises and convection slows dramatically (Caracas et al., 2019). Even in the absence of pressure effects, the late-crystallizing, iron-rich cumulates themselves may be denser than the underlying mantle, triggering overturn (Miyazaki and Korenaga, 2019). Overturn of ilmenite (FeTiO₃-bearing cumulates) is a well-studied scenario to explain mare volcanism on the Moon (Li et al., 2019; Yu et al., 2019; Zhao et al.,

2019).

Magma ocean chemistry can also evolve due to evaporation (Schaefer and Fegley, 2009; Perez-Becker and Chiang, 2013; Kite et al., 2016). This is the case when surface temperature exceed 2000 K, e.g., for exoplanets like CoRoT 7-b or 55 Cnc e on very close orbits around solar-type host stars (Sec. 5.3). In the case of planets with tenuous atmospheres, evaporates can condense at cooler regions, i.e. the poles or, in the case of tidally-locked planets, near the day-night boundary or terminator (Fig. 1), influencing the surface chemistry there. The vapor can also escape to space from small planets with low gravity, causing permanent changes in the composition of the magma ocean. "Evaporating planets" – highly periodic occultation of stars by dust tails from small, undetected planets on ultra-short period orbits – are evidence for a process of simultaneous evaporation and dust condensation (Rappaport et al., 2012; Sanchis-Ojeda et al., 2015).

Kite et al. (2016) explored the consequences of evaporation on the physical and chemical evolution of a magma ocean or "lava pond" centered at the sub-stellar point on a tidally-locked planet. The evaporation from a silicate melt proceeds from most to least volatile: Na > K > Fe > (Si, Mg) > Ca > Al. Since Na and K have a comparatively low atomic weight, their loss will increase the density of the residual melt, at least in a chemical boundary layer at the surface, which will eventually mix into the magma column. In steady-state, there is compensatory melting of the silicate mantle at the base of the magma ocean which dilutes this enrichment. As evaporation proceeds, the elimination of Fe lowers the density of the boundary layer and could stabilize it as a "lag". The appearance of lags depends on the substellar temperature and Fe content of the mantle and is a potential observable that could be used to constrain planet composition (Kite et al., 2016). Composition might also be inferred by probing the mineralogy of the dust grains that condense in an escaping silicate vapor atmosphere (Bodman et al., 2018a).

More complex situations could include both crystallization, which increases the Fe content and density of the melt, and evaporation, which could either increase or decrease the density, with the relative importance of these two effects depending on the mass (surface gravity) and equilibrium temperature of the planet. Evaporation will dominate on smaller, hotter planets and crystallization will dominate on cooler, more massive planets (Fig. 8).

6.2. Effect of Rotation

The rotation of the planet can also affect the behavior of a magma ocean via its effect on circulation and overturn (Maas and Hansen, 2019). Vigorous convection of a crystallizing magma ocean stirs the minerals grains and distributes them throughout the magma ocean, homogenizing the crystallization process. On a rotating planet, the Coriolis acceleration tends to suppress meridional (north-south) flow (Sec. 2.2) and three-dimensional flow patterns tend to become more two-dimensional (vertical and equatorial) and there is less mixing between latitudes. The effect is larger on planets with

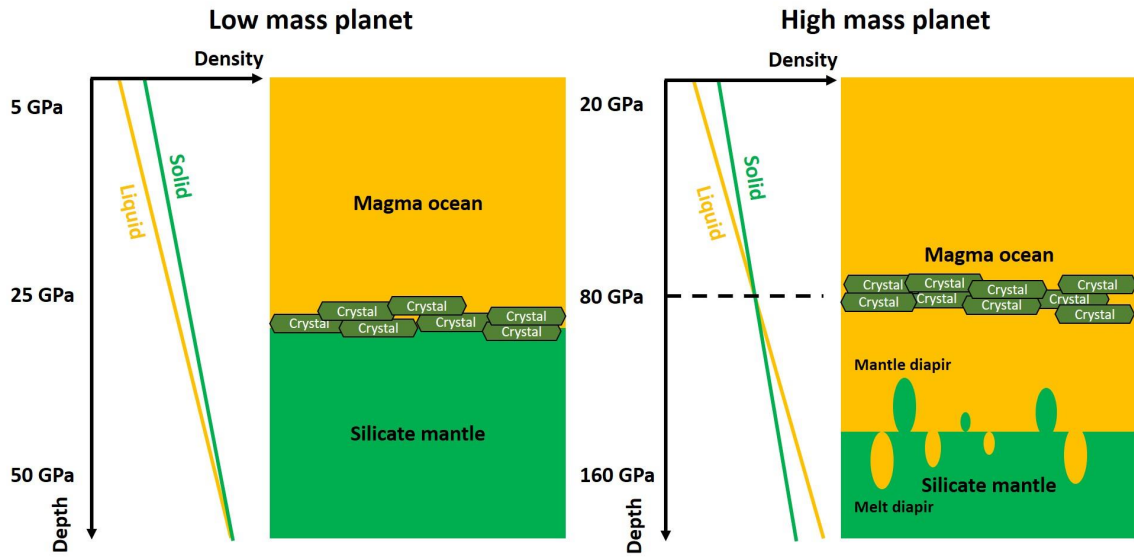


Figure 7: Difference in magma ocean behavior on a low mass planet with low gravity (left) and a high mass planet with high gravity (right). In the former, the magma ocean is shallower than the cross-over depth where the liquid phase has a density equal to the crystallizing solids, and crystals accumulate at the base of the ocean. In the latter, the cross-over depth is within the magma ocean column, the ocean bifurcates, and the lower ocean can become denser than the underlying mantle and destabilize.

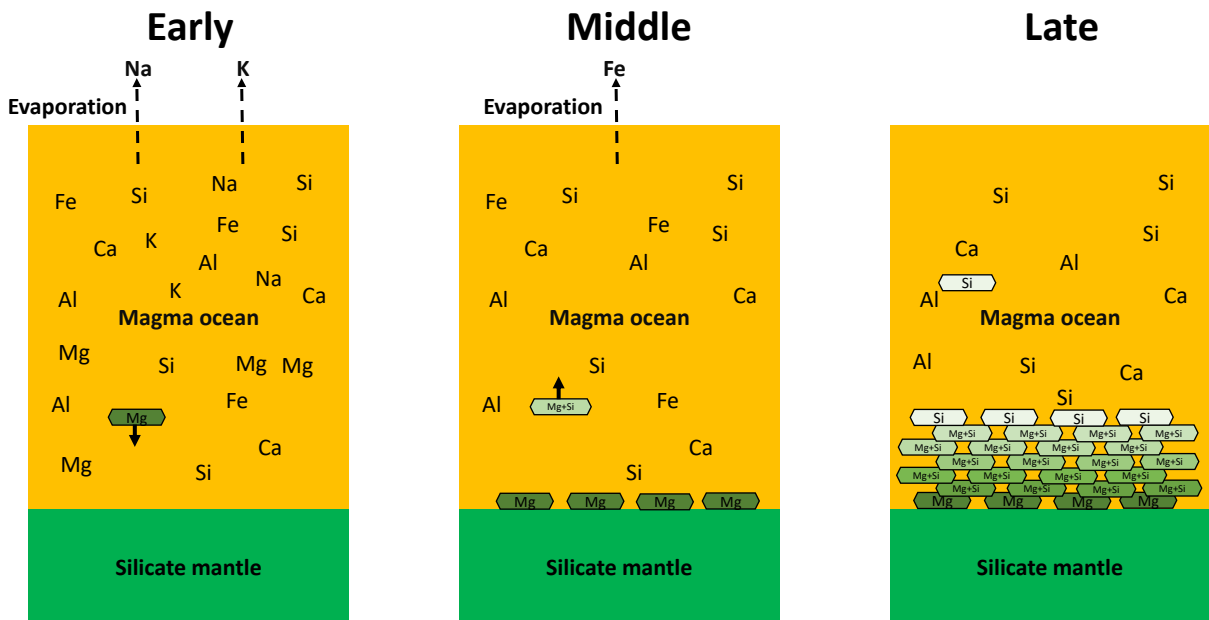


Figure 8: Possible stages in the evolution of a magma ocean experiencing chemical evolution due to both crystallization and evaporation. Left: At lower temperatures or early stages of magma ocean evaporation/crystallization, volatile Na and K evaporate and refractory Mg-rich minerals crystallize and sink, both increasing the relative Fe content and density of the melt. Middle: The progressive evolution of the melt eventually causes later crystallizing to be buoyant. At higher temperatures Fe is volatile and evaporates, and the density of the melt decreases. Right: At late stages, crystallizing Si-rich minerals tend to be neutrally or slightly negatively buoyant in the Fe-poor but Ca- and Al-rich melt. The timescales for crystallization and evaporation need not be comparable and the order of stages could be reversed.

a smaller global Rossby number Ro (faster rotation). Since the *local* Rossby number $\propto 1/\sin\theta$ (Eqn. 12), the effects of rotation are negligible at the equator but can become important towards the poles.

Suppression of circulation will have two major effects. First, on synchronously-rotating planets with thin atmospheres, circulation from the substellar point towards the terminator will be suppressed towards the poles. This will not affect the extent of the magma ocean, since heat transport by a circulating magma ocean is small compared to the radiation terms in the surface energy balance equation (Eqn. 13) (Kite et al., 2016), but will allow different latitudes to become chemically segregated. Second, at higher latitude the vigor of convection will decrease and settling of mineral grains will increase, leading to meridional gradients in the chemistry of the melt (Maas and Hansen, 2019).

6.3. Interaction with the Mantle

In most scenarios the silicate portion of a planet is not completely melted and the magma ocean is in contact with a solid silicate mantle, usually below, or in the case of a basal magma ocean, above. Both the magma ocean and the mantle will be convecting – the latter by solid-state (sub-solidus) convection. Nearly all previous work has assumed that convection in these layers is self-contained and independent, but in this case the boundary between the magma ocean and the mantle is a phase-change boundary, with a comparatively small change in density, rather than a compositional boundary with a large density contrast like the core-mantle boundary. Material can cross this boundary provided the necessary latent heat of crystallization is released or absorbed (Labrosse et al., 2018). Agrusta et al. (2020) showed that the presence of a magma ocean can significantly enhanced convective heat transport in the underlying solid mantle, especially in case where a solid layer is sandwiched between upper and lower (basal) magma oceans. This essentially means the entire mantle contributes to the thermal budget of a magma ocean, which could greatly increase its longevity against complete crystallization (Agrusta et al., 2020). Such a scenario for delayed crystallization has been used to estimate the lifetime of the lunar magma ocean and to infer the Moon’s formation time (Maurice et al., 2020).

In the extreme case a density inversion could develop as a result of, e.g., partial crystallization and enrichment of Fe in the residual liquid, leading to a Rayleigh-Taylor instability and, eventually, overturn and the development of downward-propagating diapirs. Overturn could be continuous and gradual (Boukaré et al., 2018) or large-scale and catastrophic (Elkins-Tanton et al., 2003). The process could become self-sustaining as a result of the gravitational energy released during the overturn event. This can lead to the formation of a basal magma ocean.

A basal magma ocean could also affect heat transport in the metallic core of a planet, particularly as it crystallizes. The latent heat released during crystallization of a basal magma ocean would suppress heat loss from the core. Zeff and Williams (2019b), proposed that a impact-generated,

crystallizing magma ocean in the Fe-rich mantle of Mars would be susceptible to sinking to the core-mantle boundary as a result of Fe enrichment. This chemically distinct layer with its supply of latent heat and relatively low thermal conductivity would insulate the core, hindering heat flow, and could explain the cessation of the Martian dynamo early (≈ 4.3 Gyr ago) in the planet’s history (see Sec. 4.3).

7. Atmospheres of Lava Worlds

7.1. The Role of an Atmosphere

Any atmosphere on a lava world can significantly influence the stability, extent and lifetime of the magma ocean (Elkins-Tanton, 2008; Lebrun et al., 2013; Nikolaou et al., 2019), as well as its detectability (Fig. 1). Atmospheres can greatly elevate surface temperatures by the “greenhouse” effect and will transport heat to the night side and/or poles of a planet (Sec. 2.2), causing surface temperatures to be more uniform and enlarging any magma ocean. Atmospheres also provide a reservoir and transport for volatiles that are exchanged with the magma ocean, and since these gaseous species also affect the radiative properties and structure of the atmosphere, e.g., via clouds, complex feedbacks can develop (Olson and Sharp, 2019). These atmospheres will be dynamic (short residence times), and this exchange with the interior could be crucial for their evolution, since often the proximity of the planet to the host star, which causes elevated surface temperatures permissive of a magma ocean, also drives the erosion of an atmosphere by elevated X-ray, UV, and particle fluxes. Finally, an atmosphere can prevent direct observations of the surface and any magma ocean; thus it is through an interpretation of observations of the intermediary atmosphere that the existence and properties of a magma ocean might have to be established.

Most of our understanding of planetary atmospheres is based on studies of the present Solar System or, by chemical inference and modeling, the early Solar System, with Mercury (possessing only a sputter-produced, low-density exosphere) and Venus (with a thick CO_2 -dominated atmosphere) serving as two useful end-member analogs (Fig. 1). The theory for many of the underlying physical and chemical processes, including the greenhouse effect (Ekholm, 1901; Ingersoll, 1969; Komabayasi, 1967) have been derived from studies of Earth’s atmosphere and oceans as applied to the rest of the Solar System. However, the diversity of rocky planet atmospheres is undoubtedly far greater than is represented by the inner Solar System, with H/He rich atmospheres (Tian et al., 2005; Pierrehumbert and Gaidos, 2011; Ramirez and Kaltenegger, 2017), and more reducing CO and CH_4 -rich atmospheres as plausible scenarios (Rimmer and Rugheimer, 2019; Zilinskas et al., 2020). Also unrepresented are more “exotic” phenomena such electromagnetic interactions (Castan and Menou, 2011; Pu and Valencia, 2017; Kislyakova et al., 2018) for which we have only theory and laboratory experiments. Here, we restrict our consideration to plausible primordial or proto-atmospheres that could have co-existed with early magma-oceans, including those pro-

posed for the early Solar System (Massol et al., 2016), the processes that drove evolution of those atmospheres, and two possible end-states: the complete loss of an atmosphere as on Mercury, and a thick high-molecular weight greenhouse atmosphere such as on Venus.

7.2. Primordial Atmospheres

Due to the release of gravitational energy (Sec. 2.1), the latter stages of the accretion of an Earth-sized planet will be highly energetic (Eqn. 1), and accompanied by melting and intense shocking which will drive volatiles such as H_2O and carbon-bearing molecules (e.g., CO , CO_2 , CH_4) into an atmosphere (Abe and Matsui, 1988; Schaefer and Fegley, 2007, 2017). In the canonical picture of rocky planet formation, accretion proceeds with successively larger bodies (Morbidelli et al., 2012); for Earth these included the Moon-forming impactor or impactors (see Sec. 4.1). For Earth, at least, the abundance of highly siderophilic elements in the mantle are evidence for the accretion of a “late veneer” consisting of a comparatively small amount of chondritic-like material after the giant impact and magma ocean phase. This may have been responsible for a significant fraction of the volatile inventory, including water, at Earth’s surface (Albarede, 2009; Peron et al., 2017). The composition of the atmosphere will depend greatly on the oxidation state of mantle silicates and a magma ocean; this in turn will depend on the composition of the progenitor planetesimals but also on pressure effects in the mantle: in the deep mantle of Earth-sized planets, charge disproportionation of Fe^{2+} into (metallic) Fe^0 and Fe^{3+} and migration of the former to the core will lead to a more oxidized mantle (see Sec. 4.8) and thus a more oxidized primordial atmosphere rich in H_2O , CO_2 , and N_2 . A late veneer of unaltered planetesimals, however, could drive atmospheric chemistry towards a more reducing state (Zahnle et al., 2020).

Some volatiles, particularly H_2O , are highly soluble in silicate magma and thus the surface pressure of a steam atmosphere will be set by the total H_2O inventory and its solubility in the magma. With an optically thick atmosphere the surface temperature is related to the surface pressure via the adiabatic gradient; since a magma ocean will exist only if the surface temperature exceeds ≈ 1300 K, this produces a stabilizing feedback that will tend to maintain the surface inventory of water (as steam) at the level required to maintain a magma ocean, e.g. about 300 bars (or one terrestrial ocean) in the case of Earth (Matsui and Abe, 1986; Zahnle et al., 2007). A substantial CO_2 atmosphere suppresses magma crystallization and outgassing of H_2O , allowing a planet to retain more water, long term, in its interior (Bower et al., 2019).

Earth-mass planets can also accrete H/He-rich gas directly from a planet-forming circumstellar disk (e.g., Lee and Chiang, 2015), and the mass of the envelope will increase with planet mass. The radius distribution of *Kepler* planets is indirect evidence that rocky planets often capture (and sometimes lose) a H/He envelope that contributes substantially to their radius but only a few percent to their mass (Fulton et al.,

2017). A molecular hydrogen-rich atmosphere can produce significant surface warming by collision-induced absorption in the infrared (Pierrehumbert and Gaidos, 2011) and will buffer the magma ocean to reducing conditions (Olson and Sharp, 2019). However, the light elements H and He are expected to readily escape as the upper atmosphere is heated by X-ray and UV radiation from the central star (Owen, 2019). The less massive the body, the less H/He accreted and the shorter the lifetime of such an atmosphere (Ikoma and Hori, 2012). On the other hand, Kite et al. (2019) showed that a sufficiently thick H/He atmosphere can maintain a magma ocean on a rocky planet, into which that atmosphere can dissolve: this could limit the radii of “sub-Neptune” planets discovered by *Kepler*.

A primordial atmosphere and an underlying magma ocean can be sustained by continued impact input of energy and volatiles, depending on the irradiance from the host star. Planets sufficiently close to the star can maintain their magma oceans almost indefinitely (Hamano et al., 2015), even if they lose their primordial H/He, as long as it retain a sufficient inventory of volatiles (chiefly H_2O and CO_2) to constitute a thick greenhouse atmosphere, i.e. the planet is sufficiently massive and/or far enough away from the star. Planets that are somewhat closer will lose this atmosphere (see below) and the magma ocean will crystallize. Planets that are very close-in, e.g. the USPs (Sec. 5.2.1) can maintain a magma ocean without the benefit of a greenhouse atmosphere. Figure 9 illustrates the dependence of magma ocean evolution based on stellar irradiance and water content.

7.3. Evolution of Atmospheres on Lava Worlds

Atmospheres will evolve by any continued accretion of residual planetesimals, escape of light elements to space, exchange with the interior, including any surface or near-surface magma ocean, and irradiance, including photochemically active UV irradiance, by the central star (Fig. 3). This evolution may be regulated or destabilized by negative or positive feedbacks, e.g. the solubility of a steam greenhouse atmosphere in molten silicates (Matsui and Abe, 1986; Abe and Matsui, 1988).

The presence of highly siderophilic elements in Earth’s mantle indubitably supports accretion of a “late veneer” of chondritic-like planetesimals after crystallization of the magma ocean effectively segregated Earth’s core and mantle but the exact timing of this input, its relation to both the “Late Heavy Bombardment” recorded by large lunar impact basins and to the handful of known early Archean impact structures, and the causative dynamic, e.g., migration of the outer giant planets, are areas of active research (Bottke and Norman, 2017; Lowe and Byerly, 2018; Mojzsis et al., 2019). Presumably many planetary systems experience such episodes, depending sensitively on their specific orbital geometry. While impacts can erode an Earth-like atmosphere, recent three-dimensional calculations by Kegerreis et al. (2020) suggest that, for Earth-mass planets, atmospheric erosion is efficient only for those impacts approaching the scale of the Moon-forming event. This is also predicted by new scaling laws

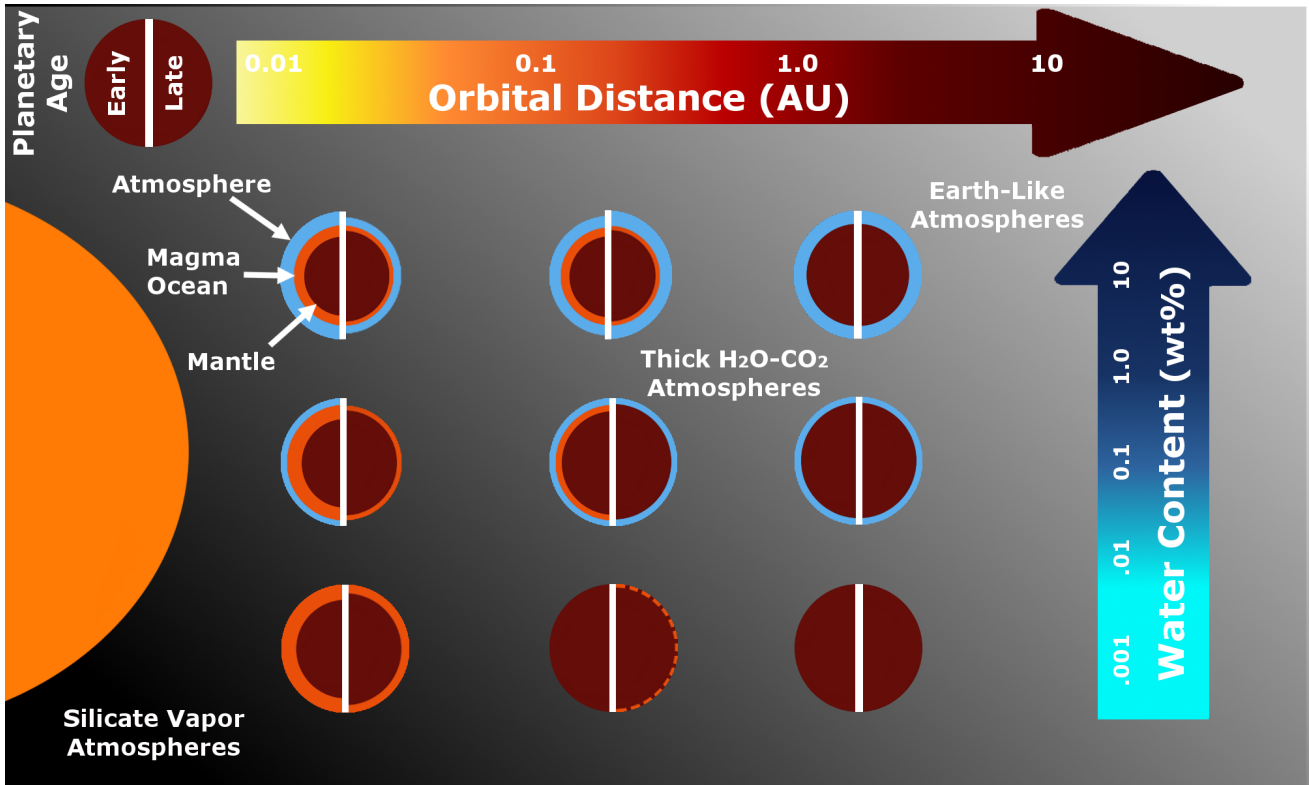


Figure 9: Different scenarios for the appearance and evolution of magma oceans on rocky planets depending on orbital distance and initial water content (which also is a proxy for other volatiles). Each circle represents a planet in its early (proto-atmosphere but post-accretionary magma ocean) and late (Gyr) phases (left and right, respectively). The orange component represents the magma ocean and the blue component represents the atmosphere. The background represents zones where the outcomes are silicate vapor atmospheres (lower left), Venus-like steam-CO₂ atmospheres (middle) and Earth-like atmospheres (upper right). Ultra-short period planets (left column) will experience massive loss of volatiles via atmospheric escape; only very volatile-rich planets might retain any atmosphere. Magma oceans will be widespread on such planets, depending on the luminosity of the host star. Planets on short-period orbits (middle column) will experience a runaway greenhouse and moderate loss of volatiles; magma oceans will appear only if the greenhouse effect is sufficiently strong, or late when the star is evolving into a luminous giant, the planet is tidally locked, and has no atmosphere (bottom scenario). Gradual crystallization of such magma oceans will expel volatiles into atmospheres. Temperate planets (right column) will have no long-term magma oceans nor experience significant atmospheric escape or a runaway greenhouse. A moderate volatile content can form an “Earth-like” atmosphere.

derived by Denman et al. (2020) from numerical smooth particle hydrodynamics experiments. Nonetheless, this process could be much more important for H/He-rich atmospheres (Biersteker and Schlichting, 2019).

Light elements can escape to space from Earth-mass planets with upper atmospheres heated by X-ray and UV radiation from the host star (Catling and Kasting, 2017; Owen, 2019). An important figure of merit for such a mode of escape is the Jean’s parameter, which is the ratio of the gravitational to thermal energy of atoms or molecules at an altitude h where the mean free path between collisions becomes comparable to the atmospheric scale height (the exobase),

$$\Lambda = \frac{GM_p \mu}{(R_p + h)k_B T}, \quad (20)$$

where k_B is the Boltzmann constant, and μ the atomic weight of the atom or molecule considered. Due to gravitational settling and condensation, only light atomic species are present at these altitudes and only ionizing X-ray and UV (XUV) ra-

diation with wavelength $\lambda < 91.2$ nm from the star can be absorbed. Nevertheless, inefficient cooling allows temperatures to reach many 1000s of K. If $\Lambda > 3$ molecular escape occurs. In hot, extended atmospheres of light elements, i.e. H and He, $\Lambda \lesssim 2$ and escape occurs as a hydrodynamic flow (Volkov et al., 2011). Such a flow can drag heavier C, N, and O atoms into space (Catling and Zahnle, 2009).

Hydrogen contained in molecular form, principally the H₂O of a steam atmosphere and oceans, but also less abundant constituents such as CH₄ and HCN can be lost by UV photodissociation and diffusive and turbulent transport to the exobase where it can escape. This is the standard explanation for the loss of any initial water inventory on Venus, and similar processes may be widespread among rocky planets close to young stars (Tian et al., 2018). Due to the intense greenhouse effect, a thick H₂O-dominated atmosphere on a planet that is irradiated at a level exceeding modern Venus can maintain a magma ocean for significantly longer than on a planet further out. One consequence of this long-lived

atmosphere is the loss of water by photodissociation and H escape, which can ultimately lead to lower surface temperatures and crystallization of the magma ocean (Hamano et al., 2013).

A major question concerns the fate of the oxygen produced by the photodissociation of H₂O and escape of H and whether O₂ will accumulate in the atmosphere (Tian, 2015; Luger and Barnes, 2015). In isolation from the interior, an atmosphere will become more oxidizing, e.g. any CO or CH₄ replaced by CO₂, as has been proposed for the Archean Earth (Catling et al., 2001; Zahnle et al., 2013). This process could ultimately lead to the accumulation of significant O₂ – considered an important biosignature – and potential “false positives” for biosignatures (Luger and Barnes, 2015) (see discussion by Meadows Meadows, 2017). This is distinct from photodissociation of CO₂ (see Sec. 7.4.1). Free oxygen will react with any reducing elements like ferrous Fe on the surface, and especially throughout a rapidly convecting magma ocean (Schaefer et al., 2016; Wordsworth et al., 2018). This oxygen can also react with impact ejecta during any tail-end of the accretionary phase of rocky planets (Kurosawa, 2015). Massive water loss may occur on highly irradiated planets close to active stars (Johnstone, 2020); at such high XUV irradiance, ionization of both H and O strongly couples the species and leads to efficient loss of O along with H (Guo, 2019; Johnstone, 2020). Quantifying the evolution of XUV radiation from stellar hosts over timescales of Myr to Gyr is crucial to understanding these processes (Tu et al., 2015).

Non-thermal escape mechanisms can play an equal or even larger role in the removal of atmospheres from planets on close-in orbits, particularly in removing heavier atoms of C, N, and O. The rates of escape depend on the behavior of the star and the interaction with the planet and any magnetic field, as well as XUV heating of the upper atmosphere, which determines its vertical structure. The kinetic energy imparted to the atom is variously derived from recombination after photoionization or even photodissociation (Shematovich and Marov, 2018; Howe et al., 2020), collisions with ions from star or planet planetary ions accelerated by the magnetic field in the stellar wind (Lundin et al., 2007), or electromagnetic interactions with the stellar wind (Catling and Kasting, 2017). The foundations of a better understanding of these phenomena is being laid with statistical determinations of flaring rates of stars with a range of spectral type and rotation rates/ages. However, in the case of solar-type host stars of magma ocean planets, flares have low contrast with respect to the stellar photosphere and even the most sensitive space-based surveys can only detect the largest events. For example, the average energy of flares detected in *Kepler* data is ≈ 400 times the *maximum* observed on the Sun. On dimmer M dwarf stars the higher contrast allows detection by ground- and space-based surveys (Rodríguez Martínez et al., 2020; Günther et al., 2020). Detection of coronal mass ejections, e.g. by spectroscopy, is even more challenging and remains frontier work (Leitzinger et al., 2020; Odert et al., 2020).

It is also important to place this activity within a temporal context, since elevated activity when stars are younger and more rapidly rotating could mean that most non-thermal mass escape occurs then as well. Here the all-sky photometry obtained by the *TESS* mission of stars with a range of established ages will contribute (Feinstein et al., 2020). Also just as important but uncertain is how the planet’s magnetic field, if any, will influence this escape, since it can have opposing roles of concentrating stellar wind particles onto an atmosphere while simultaneously reducing the kinetic energy per particle (Blackman and Tarduno, 2018). Nonetheless, extensive modeling efforts have been made in order to quantify atmospheric escape as a function of different parameters such XUV emission (e.g., Rodríguez-Mozos and Moya, 2019).

Broadly speaking, it is expected that less massive planets on closer orbits will be less likely to retain a significant atmosphere, but the boundaries are unclear and the extent to which the interior will out-gas is important (Kite and Barnett, 2020). Olson and Sharp (2019) predict that a planet less massive than 0.5 M_⊕ will lose most of its atmosphere in ~ 100 Myr.

7.4. End-State Atmospheres

7.4.1. Thick H₂O-CO₂ Atmospheres

Thick, Venus-like atmospheres of CO₂ and variable amounts of H₂O are the outcome on planets with significant volatile content and that are sufficiently massive, distant, and/or have a magnetic field which can protect against significant erosion such that the atmosphere is largely retained over Gyr (Fig. 9. Surface temperatures on Venus (740K) are well below the solidus of an Earth-like mantle, but Venus may have maintained a magma ocean for a significant amount of time (Chassefière et al., 2012). If Venus was significantly closer to the Sun, had a thicker or wetter atmosphere, and/or a lower albedo it could sustain a global magma ocean indefinitely (Hamano et al., 2015). Assuming a modified adiabatic profile that accounts for changes in the gas properties with temperature, the surface temperature T_s for a given surface pressure P_s will be

$$T_s \approx T_{\text{eq}} \left(P_s / P_{\text{rc}} \right)^{\zeta \frac{\gamma-1}{\gamma}}, \quad (21)$$

where for a Venus-like CO₂-dominated atmosphere, the ratio of specific heats $\gamma = 1.3$, $\zeta = 0.78$ (Robinson and Catling, 2012), the pressure at the radiative-convective boundary $P_{\text{rc}} \sim 0.1$ bar (Robinson and Catling, 2014), and the equilibrium heat flux is $230(0.72/a)^2 \text{ W m}^{-2}$. A Venus twin orbiting interior to 0.23 au, or out to about 0.3 au if the atmosphere was thicker or the planet more massive, or had a lower albedo, would have $T_s > 1300$ K. Water would be highly soluble in a magma ocean; CO₂ much less so: at 0.57 wt ppm bar⁻¹ (Ni and Keppler, 2013). Only 1.5% of the mass of Venus’ CO₂ atmosphere would dissolve into a 100 km deep ocean; less if H₂O were also dissolved, displacing CO₂.

CO₂ absorption of UV ($\lambda = 120 - 210$ nm) photons can lead to dissociation: CO₂ \rightarrow CO + O or possibly CO₂ \rightarrow C + O₂ (Lu et al., 2014). The extent to which this could lead to

the buildup of molecular O_2 is debated, since molecular oxygen can react with ferrous iron in the surface (in this case, a magma ocean) and lightning in the atmosphere can catalyze the reverse reaction (Harman et al., 2018). However, rates of electrical discharge on Venus – and more broadly in dry, hot atmospheres – are uncertain (Lorenz, 2018; Lorenz et al., 2019). It is possible that while the accumulation of O_2 may be limited, CO can gradually accumulate as the magma ocean and interior are oxidized. (CO is only a trace component in the present Venusian atmosphere). A Venus-like atmosphere enriched in CO, as well as SO_2 , given the expected destabilization of sulfide-bearing minerals known to exist on the surface of Venus higher temperatures (Zolotov, 2019), could be a model for many of the Earth and super-Earth exoplanets discovered on short-period orbits (Sec. 5).

7.4.2. Silicate Vapor Atmospheres

Depending on their mass, planets on very short period orbits could be depleted in volatiles due to their formation close to the parent star (Lissauer, 2007; Lopez, 2017) and/or lose virtually their entire atmosphere through XUV- and particle-driven loss. They would become more Mercury-like, albeit with significantly higher surface temperatures and stellar particle fluxes, depending on the planet's magnetic field. Unlike Mercury, tidal locking is expected to lead to 1:1 synchronous rotation, extreme day-night temperature contrasts, and the presence of a hemispheric magma ocean at the surface (Fig. 1). As temperatures exceed 2000 K, the vapor pressure of more volatile constituents of silicate mantles / magma oceans, i.e. Na and K, along with O for valence balance, become appreciable, forming a tenuous atmosphere (Schaefer and Fegley, 2009) (Fig. 10). With increasing temperature, more refractory elements contribute to this atmosphere: Fe, Si, Mg, and lastly Al and Ca when the temperature approaches 3000 K (Fig. 10). The gradient in vapor pressure from the sub-stellar point towards the terminator will drive a thermal wind, with atoms being deposited at the margins of the magma ocean or possibly near the terminator (Schaefer and Fegley, 2009; Kite et al., 2016) (Fig. 1). This wind can be partially ionized and to the extent it is collisional, will be affected by any planetary magnetic field (Castan and Menou, 2011) or potential removal by the electric and magnetic fields of the stellar wind. If the removal of elements is more efficient from mixing of the magma ocean due to the gradient in temperature than a chemical residual layer or "lag" can develop, which can be less or more dense depending on the stage of evaporation, i.e. the atomic mass of the evaporated constituents. Depending on the FeO content of the mantle, evaporation of lighter Na and K produces a heavier, unstable lag, while evaporation of heavier Fe (at a later stage) produces a stable lag (Kite et al., 2016).

In the extreme cases, vaporization of a highly irradiated planet and loss of the vapor or dust condensates to space could significantly erode the planet. The dusty cometary winds of such evaporating planets will obscure the star if the planet is on a transiting orbit and candidate systems have been identified, including Kepler-1520b (Rappaport et al.,

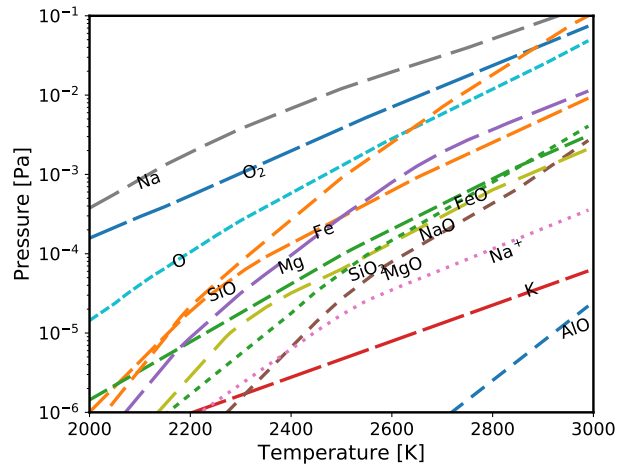


Figure 10: Approximate vapor pressure of constituents of a rock vapor atmosphere at 2000–3000 K in equilibrium with a surface with the bulk composition of Earth's mantle. Based on Schaefer and Fegley (2009) with some extrapolation. The dominant species in such an atmosphere are Na, O_2 , and, at the highest temperature, Fe.

2012), K2-22b (Sanchis-Ojeda et al., 2015), and HD 240779 (Gaidos et al., 2019b). Vaporization reduces the mass and the surface gravity, which in turn allows vaporization to proceed more quickly, leading to the potential runaway evaporation of the entire planet (Perez-Becker and Chiang, 2013). However, the process could potentially self-arrest if a buoyant, refractory (i.e. Mg, Ca, Al-rich) magma ocean and crust were to develop that does not mix with the interior. These dust tails, back-lit by the star, provide a means of probing the interior composition of such objects that would otherwise not be accessible (Budaj et al., 2015; van Lieshout et al., 2016; Gaidos et al., 2019a).

8. Summary and Future Directions

8.1. Significant Advances

While evidence for past magma oceans in the Solar System has been accumulating for the past half century, beginning with the analysis of Apollo 11 samples, it is only in the last decade that a magma ocean as a near-universal phase of early rocky planet evolution has become both widely appreciated and investigated. With the detection of rocky planets on short-period orbits around other stars it has also become more likely that we can study *extant* magma oceans directly, albeit from a great distance. Arguably the most significant advance in the realm of Solar System exploration was the *Dawn* mission to Vesta, which greatly strengthened the connection between the asteroid and the HED meteorite suite which are products of magma ocean crystallization (McSween Jr et al., 2013). A preliminary understanding of Vesta's interior structure was provided by measurements of its gravity field; more might be learned once any remnant magnetic field, like that suggested by the HED meteorites (Fu et al., 2012), is measured. Measurements of Mercury and Mars

have provided intriguing but indirect evidence for magma oceans. For the time being, evidence for Earth's possible magma ocean phase will be restricted to improving measurements of the isotopic composition of the mantle relative to the hypothetical Earth-forming reservoir. Venus will remain an enigma until surface exploration is resumed.

Space-based photometry has ushered in an era of detection via transits of Earth-size planets around other stars; the limited Doppler RV measurements of mass that have been possible thus far indicate rocky-metal compositions similar to Earth. Due to detection bias, known planets tend to be on short-period orbits of a few days or less, and equilibrium temperatures exceeding the solidus raise the prospect of observable, stable magma oceans. Transits of three well-characterized examples (CoRoT-7b, 55 Cnc e, and Kepler-78b) were detected by three different missions: *CoRoT*, *MOST*, and *Kepler* and have been the most extensively characterized in terms of mass, equilibrium temperature, and the presence or absence of an atmosphere. Nevertheless, the limited accuracy and degeneracy of interpretation of some measurements, particularly mass, leave room for substantial controversy such as composition of the interior and the presence or absence of an atmosphere, (e.g., Dai et al., 2019).

8.2. Major Outstanding Questions and Key Needs

Our understanding of the behavior of lavas/magma on Earth, elsewhere in the Solar System, or on ultra-short period planets around other stars is only as good as our knowledge of the rheologic and thermodynamic properties of those materials. Properties can be determined by laboratory measurements (e.g., Hofmeister et al., 2016; Heap et al., 2020), empirical fits to data collected in the field (e.g., Castruccio et al., 2013), or, more rarely, direct measurement in the field (e.g., Chevrel et al., 2018). Volatiles play a key role in determining lava lake behavior, and our knowledge of volatile solubility, speciation, and diffusivity have come in large part from experiments (e.g., Wallace et al., 2015; Ni and Zhang, 2018; Zhang et al., 2010). More data are needed, particularly for compositions that radically deviate from the calc-alkaline compositions of the terrestrial trend between basalt and rhyolite. For example, Léger et al. (2011) predicted an eventual magma ocean composition of mixed CaO-Al₂O₃ on CoRoT-7b. Recent studies by Morrison et al. (2019) and Sehlke and Whittington (2020) used laboratory measurements to determine the rheology of both primary and impact-induced predicted lunar melts. More data on carbon- and sulfur-rich melts are needed to understand a possible magma ocean and volcanism on Mercury and perhaps planets with analogous, reduced compositions. The exploration of lakes of liquid sulfur in undersea volcanoes (de Ronde et al., 2015) may offer insight into phenomena on Io.

Almost certainly Vesta was *not* the only small body to host a magma ocean in the Main Asteroid Belt, simply perhaps the largest intact survivor. The energetics of planetary accretion seem to have been sufficient to melt and even vaporize a significant mass fraction (Davies et al., 2020). Enrichment of heavy isotopes of Si and Mg in planets with re-

spect to chondritic meteorites has been interpreted as evidence for isotopic fractionation during evaporation from molten planetesimals (Young et al., 2019). There have been several surveys that have identified a few basaltic asteroids that, unlike the "Vestoid" asteroid family, cannot be dynamically linked to Vesta (Lazzaro et al., 2000; Moskovitz et al., 2008; Roig et al., 2008; Oszkiewicz et al., 2017). Finds and falls of unique basaltic as well as the anorthosite-rich meteorites (Bland et al., 2009; Frossard et al., 2019) also hint at additional diversity in similar bodies, obscured, in part, by the effects of space weathering (Yamamoto et al., 2018). Expanded surveys of the asteroid belt, as well as systematic analysis of current and future meteorites collected, e.g. Antarctica, may provide a fuller picture of the diversity of parent bodies that hosted or are fragments of crystallized magma oceans.

8.3. Future Solar System Missions

Several planned or proposed missions to planets and satellites should yield more definitive and detailed information on magma oceans or lava lakes they hosted or host. First in line is *Bepi-Columbo*, due at Mercury (i.e., its first flyby) in October 2021 (Spohn et al., 2001; Schulz and Benkhoff, 2006; Milillo et al., 2010). *Bepi-Columbo* will further the investigation of the composition of the Hermian crust and the planet's magnetic field (Rothery et al., 2020). This includes potentially confirming *Messenger's* tentative detection of carbon by the MIXS X-ray and MGNS γ -ray and neutron spectrometers (Rothery et al., 2020) as a test of the hypothesis that a Hermian magma ocean had a graphite flotation crust (Peplowski et al., 2016). Ultimately, a sample return mission could provide definitive answers to the history of the planet and its putative magma ocean (Vander Kaaden et al., 2019).

Ever since volcanism was detected by Voyager 1, Io has remained a compelling but hazardous target for spacecraft missions, with only limited data from *Galileo* and now *Juno* (Mura et al., 2020). The Io Volcano Observer (IVO) is a proposed mission that would orbit Jupiter and study the satellite via a series of flybys to determine how and where heat is produced by tidal dissipation, and whether Io hosts a subsurface magma ocean via measurements of the induced magnetic field produced by eddy currents, the distribution of heat and volcanism, and its gravity field (McEwen and IVO Science Team, 2020).

Future missions to the Moon include the Chang'e 5 sample return from Mons Rümker, scheduled at the end of 2020 (Zhao et al., 2017), and, possibly, a continuation of the Soviet/Russian *Luna* series in 2021 with the *Luna 25* lander and continuing with planned rovers and sample return from the south pole (Tretyakov et al., 2020). Mons Rümker is a 3.5 Gyr-old basaltic volcanic dome complex which could be informative about late-stage volcanism on the Moon (Zhao et al., 2017). Of course, human return to the Moon would bring with it the opportunity for high volume sampling, although perhaps from a limited region of the surface. And there may be surprises in store "for free" from the curated

Apollo samples that are being released for analysis for the first time⁹.

Sample return from Mars is a long-term goal of the planetary science community (Muirhead et al., 2020), and the first concrete step will be taken with sample caching by the *Perseverance* (Mars 2020) mission to Jezero Crater (Grady et al., 2020). Although the goals of the mission are to search for evidence of past life in the sedimentary deposits around the landing site, any returned samples would ultimately provide counterparts to the Martian meteorites (SNCs) and/or indirect evidence for or constraints on any past magma ocean (e.g., the composition of the mantle). A potential alternative to collecting Martian material would be to return samples from one of Mars' satellites Phobos and Deimos. The *Martian Moons eXploration* (MMX) mission will return samples from Phobos at the end of the 2020s (Kuramoto et al., 2018). If these satellites accreted from an impact generated disk, as has been proposed, they will consist of an admixture of Martian and impactor material (Hyodo et al., 2017; Pignatale et al., 2018) that is far easier to retrieve (but probably much more difficult to interpret) than the crust of Mars itself.

Venus will continue to remain an enigma for some time. There are no approved missions to return to the planet, although many have been proposed or are under current study. Missions to investigate the structure and composition of the atmosphere (Garvin et al., 2020) could reveal whether volcanism still persists, as suspected, while high-resolution radar and gravity surveys will better characterize the planet's interior structure and response to tidal deformation (Widemann et al., 2020) and thus describe the crust which could rule out or possibly detect a basal magma ocean. Sample return from Venus, while obviously desirable, is an enormous technical challenge and is not on the horizon (Sweetser et al., 2003).

8.4. Beyond the Solar System

While we await these Solar System missions, some of the most fruitful observations and ground-breaking discoveries may occur for much more distant objects, i.e. exoplanets. The first of what could be multiple extended missions for the *TESS* satellite has now started. This promises to expand and refine our sample of close-in planets around bright stars (Barclay et al., 2018). The longer baseline and faster 10-minute cadence for the full dataset, which will better resolve short-duration transits, will allow *TESS* to improve the statistics of Earth- to super-Earth-size ultra-short period planets and identify many that are suitable for follow-up.

New RV spectrographs such as ESPRESSO should allow more USPs to be "weighed" with greater precision. Spectrographs such as SPIRou (Donati et al., 2018) and NIRPS (Wildi et al., 2017) which observe at infrared wavelengths are, in principle, less affected by stellar photosphere noise ("jitter" Marchwinski et al., 2015), likely to be the limiting source of noise in many systems. SPIRou and NIRPS also simultaneously measure polarization, which can be used to constrain the strength and configuration of the stellar mag-

netic fields and the positions of active regions, information useful for mitigating jitter. Of particular interest is whether continued population of the mass-radius diagram of USPs (Fig. 6) will uncover denser planets with Mercury-like interiors and massive iron cores like Kepler-974c produced by collisions or segregation of metal and silicates (Scora et al., 2020).¹⁰ This decade will also see "first light" at one or more ≥ 30 m-aperture Extremely Large Telescopes, eventually with instrumentation that can obtain informative spectra of the atmospheres of Earth-size planets during transits (Marconi et al., 2018; Szentgyorgyi et al., 2018; Mawet et al., 2019).

Perhaps the biggest leap forward will be provided by the infrared *JWST*, scheduled for launch in late 2021, which will be able to detect the secondary eclipses and/or measure the phase curve of many hot Earth-size planets and by doing so estimate their equilibrium temperature, albedo and efficacy of heat transport from the day to night sides (Beichman and Greene, 2018). A smaller optical-infrared space telescope (*ARIEL*) dedicated to exoplanet observations should follow several years later (Edwards et al., 2019). Time variability and eclipse mapping of the offset of any hot spot should provide more insight into the circulation of any atmosphere; in the absence of an atmosphere, peak temperatures would be indicative of the presence or absence of a magma ocean. Infrared spectra of the largest/brightest examples could also be used to constrain the mineralogy of any solid surface (Hu et al., 2012). Even with a thick atmosphere obscuring the surface, a magma ocean might reveal itself via the relative solubility of important atmospheric gases and hence their abundance in the atmosphere, e.g. CO, CO₂, and H₂O (Pawley et al., 1992; Wetzel et al., 2013; Armstrong et al., 2015; Yoshioka et al., 2019) as well as H/He (Kite et al., 2019). Over the horizon are the next generation of proposed space observatories like *Origins Space Telescop* (Cooray et al., 2019), *HabEx* (Gaudi et al., 2018b), and *LUVVOIR* (Gaudi et al., 2018a); these offer the greater sensitivity and angular resolution, enhancing our ability to explore lava worlds from afar.

Acknowledgements

R. D. acknowledges fruitful discussions with J. Birnbaum and T. Keller. F. Nimmo, E. Kite, and two anonymous reviewers gave expert and constructive comments on the manuscript.

9. Bibliography

- Abe, Y., Matsui, T., 1988. Evolution of an impact-generated H₂O-CO₂ atmosphere and formation of a hot proto-ocean on Earth. *Journal of the Atmospheric Sciences* 45, 3081–3101.
- Agol, E., Jansen, T., Lacy, B., Robinson, T.D., Meadows, V., 2015. The center of light: spectroastrometric detection of exomoons. *The Astrophysic-*

¹⁰The composition of former short-period planets can be investigated *post mortem* as elemental debris in the atmosphere of the white dwarfs that disrupted them (Doyle et al., 2019).

⁹<https://sservi.nasa.gov/articles/apollo-next-generation-sample-analysis-program/>

- cal Journal 812, 5. URL: <http://dx.doi.org/10.1088/0004-637X/812/1/5>, doi:10.1088/0004-637X/812/1/5.
- Agrusta, R., Morison, A., Labrosse, S., Deguen, R., Alboussière, T., Tackley, P.J., Dubuffet, F., 2020. Mantle convection interacting with magma oceans. *Geophysical Journal International* 220, 1878–1892. doi:10.1093/gji/ggz549.
- Aitta, A., 2012. Venus' internal structure, temperature and core composition. *Icarus* 218, 967–974.
- Aiuppa, A., de Moor, J.M., Arellano, S., Coppola, D., Francofonte, V., Galle, B., Giudice, G., Liuzzo, M., Mendoza, E., Saballos, A., Tamburello, G., Battaglia, A., Bitetto, M., Gurrieri, S., Laiolo, M., Mastrolia, A., Moretti, R., 2018. Tracking Formation of a Lava Lake From Ground and Space: Masaya Volcano (Nicaragua), 2014–2017. *Geochemistry, Geophysics, Geosystems* 19, 496–515. URL: <https://agupubs.onlinelibrary.wiley.com/doi/abs/10.1002/2017GC007227>, doi:10.1002/2017GC007227, arXiv:<https://agupubs.onlinelibrary.wiley.com/doi/pdf/10.1002/2017GC007227>.
- Albarede, F., 2009. Volatile accretion history of the terrestrial planets and dynamic implications. *Nature* 461, 1227–1233.
- Albarède, F., Blichert-Toft, J., 2007. The split fate of the early Earth, Mars, Venus, and Moon. *Comptes Rendus Geoscience* 339, 917–927. doi:10.1016/j.crte.2007.09.006.
- Alonso, R., 2018. Characterization of Exoplanets: Secondary Eclipses, in: Deeg, H.J., Belmonte, J.A. (Eds.), *Handbook of Exoplanets*, p. 40. doi:10.1007/978-3-319-55333-7_40.
- Angelo, I., Hu, R., 2017. A Case for an Atmosphere on Super-Earth 55 Cancri e. *The Astronomical Journal* 154, 232. URL: <https://doi.org/10.3847/1538-3881/aa9278>, doi:10.3847/1538-3881/aa9278.
- Angelo, I., Rowe, J.F., Howell, S.B., Quintana, E.V., Still, M., Mann, A.W., Burningham, B., Barclay, T., Ciardi, D.R., Huber, D., Kane, S.R., 2017. Kepler-1649b: An Exo-Venus in the Solar Neighborhood. *The Astronomical Journal* 153, 162. URL: <https://doi.org/10.3847/1538-3881/aa615f>, doi:10.3847/1538-3881/aa615f.
- Angerhausen, D., DeLarme, E., Morse, J.A., 2015. A Comprehensive Study of Kepler Phase Curves and Secondary Eclipses: Temperatures and Albedos of Confirmed Kepler Giant Planets. *PASP* 127, 1113. doi:10.1086/683797, arXiv:1404.4348.
- Armstrong, K., Frost, D.J., McCammon, C.A., Rubie, D.C., Boffa Ballaran, T., 2019. Deep magma ocean formation set the oxidation state of Earth's mantle. *Science* 365, 903–906. doi:10.1126/science.aax8376.
- Armstrong, L.S., Hirschmann, M.M., Stanley, B.D., Falksen, E.G., Jacobsen, S.D., 2015. Speciation and solubility of reduced C-O-H-N volatiles in mafic melt: Implications for volcanism, atmospheric evolution, and deep volatile cycles in the terrestrial planets. *Geochim. Cosmochim. Acta* 171, 283–302. doi:10.1016/j.gca.2015.07.007.
- Asphaug, E., 2014. Impact Origin of the Moon? *Annual Review of Earth and Planetary Sciences* 42, 551–578. doi:10.1146/annurev-earth-050212-124057.
- Baglin, A., Auvergne, M., Barge, P., Deleuil, M., Catala, C., Michel, E., Weiss, W., COROT Team, 2006. Scientific Objectives for a Minisat: CoRoT, in: Fridlund, M., Baglin, A., Lochard, J., Conroy, L. (Eds.), *The CoRoT Mission Pre-Launch Status - Stellar Seismology and Planet Finding*, p. 33.
- Barclay, T., Pepper, J., Quintana, E.V., 2018. A Revised Exoplanet Yield from the Transiting Exoplanet Survey Satellite (TESS). *The Astrophysical Journal Supplement Series* 239, 2. doi:10.3847/1538-4365/aac3e9, arXiv:1804.05050.
- Barnes, R., Raymond, S.N., Greenberg, R., Jackson, B., Kaib, N.A., 2010. CoRoT-7b: Super-Earth or Super-Io? *ApJ* 709, L95–L98. doi:10.1088/2041-8205/709/2/L95, arXiv:0912.1337.
- Barr, A.C., Dobos, V., Kiss, L.L., 2018. Interior structures and tidal heating in the TRAPPIST-1 planets. *A&A* 613, A37. doi:10.1051/0004-6361/201731992, arXiv:1712.05641.
- Batalha, N.M., Borucki, W.J., Bryson, S.T., Buchhave, L.A., Caldwell, D.A., Christensen-Dalsgaard, J., Ciardi, D., Dunham, E.W., Fressin, F., Gautier, T.N., Gilliland, R.L., Haas, M.R., Howell, S.B., Jenkins, J.M., Kjeldsen, H., Koch, D.G., Latham, D.W., Lissauer, J.J., Marcy, G.W., Rowe, J.F., Sasselov, D.D., Seager, S., Steffen, J.H., Torres, G., Basri, G.S., Brown, T.M., Charbonneau, D., Christiansen, J., Clarke, B., Cochran, W.D., Dupree, A., Fabrycky, D.C., Fischer, D., Ford, E.B., Fortney, J., Girouard, F.R., Hekman, M.J., Johnson, J., Isaacson, H., Klaus, T.C., Machalek, P., Moorehead, A.V., Morehead, R.C., Ragozzine, D., Tenenbaum, P., Twicken, J., Quinn, S., VanCleve, J., Walkowicz, L.M., Welsh, W.F., Devore, E., Gould, A., 2011. Kepler's first rocky planet: Kepler-10b. *The Astrophysical Journal* 729, 27. URL: <https://doi.org/10.1088/2F0004-637X/729/2F27>, doi:10.1088/0004-637X/729/1/27.
- Beichman, C.A., Greene, T.P., 2018. Observing Exoplanets with the James Webb Space Telescope, in: Deeg, H.J., Belmonte, J.A. (Eds.), *Handbook of Exoplanets*, p. 85. doi:10.1007/978-3-319-55333-7_85.
- Belbruno, E., Gott, J. Richard, I., 2005. Where Did the Moon Come From? *AJ* 129, 1724–1745. doi:10.1086/427539, arXiv:astro-ph/0405372.
- Berger, T.A., Huber, D., van Saders, J.L., Gaidos, E., Tayar, J., Kraus, A.L., 2020. The *Gaia-Kepler* Stellar Properties Catalog I: Homogeneous Fundamental Properties for 186,000 *Kepler* Stars. arXiv e-prints, arXiv:2001.07737arXiv:2001.07737.
- Biersteker, J.B., Schlichting, H.E., 2019. Atmospheric mass-loss due to giant impacts: the importance of the thermal component for hydrogen-helium envelopes. *MNRAS* 485, 4454–4463. doi:10.1093/mnr/stz738, arXiv:1809.06810.
- Bindi, L., Shim, S.H., Sharp, T.G., Xie, X., 2020. Evidence for the charge disproportionation of iron in extraterrestrial bridgmanite. *Science Advances* 6. URL: <https://advances.sciencemag.org/content/6/2/eaay7893>, doi:10.1126/sciadv.aay7893, arXiv:<https://advances.sciencemag.org/content/6/2/eaay7893.full.pdf>.
- Binzel, R.P., Xu, S., 1993. Chips off of asteroid 4 Vesta: Evidence for the parent body of basaltic achondrite meteorites. *Science* 260, 186–191.
- Birkby, J.L., 2018. Spectroscopic Direct Detection of Exoplanets, in: Deeg, H.J., Belmonte, J.A. (Eds.), *Handbook of Exoplanets*, p. 16. doi:10.1007/978-3-319-55333-7_16.
- Birnbaum, J., Keller, T., Suckale, J., Lev, E., 2020. "Periodic outgassing as a result of unsteady convection in Ray lava lake, Mount Erebus, Antarctica". *Earth and Planetary Science Letters* 530.
- Blackman, E.G., Tarduno, J.A., 2018. Mass, energy, and momentum capture from stellar winds by magnetized and unmagnetized planets: implications for atmospheric erosion and habitability. *MNRAS* 481, 5146–5155. doi:10.1093/mnr/sty2640, arXiv:1801.00895.
- Bland, P.A., Spurný, P., Towner, M.C., Bevan, A.W.R., Singleton, A.T., Botke, W.F., Greenwood, R.C., Chesley, S.R., Shrubbený, L., Borovička, J., Ceplecha, Z., McClafferty, T.P., Vaughan, D., Benedix, G.K., Deacon, G., Howard, K.T., Franchi, I.A., Hough, R.M., 2009. An Anomalous Basaltic Meteorite from the Innermost Main Belt. *Science* 325, 1525. doi:10.1126/science.1174787.
- Blöcker, A., Saur, J., Roth, L., Strobel, D.F., 2018. MHD Modeling of the Plasma Interaction With Io's Asymmetric Atmosphere. *Journal of Geophysical Research: Space Physics* 123, 9286–9311. URL: <https://agupubs.onlinelibrary.wiley.com/doi/abs/10.1029/2018JA025747>, doi:10.1029/2018JA025747, arXiv:<https://agupubs.onlinelibrary.wiley.com/doi/pdf/10.1029/2018JA025747>.
- Bodman, E., Wright, J., Boyajian, T., Ellis, T., 2018a. The Variable Wavelength Dependence of the Dipping event of KIC 8462852. arXiv e-prints, arXiv:1806.08842arXiv:1806.08842.
- Bodman, E.H.L., Wright, J.T., Desch, S.J., Lisse, C.M., 2018b. Inferring the Composition of Disintegrating Planet Interiors from Dust Tails with Future James Webb Space Telescope Observations. *AJ* 156, 173. doi:10.3847/1538-3881/aadc60, arXiv:1808.07043.
- Boisse, I., Bouchy, F., Hébrard, G., Bonfils, X., Santos, N., Vauclair, S., 2011. Disentangling between stellar activity and planetary signals. *A&A* 528, A4. URL: <https://doi.org/10.1051/0004-6361/201014354>, doi:10.1051/0004-6361/201014354.
- Bonati, I., Lichtenberg, T., Bower, D.J., Timpe, M.L., Quanz, S.P., 2019. Direct imaging of molten protoplanets in nearby young stellar associations. *A&A* 621, A125. doi:10.1051/0004-6361/201833158, arXiv:1811.07411.
- Borg, L.E., Gaffney, A.M., Kruijjer, T.S., Marks, N.A., Sio, C.K., Wimpenny, J., 2019. Isotopic evidence for a young lunar magma ocean. *Earth*

- and Planetary Science Letters 523, 115706. doi:10.1016/j.epsl.2019.07.008.
- Borg, L.E., Nyquist, L.E., Taylor, L.A., Wiesmann, H., Shih, C.Y., 1997. Constraints on Martian differentiation processes from Rb Sr and Sm Nd isotopic analyses of the basaltic shergottite QUE 94201. *Geochimica et Cosmochimica Acta* 61, 4915–4931.
- Bottke, W.F., Norman, M.D., 2017. The Late Heavy Bombardment. *Annual Review of Earth and Planetary Sciences* 45, 619–647. doi:10.1146/annurev-earth-063016-020131.
- Boukaré, C.E., Parmentier, E.M., Parman, S.W., 2018. Timing of mantle overturn during magma ocean solidification. *Earth and Planetary Science Letters* 491, 216–225. doi:10.1016/j.epsl.2018.03.037.
- Bourrier, V., Dumusque, X., Dorn, C., Henry, G.W., Astudillo-Defru, N., Rey, J., Benneke, B., Hébrard, G., Lovis, C., Demory, B.O., et al., 2018a. The 55 Cancri system reassessed. *Astronomy & Astrophysics* 619, A1. URL: <http://dx.doi.org/10.1051/0004-6361/201833154>, doi:10.1051/0004-6361/201833154.
- Bourrier, V., Ehrenreich, D., Lecavelier des Etangs, A., Louden, T., Wheatley, P.J., Wyttenbach, A., Vidal-Madjar, A., Lavie, B., Pepe, F., Udry, S., 2018b. High-energy environment of super-Earth 55 Cancri e. *Astronomy & Astrophysics* 615, A117. URL: <http://dx.doi.org/10.1051/0004-6361/201832700>, doi:10.1051/0004-6361/201832700.
- Bourrier, V., Hébrard, G., 2014. Detecting the spin-orbit misalignment of the super-Earth 55 Cancri e. *Astronomy & Astrophysics* 569, A65. URL: <http://dx.doi.org/10.1051/0004-6361/201424266>, doi:10.1051/0004-6361/201424266.
- Bouvier, L.C., Costa, M.M., Connelly, J.N., Jensen, N.K., Wielandt, D., Storey, M., Nemchin, A.A., Whitehouse, M.J., Snape, J.F., Bellucci, J.J., Moynier, F., Agranier, A., Gueguen, B., Schönbächler, M., Bizzarro, M., 2018. Evidence for extremely rapid magma ocean crystallization and crust formation on Mars. *Nature* 558, 586–589. doi:10.1038/s41586-018-0222-z.
- Bower, D.J., Kitzmann, D., Wolf, A.S., Sanan, P., Dorn, C., Oza, A.V., 2019. Linking the evolution of terrestrial interiors and an early outgassed atmosphere to astrophysical observations. *A&A* 631, A103. doi:10.1051/0004-6361/201935710, arXiv:1904.08300.
- Bowler, B.P., 2016. Imaging Extrasolar Giant Planets. *PASP* 128, 102001. doi:10.1088/1538-3873/128/968/102001, arXiv:1605.02731.
- Boyett, M., Carlson, R.W., 2005. 142Nd evidence for early (> 4.53 Ga) global differentiation of the silicate Earth. *Science* 309, 576–581.
- Bromley, B.C., Kenyon, S.J., 2019. Ohmic Heating of Asteroids around Magnetic Stars. *ApJ* 876, 17. doi:10.3847/1538-4357/ab12e9, arXiv:1903.11533.
- Budaj, J., Kocifaj, M., Salmeron, R., Hubeny, I., 2015. Tables of phase functions, opacities, albedos, equilibrium temperatures, and radiative accelerations of dust grains in exoplanets. *MNRAS* 454, 2–27. doi:10.1093/mnras/stv1711, arXiv:1505.08013.
- Buratti, B.J., Hillier, J.K., Wang, M., 1996. The Lunar Opposition Surge: Observations by Clementine. *Icarus* 124, 490–499. doi:10.1006/icar.1996.0225.
- Cameron, A.G.W., Ward, W.R., 1976. The Origin of the Moon, in: *Lunar and Planetary Science Conference*, p. 120.
- Campion, R., 2014. New lava lake at Nyamuragira volcano revealed by combined ASTER and OMI SO₂ measurements. *Geophysical Research Letters* 41, 7485–7492. URL: <https://agupubs.onlinelibrary.wiley.com/doi/abs/10.1002/2014GL061808>, doi:10.1002/2014GL061808, arXiv:https://agupubs.onlinelibrary.wiley.com/doi/pdf/10.1002/2014GL061808.
- Cano, E.J., Sharp, Z.D., Shearer, C.K., 2020. Distinct oxygen isotope compositions of the Earth and Moon. *Nature Geoscience* 13, 270–274.
- Canup, R.M., 2012. Forming a Moon with an Earth-like composition via a giant impact. *Science* 338, 1052–1055.
- Caracas, R., Hirose, K., Nomura, R., Ballmer, M.D., 2019. Melt–crystal density crossover in a deep magma ocean. *Earth and Planetary Science Letters* 516, 202–211.
- Caro, G., Bourdon, B., Birck, J.L., Moorbath, S., 2006. High-precision 142Nd/144Nd measurements in terrestrial rocks: constraints on the early differentiation of the Earth's mantle. *Geochimica et Cosmochimica Acta* 70, 164–191.
- Caro, G., Bourdon, B., Wood, B.J., Corgne, A., 2005. Trace-element fractionation in Hadean mantle generated by melt segregation from a magma ocean. *Nature* 436, 246–249.
- Cartier, C., 2019. The Role of Reducing Conditions in Building Mercury Evolution and differentiation of early planetoids View project Element volatilities in the early solar system View project The Role of Reducing Conditions in Building Mercury. *Elements* 15, 39–45. URL: <https://www.researchgate.net/publication/331031844>, doi:10.2138/gselements.15.1.39.
- Cashman, K.V., Sparks, R.S.J., 2013. How volcanoes work: A 25 year perspective. *GSA bulletin* 125, 664–690.
- Cassidy, T.A., Mendez, R., Arras, P., Johnson, R.E., Skrutskie, M.F., 2009. Massive Satellites of Close-In Gas Giant Exoplanets. *ApJ* 704, 1341–1348. doi:10.1088/0004-637X/704/2/1341, arXiv:0909.0770.
- Castan, T., Menou, K., 2011. Atmospheres of Hot Super-Earths. *ApJ* 743, L36. doi:10.1088/2041-8205/743/2/L36, arXiv:1109.0659.
- Castruccio, A., Rust, A., Sparks, R., 2013. Evolution of crust-and core-dominated lava flows using scaling analysis. *Bulletin of volcanology* 75, 681.
- Catling, D.C., Kasting, J.F., 2017. Atmospheric Evolution on Inhabited and Lifeless Worlds.
- Catling, D.C., Zahnle, K.J., 2009. The planetary air leak. *Scientific American* 300, 36–43.
- Catling, D.C., Zahnle, K.J., McKay, C.P., 2001. Biogenic methane, hydrogen escape, and the irreversible oxidation of early earth. *Science* 293, 839–843. URL: <https://science.sciencemag.org/content/293/5531/839>, doi:10.1126/science.1061976, arXiv:https://science.sciencemag.org/content/293/5531/839.full.pdf.
- Chassefière, E., Wieler, R., Marty, B., Leblanc, F., 2012. The evolution of Venus: Present state of knowledge and future exploration. *Planetary and Space Science* 63-64, 15–23. doi:10.1016/j.pss.2011.04.007.
- Chatterjee, S., Tan, J.C., 2014. Inside-out Planet Formation. *ApJ* 780, 53. doi:10.1088/0004-637X/780/1/53, arXiv:1306.0576.
- Cheek, L.C., Donaldson Hanna, K.L., Pieters, C.M., Head, J.W., Whitten, J.L., 2013. The distribution and purity of anorthosite across the Orientale basin: New perspectives from Moon Mineralogy Mapper data. *Journal of Geophysical Research (Planets)* 118, 1805–1820. doi:10.1002/jgre.20126.
- Chevrel, M., Harris, A.J.L., James, M.R., Calabrò, L., Gurioli, L., Pinkerton, H., 2018. "The viscosity of pahoehoe lava: In situ syn-eruptive measurements from Kilauea, Hawaii". *Earth and Planetary Science Letters* 493, 161–171. URL: <https://doi.org/10.1016/j.epsl.2018.04.028>, doi:10.1016/j.epsl.2018.04.028.
- Chiang, E., Laughlin, G., 2013. The minimum-mass extrasolar nebula: in situ formation of close-in super-Earths. *MNRAS* 431, 3444–3455. doi:10.1093/mnras/stt424, arXiv:1211.1673.
- Ciardi, D.R., Bean, J., Burt, J., Dragomir, D., Gaidos, E., Johnson, M.C., Kempton, E., Konopacky, Q., Meyer, M., Teske, J., Weiss, L., Zhou, G., 2019. Astro2020 Science White Paper: Toward Finding Earth 2.0: Masses and Orbits of Small Planets with Extreme Radial Velocity Precision. arXiv:1903.05665.
- Cipar, J.J., Anderson, G.P., Cooley, T.W., 2012. Temperature and Power Output of the Lava Lake in Halema'uma'u Crater, Hawaii, Using a Space-Based Hyperspectral Imager. *IEEE Journal of Selected Topics in Applied Earth Observations and Remote Sensing* 5, 617–624.
- Cipriani, A., Bonatti, E., Carlson, R.W., 2011. Nonchondritic ¹⁴²Nd in suboceanic mantle peridotites. *Geochemistry, Geophysics, Geosystems* 12, Q03006. doi:10.1029/2010GC003415.
- Clausen, N., Tilgner, A., 2015. Dissipation in rocky planets for strong tidal forcing. *A&A* 584, A60. doi:10.1051/0004-6361/201526082.
- Colburn, D.S., 1980. Electromagnetic heating of Io. *J. Geophys. Res.* 85, 7257–7261. doi:10.1029/JB085iB12p07257.
- Conrad, A., De Kleer, K., Leisenring, J., La Camera, A., Arcidiacono, C., Bertero, M., Boccacci, P., Defrère, D., De Pater, I., Hinz, P., et al., 2015. Spatially resolved m-band emission from Io's Loki Patera–Fizeau imaging at the 22.8 m LBT. *The Astronomical Journal* 149, 175.
- Cooray, A., Meixner, M., Leisawitz, D., Staguhn, J., Armus, L., Battersby, C., Bauer, J., Bergin, E., Bradford, M., Ennico-Smith, K., Fortney, J.,

- Kataria, T., Melnick, G., Milam, S., Narayanan, D., Padgett, D., Pontoppidan, K., Pope, A., Roellig, T., Sandstrom, K., Stevenson, K., Su, K., Vieira, J., Wright, N., Zmuidzinas, J., Carter, R., Sheth, K., Benford, D., Mamajek, E., Neff, S., DiPirro, M., Wu, C., Amatucci, E., De Beck, E., Aalto, S., Gerin, M., Helmich, F., Sakon, I., Scott, D., Vavrek, R., Wieder, M., Burgarella, D., 2019. Origins Space Telescope: From First Light to Life, in: *Bulletin of the American Astronomical Society*, p. 59.
- Coppola, D., Campion, R., Laiolo, M., Cuoco, E., Balagizi, C., Ripepe, M., Cigolini, C., Tedesco, D., 2016. Birth of a lava lake: Nyamulagira volcano 2011–2015. *Bulletin of Volcanology* 78, 20. URL: <https://doi.org/10.1007/s00445-016-1014-7>, doi:10.1007/s00445-016-1014-7.
- Costa, A., Caricchi, L., Bagdassarov, N., 2009. A model for the rheology of particle-bearing suspensions and partially molten rocks. *Geochemistry, Geophysics, Geosystems* 10. URL: <https://agupubs.onlinelibrary.wiley.com/doi/abs/10.1029/2008GC002138>, doi:10.1029/2008GC002138.
- Creech, J.B., Baker, J.A., Handler, M.R., Lorand, J.P., Storey, M., Wainwright, A.N., Luguët, A., Moynier, F., Bizzarro, M., 2016. Late accretion history of the terrestrial planets inferred from platinum stable isotopes. *Geochemical Perspectives Letters* 3, 94–104. URL: <http://www.geochemicalperspectivesletters.org/article1710>.
- Crossfield, I.J.M., 2015. Observations of Exoplanet Atmospheres. *Publications of the Astronomical Society of the Pacific* 127, 941–960. URL: <https://doi.org/10.1086/2F683115>, doi:10.1086/683115.
- Crossfield, I.J.M., Petigura, E., Schlieder, J.E., Howard, A.W., Fulton, B.J., Aller, K.M., Ciardi, D.R., Lépine, S., Barclay, T., de Pater, I., de Kleer, K., Quintana, E.V., Christiansen, J.L., Schlafly, E., Kaltenegger, L., Crepp, J.R., Henning, T., Obermeier, C., Deacon, N., Weiss, L.M., Isaacson, H.T., Hansen, B.M.S., Liu, M.C., Greene, T., Howell, S.B., Barman, T., Mordasini, C., 2015. A Nearby M Star with Three Transiting Super-Earths Discovered by K2. *ApJ* 804, 10. doi:10.1088/0004-637X/804/1/10, arXiv:1501.03798.
- Culha, C., Suckale, J., Keller, T., Qin, Z., 2020. Crystal Fractionation by Crystal-Driven Convection. *Geophys. Res. Lett.* 47, e86784. doi:10.1029/2019GL086784.
- Dai, F., Masuda, K., Winn, J.N., 2018. Larger Mutual Inclinations for the Shortest-period Planets. *ApJ* 864, L38. doi:10.3847/2041-8213/aadd4f, arXiv:1808.08475.
- Dai, F., Masuda, K., Winn, J.N., Zeng, L., 2019. Homogeneous Analysis of Hot Earths: Masses, Sizes, and Compositions. *The Astrophysical Journal* 883, 79. URL: <http://dx.doi.org/10.3847/1538-4357/ab3a3b>, doi:10.3847/1538-4357/ab3a3b.
- Dai, F., Winn, J.N., Gandolfi, D., Wang, S.X., Teske, J.K., Burt, J., Albrecht, S., Barragán, O., Cochran, W.D., Endl, M., Fridlund, M., Hatzes, A.P., Hirano, T., Hirsch, L.A., Johnson, M.C., Justesen, A.B., Livingston, J., Persson, C.M., Prieto-Arranz, J., Vanderburg, A., Alonso, R., Antoniciello, G., Arriagada, P., Butler, R.P., Cabrera, J., Crane, J.D., Cusano, F., Csizmadia, S., Deeg, H., Dieterich, S.B., Eigmüller, P., Erikson, A., Everett, M.E., Fukui, A., Grziwa, S., Guenther, E.W., Henry, G.W., Howell, S.B., Johnson, J.A., Korth, J., Kuzuhara, M., Narita, N., Nespral, D., Nowak, G., Palle, E., Pätzold, M., Rauer, H., Rodríguez, P.M., Shectman, S.A., Smith, A.M.S., Thompson, I.B., Eylen, V.V., Williamson, M.W., Wittenmyer, R.A., 2017. The Discovery and Mass Measurement of a New Ultra-short-period Planet: K2-131b. *The Astronomical Journal* 154, 226. URL: <https://doi.org/10.3847/1538-3881/2Faa9065>, doi:10.3847/1538-3881/aa9065.
- Dang, L., Cowan, N.B., Schwartz, J.C., Rauscher, E., Zhang, M., Knutson, H.A., Line, M., Dobbs-Dixon, I., Deming, D., Sundararajan, S., Fortney, J.J., Zhao, M., 2018. Detection of a westward hotspot offset in the atmosphere of hot gas giant CoRoT-2b. *Nature Astronomy* 2, 220–227. doi:10.1038/s41550-017-0351-6, arXiv:1801.06548.
- Dauphas, N., Chaussidon, M., 2011. A Perspective from Extinct Radionuclides on a Young Stellar Object: The Sun and Its Accretion Disk. *Annual Review of Earth and Planetary Sciences* 39, 351–386. doi:10.1146/annurev-earth-040610-133428, arXiv:1105.5172.
- Davenport, J.R.A., Covey, K.R., Clarke, R.W., Boeck, A.C., Cornet, J., Hawley, S.L., 2019. The Evolution of Flare Activity with Stellar Age. *ApJ* 871, 241. doi:10.3847/1538-4357/aafb76, arXiv:1901.00890.
- Davies, A.G., 2003. Temperature, age and crust thickness distributions of Loki Patera on Io from Galileo NIMS data: Implications for resurfacing mechanism. *Geophysical research letters* 30.
- Davies, A.G., Keszhelyi, L.P., Williams, D.A., Phillips, C.B., McEwen, A.S., Lopes, R.M.C., Smythe, W.D., Kamp, L.W., Soderblom, L.A., Carlson, R.W., 2001. "Thermal signature, eruption style, and eruption evolution at Pele and Pillan on Io". *Journal of Geophysical Research* 106, 33079–33103.
- Davies, E.J., Carter, P.J., Root, S., Kraus, R.G., Spaulding, D.K., Stewart, S.T., Jacobsen, S.B., 2020. Silicate Melting and Vaporization During Rocky Planet Formation. *Journal of Geophysical Research (Planets)* 125, e06227. doi:10.1029/2019JE006227, arXiv:2002.00998.
- de Kleer, K., Nimmo, F., Kite, E., 2019. Variability in Io's Volcanism on Timescales of Periodic Orbital Changes. *Geophys. Res. Lett.* 46, 6327–6332. doi:10.1029/2019GL082691.
- de Kleer, K., Skrutskie, M., Leisenring, J., Davies, A.G., Conrad, A., de Pater, I., Resnick, A., Bailey, V., Defrère, D., Hinz, P., Skemer, A., Spalding, E., Vaz, A., Veillet, C., Woodward, C.E., 2017. Multi-phase volcanic resurfacing at Loki Patera on Io. *Nature* 545, 199–202. doi:10.1038/nature22339.
- de Vries, J., Nimmo, F., Melosh, H.J., Jacobson, S.A., Morbidelli, A., Rubie, D.C., 2016. Impact-induced melting during accretion of the Earth. *Progress in Earth and Planetary Science* 3, 7. doi:10.1186/s40645-016-0083-8, arXiv:1603.08682.
- Debaile, V., Brandon, A.D., Yin, Q.Z., Jacobsen, B., 2007. Coupled ^{142}Nd - ^{143}Nd evidence for a protracted magma ocean in Mars. *Nature* 450, 525–528. doi:10.1038/nature06317.
- Deeg, H.J., Alonso, R., 2018. Transit Photometry as an Exoplanet Discovery Method. *Handbook of Exoplanets*, 633–657. URL: http://dx.doi.org/10.1007/978-3-319-55333-7_117, doi:10.1007/978-3-319-55333-7_117.
- Delgado Mena, E., Israelian, G., González Hernández, J.I., Bond, J.C., Santos, N.C., Udry, S., Mayor, M., 2010. Chemical clues on the formation of planetary systems: C/O versus Mg/Si for HARPS GTO sample. *The Astrophysical Journal* 725, 2349–2358. URL: <http://dx.doi.org/10.1088/0004-637X/725/2/2349>, doi:10.1088/0004-637X/725/2/2349.
- Deming, D., Louie, D., Sheets, H., 2019. How to Characterize the Atmosphere of a Transiting Exoplanet. *PASP* 131, 013001. doi:10.1088/1538-3873/aae5c5, arXiv:1810.04175.
- Demory, B.O., Gillon, M., Deming, D., Valencia, D., Seager, S., Benneke, B., Lovis, C., Cubillos, P., Harrington, J., Stevenson, K.B., et al., 2011. Detection of a transit of the super-Earth 55 Cancri e with warm Spitzer. *Astronomy & Astrophysics* 533, A114. URL: <http://dx.doi.org/10.1051/0004-6361/201117178>, doi:10.1051/0004-6361/201117178.
- Demory, B.O., Gillon, M., Madhusudhan, N., Queloz, D., 2015. Variability in the super-Earth 55 Cnc e. *Monthly Notices of the Royal Astronomical Society* 455, 2018–2027. URL: <http://dx.doi.org/10.1093/mnras/stv2239>, doi:10.1093/mnras/stv2239.
- Demory, B.O., Gillon, M., de Wit, J., Madhusudhan, N., Bolmont, E., Heng, K., Kataria, T., Lewis, N., Hu, R., Krick, J., et al., 2016. A map of the large day–night temperature gradient of a super-Earth exoplanet. *Nature* 532, 207–209. URL: <http://dx.doi.org/10.1038/nature17169>, doi:10.1038/nature17169.
- Deng, J., Du, Z., Karki, B.B., Ghosh, D.B., Lee, K.K.M., 2020. A magma ocean origin to divergent redox evolutions of rocky planetary bodies and early atmospheres. *Nature Communications* 11, 2007. doi:10.1038/s41467-020-15757-0.
- Denman, T.R., Leinhardt, Z.M., Carter, P.J., Mordasini, C., 2020. Atmosphere loss in planet-planet collisions. *MNRAS* 496, 1166–1181. doi:10.1093/mnras/staa1623, arXiv:2006.01881.
- Dittmann, J.A., Irwin, J.M., Charbonneau, D., Bonfils, X., Astudillo-Defru, N., Haywood, R.D., Berta-Thompson, Z.K., Newton, E.R., Rodriguez, J.E., Winters, J.G., Tan, T.G., Almenara, J.M., Bouchy, F., Delfosse, X., Forveille, T., Lovis, C., Murgas, F., Pepe, F., Santos, N.C., Udry, S., Wünsche, A., Esquerdo, G.A., Latham, D.W., Dressing, C.D., 2017. A temperate rocky super-Earth transiting a nearby cool star. *Nature* 544, 333–336. doi:10.1038/nature22055, arXiv:1704.05556.
- Donati, J.F., Kouch, D., Lacombe, M., Baratchat, S., Doyon, R., Delfosse, X., Artigau, É., Moutou, C., Hébrard, G., Bouchy, F., Bouvier, J., Alen-

- car, S., Saddlemyer, L., Parès, L., Rabou, P., Micheau, Y., Dolon, F., Barrick, G., Hernandez, O., Wang, S.Y., Reshetov, V., Striebig, N., Challin, Z., Carmona, A., Tibault, S., Martioli, E., Figueira, P., Boisse, I., Pepe, F., 2018. SPIRou: A NIR Spectropolarimeter/High-Precision Velocimeter for the CFHT, in: Deeg, H.J., Belmonte, J.A. (Eds.), *Handbook of Exoplanets*, p. 107. doi:10.1007/978-3-319-55333-7_107.
- Dorn, C., Harrison, J.H.D., Bonsor, A., Hands, T.O., 2018. A new class of Super-Earths formed from high-temperature condensates: HD219134 b, 55 Cnc e, WASP-47 e. *Monthly Notices of the Royal Astronomical Society* 484, 712–727. URL: <http://dx.doi.org/10.1093/mnras/sty3435>, doi:10.1093/mnras/sty3435.
- Dorn, C., Hinkel, N.R., Venturini, J., 2017. Bayesian analysis of interiors of HD 219134b, Kepler-10b, Kepler-93b, CoRoT-7b, 55 Cnc e, and HD 97658b using stellar abundance proxies. *A&A* 597, A38. doi:10.1051/0004-6361/201628749.
- Dotter, A., Chaboyer, B., Jevremović, D., Kostov, V., Baron, E., Ferguson, J.W., 2008. The Dartmouth Stellar Evolution Database. *ApJS* 178, 89–101. doi:10.1086/589654, arXiv:0804.4473.
- Dowty, S., Keil, K., Prinz, M., Gros, J., Takahashi, H., 1976. Meteorite-free Apollo 15 crystalline KREEP, in: *Lunar and Planetary Science Conference Proceedings*, pp. 1833–1844.
- Doyle, A.E., Young, E.D., Klein, B., Zuckerman, B., Schlichting, H.E., 2019. Oxygen fugacities of extrasolar rocks: Evidence for an Earth-like geochemistry of exoplanets. *Science* 366, 356–359. doi:10.1126/science.aax3901, arXiv:1910.12989.
- Dressing, C.D., Charbonneau, D., 2015. The Occurrence of Potentially Habitable Planets Orbiting M Dwarfs Estimated from the Full Kepler Dataset and an Empirical Measurement of the Detection Sensitivity. *ApJ* 807, 45. doi:10.1088/0004-637X/807/1/45, arXiv:1501.01623.
- Driscoll, P.E., Barnes, R., 2015a. Tidal Heating of Earth-like Exoplanets around M Stars: Thermal, Magnetic, and Orbital Evolutions. *Astrobiology* 15, 739–760. doi:10.1089/ast.2015.1325, arXiv:1509.07452.
- Driscoll, P.E., Barnes, R., 2015b. Tidal Heating of Earth-like Exoplanets around M Stars: Thermal, Magnetic, and Orbital Evolutions. *Astrobiology* 15, 739–760. doi:10.1089/ast.2015.1325, arXiv:1509.07452.
- Duprat, J., Tatischeff, V., 2007. Energetic Constraints on In Situ Production of Short-Lived Radionuclides in the Early Solar System. *ApJ* 671, L69–L72. doi:10.1086/524297.
- Dymek, R.F., Albee, A.L., Chodos, A.A., 1975. Comparative petrology of lunar cumulate rocks of possible primary origin: dunite 72415, troctolite 76535, norite 78235, and anorthosite 62237. *Lunar and Planetary Science Conference Proceedings* 1, 301–341.
- Edwards, B., Mugnai, L., Tinetti, G., Pascale, E., Sarkar, S., 2019. An Updated Study of Potential Targets for Ariel. *AJ* 157, 242. doi:10.3847/1538-3881/ab1cb9, arXiv:1905.04959.
- Ehrenreich, D., Bourrier, V., Bonfils, X., Lecavelier des Etangs, A., Hébrard, G., Sing, D.K., Wheatley, P.J., Vidal-Madjar, A., Delfosse, X., Udry, S., et al., 2012. Hint of a transiting extended atmosphere on 55 Cancri b. *Astronomy & Astrophysics* 547, A18. URL: <http://dx.doi.org/10.1051/0004-6361/201219981>, doi:10.1051/0004-6361/201219981.
- Eker, Z., Soydogan, F., Soydogan, E., Bilir, S., Yaz Gökçe, E., Steer, I., Tüysüz, M., Şenyüz, T., Demircan, O., 2015. Main-Sequence Effective Temperatures from a Revised Mass-Luminosity Relation Based on Accurate Properties. *AJ* 149, 131. doi:10.1088/0004-6256/149/4/131, arXiv:1501.06585.
- Ekholm, N., 1901. On the Variations of the Climate of the Geological and Historical Past and Their Causes. *Quarterly Journal of the Royal Meteorological Society* 27, 1–62. doi:10.1002/qj.49702711702.
- Elkins-Tanton, L.T., 2008. Linked magma ocean solidification and atmospheric growth for Earth and Mars. *Earth and Planetary Science Letters* 271, 181–191.
- Elkins-Tanton, L.T., 2012a. Magma Oceans in the Inner Solar System. *Annual Review of Earth and Planetary Sciences* 40, 113–139. doi:10.1146/annurev-earth-042711-105503.
- Elkins-Tanton, L.T., 2012b. "Magma Oceans in the Inner Solar System". *Annual Review of Earth and Planetary Sciences* 40, 113–139. doi:10.1146/annurev-earth-042711-105503.
- Elkins-Tanton, L.T., Parmentier, E.M., Hess, P.C., 2003. Magma ocean fractional crystallization and cumulate overturn in terrestrial planets: Implications for Mars. *Meteoritics and Planetary Science* 38, 1753–1771. doi:10.1111/j.1945-5100.2003.tb00013.x.
- Endl, M., Robertson, P., Cochran, W.D., MacQueen, P.J., Brugnauer, E.J., Caldwell, C., Wittenmyer, R.A., Barnes, S.I., Gullikson, K., 2012. Revisiting ρ_1 Cancri e: A new mass determination of the transiting super-Earth. *The Astrophysical Journal* 759, 19. URL: <http://dx.doi.org/10.1088/0004-637X/759/1/19>, doi:10.1088/0004-637X/759/1/19.
- Evans, L.G., Peplowski, P.N., Rhodes, E.A., Lawrence, D.J., McCoy, T.J., Nittler, L.R., Solomon, S.C., Sprague, A.L., Stockstill-Cahill, K.R., Starr, R.D., Weider, S.Z., Boynton, W.V., Hamara, D.K., Goldsten, J.O., 2012. Major-element abundances on the surface of Mercury: Results from the MESSENGER Gamma-Ray Spectrometer. *Journal of Geophysical Research (Planets)* 117, E00L07. doi:10.1029/2012JE004178.
- Feinstein, A.D., Montet, B.T., Ansdell, M., Nord, B., Bean, J.L., Günther, M.N., Gully-Santiago, M.A., Schlieder, J.E., 2020. Flare Statistics for Young Stars from a Convolutional Neural Network Analysis of TESS Data. arXiv e-prints, arXiv:2005.07710 arXiv:2005.07710.
- Ferraz-Mello, S., Tadeu dos Santos, M., Beaugé, C., Michtchenko, T. A., Rodríguez, A., 2011. On the mass determination of super-Earths orbiting active stars: the CoRoT-7 system. *A&A* 531, A161. URL: <https://doi.org/10.1051/0004-6361/201016059>, doi:10.1051/0004-6361/201016059.
- Firth, C., Handley, H., Turner, S., Cronin, S., Smith, I., 2016. Variable Conditions of Magma Storage and Differentiation with Links to Eruption Style at Ambrym Volcano, Vanuatu. *Journal of Petrology* 57, 1049–1072. URL: <https://doi.org/10.1093/petrology/egw029>, doi:10.1093/petrology/egw029.
- Fischer, D.A., Anglada-Escudé, G., Arriagada, P., Baluev, R.V., Bean, J.L., Bouchy, F., Buchhave, L.A., Carroll, T., Chakraborty, A., Crepp, J.R., et al., 2016. State of the Field: Extreme Precision Radial Velocities. *Publications of the Astronomical Society of the Pacific* 128, 066001. URL: <http://dx.doi.org/10.1088/1538-3873/128/964/066001>, doi:10.1088/1538-3873/128/964/066001.
- Fischer-Gödde, M., Elfers, B.M., Münker, C., Szilas, K., Maier, W.D., Messling, N., Morishita, T., Van Kranendonk, M., Smithies, H., 2020. Ruthenium isotope vestige of earth's pre-late-veener mantle preserved in archaean rocks. *Nature* 579, 240–244.
- Folsom, C.P., Ó Fionnagáin, D., Fossati, L., Vidotto, A.A., Moutou, C., Petit, P., Dragomir, D., Donati, J.F., 2020. Circumstellar environment of 55 Cancri. The super-Earth 55 Cnc e as a primary target for star-planet interactions. *A&A* 633, A48. doi:10.1051/0004-6361/201937186, arXiv:1912.03736.
- Forgan, D.H., 2017. On the feasibility of exomoon detection via exoplanet phase curve spectral contrast. *Monthly Notices of the Royal Astronomical Society* 470, 416–426. URL: <http://dx.doi.org/10.1093/mnras/stx1217>, doi:10.1093/mnras/stx1217.
- Frossard, P., Boyet, M., Bouvier, A., Hammouda, T., Monteux, J., 2019. Evidence for anorthositic crust formed on an inner solar system planetesimal. *Geochemical Perspectives Letters*, 28–32doi:10.7185/geochemlet.1921.
- Fu, R.R., Weiss, B.P., Shuster, D.L., Gattacceca, J., Grove, T.L., Suavet, C., Lima, E.A., Li, L., Kuan, A.T., 2012. An ancient core dynamo in asteroid Vesta. *Science* 338, 238–241.
- Fulton, B.J., Petigura, E.A., Howard, A.W., Isaacson, H., Marcy, G.W., Cargile, P.A., Hebb, L., Weiss, L.M., Johnson, J.A., Morton, T.D., Sinukoff, E., Crossfield, I.J.M., Hirsch, L.A., 2017. The California-Kepler Survey. III. A Gap in the Radius Distribution of Small Planets. *AJ* 154, 109. doi:10.3847/1538-3881/aa80eb, arXiv:1703.10375.
- Gaidos, E., Hirano, T., Ansdell, M., 2019a. Monitoring of the D doublet of neutral sodium during transits of two ‘evaporating’ planets. *MNRAS* 485, 3876–3886. doi:10.1093/mnras/stz693, arXiv:1903.06217.
- Gaidos, E., Jacobs, T., LaCourse, D., Vanderburg, A., Rappaport, S., Berger, T., Pearce, L., Mann, A.W., Weiss, L., Fulton, B., Behrman, A., Howard, A.W., Ansdell, M., Ricker, G.R., Vanderspek, R.K., Latham, D.W., Seager, S., Winn, J.N., Jenkins, J.M., 2019b. Planetesimals around stars with TESS (PAST) - I. Transient dimming of a binary solar analogue at the end of the planet accretion era. *MNRAS* 488, 4465–4476. doi:10.1093/mnras/stz1942, arXiv:1907.02476.

- Gaidos, E., Krot, A.N., Williams, J.P., Raymond, S.N., 2009. ^{26}Al and the Formation of the Solar System from a Molecular Cloud Contaminated by Wolf-Rayet Winds. *ApJ* 696, 1854–1863. doi:10.1088/0004-637X/696/2/1854, arXiv:0901.3364.
- Gaidos, E., Mann, A.W., Kraus, A.L., Ireland, M., 2016. They are small worlds after all: revised properties of Kepler M dwarf stars and their planets. *MNRAS* 457, 2877–2899. doi:10.1093/mnras/stw097, arXiv:1512.04437.
- Gaillard, F., Marziano, G.I., 2005. Electrical conductivity of magma in the course of crystallization controlled by their residual liquid composition. *Journal of Geophysical Research: Solid Earth* 110. URL: <https://agupubs.onlinelibrary.wiley.com/doi/abs/10.1029/2004JB003282>, doi:10.1029/2004JB003282, arXiv:https://agupubs.onlinelibrary.wiley.com/doi/pdf/10.1029/2004JB003282.
- Garhart, E., Deming, D., Mandell, A., Knutson, H.A., Wallack, N., Burrows, A., Fortney, J.J., Hood, C., Seay, C., Sing, D.K., Benneke, B., Fraine, J.D., Kataria, T., Lewis, N., Madhusudhan, N., McCullough, P., Stevenson, K.B., Wakeford, H., 2020. Statistical Characterization of Hot Jupiter Atmospheres Using Spitzer's Secondary Eclipses. *AJ* 159, 137. doi:10.3847/1538-3881/ab6c6f, arXiv:1901.07040.
- Garvin, J.B., Arney, G., Getty, S., Johnson, N., Kiefer, W., Lorenz, R., Ravine, M., Malespin, C., Webster, C., Campbell, B., Izenberg, N., Cottini, V., 2020. DAVINCI+: Deep Atmosphere of Venus Investigation of Noble Gases, Chemistry, and Imaging Plus, in: *Lunar and Planetary Science Conference*, p. 2599.
- Gaudi, B.S., Seager, S., Mennesson, B., Kiessling, A., Warfield, K., Kuan, G., Cahoy, K., Clarke, J.T., Domagal-Goldman, S., Feinberg, L., Guyon, O., Kasdin, J., Mawet, D., Robinson, T., Rogers, L., Scowen, P., Somerville, R., Stapelfeldt, K., Stark, C., Stern, D., Turnbull, M., Martin, S., Alvarez-Salazar, O., Amini, R., Arnold, W., Balasubramanian, B., Baysinger, M., Blais, L., Brooks, T., Calvet, R., Cormarkovic, V., Cox, C., Danner, R., Davis, J., Dorsett, L., Effinger, M., Eng, R., Garcia, J., Gaskin, J., Harris, J., Howe, S., Knight, B., Krist, J., Levine, D., Li, M., Lisman, D., Mandic, M., Marchen, L., Marrese-Reading, C., McGowen, J., Miyaguchi, A., Morgan, R., Nemati, B., Nikzad, S., Nissen, J., Novicki, M., Perrine, T., Redding, D., Richards, M., Rud, M., Scharf, D., Serabyn, G., Shaklan, S., Smith, S., Stahl, M., Stahl, P., Tang, H., Van Buren, D., Villalvazo, J., Warwick, S., Webb, D., Wofford, R., Woo, J., Wood, M., Ziemer, J., Douglas, E., Faramaz, V., Hildebrandt, S., Meshkat, T., Plavchan, P., Ruane, G., Turner, N., 2018a. The Habitable Exoplanet Observatory (HabEx) Mission Concept Study Interim Report. arXiv e-prints, arXiv:1809.09674 arXiv:1809.09674.
- Gaudi, B.S., Seager, S., Mennesson, B., Kiessling, A., Warfield, K., Kuan, G., Cahoy, K., Clarke, J.T., Domagal-Goldman, S., Feinberg, L., Guyon, O., Kasdin, J., Mawet, D., Robinson, T., Rogers, L., Scowen, P., Somerville, R., Stapelfeldt, K., Stark, C., Stern, D., Turnbull, M., Martin, S., Alvarez-Salazar, O., Amini, R., Arnold, W., Balasubramanian, B., Baysinger, M., Blais, L., Brooks, T., Calvet, R., Cormarkovic, V., Cox, C., Danner, R., Davis, J., Dorsett, L., Effinger, M., Eng, R., Garcia, J., Gaskin, J., Harris, J., Howe, S., Knight, B., Krist, J., Levine, D., Li, M., Lisman, D., Mandic, M., Marchen, L., Marrese-Reading, C., McGowen, J., Miyaguchi, A., Morgan, R., Nemati, B., Nikzad, S., Nissen, J., Novicki, M., Perrine, T., Redding, D., Richards, M., Rud, M., Scharf, D., Serabyn, G., Shaklan, S., Smith, S., Stahl, M., Stahl, P., Tang, H., Van Buren, D., Villalvazo, J., Warwick, S., Webb, D., Wofford, R., Woo, J., Wood, M., Ziemer, J., Douglas, E., Faramaz, V., Hildebrandt, S., Meshkat, T., Plavchan, P., Ruane, G., Turner, N., 2018b. The Habitable Exoplanet Observatory (HabEx) Mission Concept Study Interim Report. arXiv e-prints, arXiv:1809.09674 arXiv:1809.09674.
- Gillon, M., Demory, B.O., Benneke, B., Valencia, D., Deming, D., Seager, S., Lovis, C., Mayor, M., Pepe, F., Queloz, D., et al., 2012. Improved precision on the radius of the nearby super-Earth 55 Cnc e. *Astronomy & Astrophysics* 539, A28. URL: <http://dx.doi.org/10.1051/0004-6361/201118309>, doi:10.1051/0004-6361/201118309.
- Gillon, M., Jehin, E., Lederer, S.M., Delrez, L., de Wit, J., Burdanov, A., Van Grootel, V., Burgasser, A.J., Triaud, A.H.M.J., Opitom, C., Demory, B.O., Sahu, D.K., Bardalez Gagliuffi, D., Magain, P., Queloz, D., 2016. Temperate Earth-sized planets transiting a nearby ultracool dwarf star. *Nature* 533, 221–224. doi:10.1038/nature17448, arXiv:1605.07211.
- Goldreich, P., Lynden-Bell, D., 1969. Io, a jovian unipolar inductor. *ApJ* 156, 59–78. doi:10.1086/149947.
- González Hernández, J.I., Pepe, F., Molaro, P., Santos, N.C., 2018. ESPRESSO on VLT: An Instrument for Exoplanet Research, in: Deeg, H.J., Belmonte, J.A. (Eds.), *Handbook of Exoplanets*, p. 157. doi:10.1007/978-3-319-55333-7_157.
- Grady, C.A., Wisniewski, J.P., Schneider, G., Boccaletti, A., Gaspar, A., Debes, J.H., Hines, D.C., Stark, C.C., Thalmann, C., Lagrange, A.M., Augereau, J.C., Sezeestre, E., Milli, J., Henning, T., Kuchner, M.J., 2020. The Eroding Disk of AU Mic. *ApJ* 889, L21. doi:10.3847/2041-8213/ab65bb.
- Grasset, O., Schneider, J., Sotin, C., 2009. A Study of the Accuracy of Mass-Radius Relationships for Silicate-Rich and Ice-Rich Planets up to 100 Earth Masses. *ApJ* 693, 722–733. doi:10.1088/0004-637X/693/1/722, arXiv:0902.1640.
- Gray, D., Burton-Johnson, A., Fretwell, P., 2019. Evidence for a lava lake on mt. michael volcano, saunders island (south sandwich islands) from landsat, sentinel-2 and aster satellite imagery. *Journal of Volcanology and Geothermal Research* 379, 60 – 71. URL: <http://www.sciencedirect.com/science/article/pii/S0377027318305742>, doi:https://doi.org/10.1016/j.jvolgeores.2019.05.002.
- Greenwood, R.C., Barrat, J.A., Miller, M.F., Anand, M., Dauphas, N., Franchi, I.A., Sillard, P., Starkey, N.A., 2018. Oxygen isotopic evidence for accretion of Earth's water before a high-energy Moon-forming giant impact. *Science Advances* 4. URL: <https://advances.sciencemag.org/content/4/3/eaao5928>, doi:10.1126/sciadv.aao5928, arXiv:https://advances.sciencemag.org/content/4/3/eaao5928.full.pdf.
- Gregg, T.K.P., Lopes, R.M., 2008. "Lava lakes on Io: New perspectives from modeling". *Icarus* 194, 166–172. doi:10.1016/j.icarus.2007.08.042.
- Grunblatt, S.K., Howard, A.W., Haywood, R.D., 2015. Determining the mass of Kepler-78b with nonparametric Gaussian process estimation. *The Astrophysical Journal* 808, 127. URL: <http://dx.doi.org/10.1088/0004-637X/808/2/127>, doi:10.1088/0004-637X/808/2/127.
- Guenther, E. W., Cabrera, J., Erikson, A., Fridlund, M., Lammer, H., Mura, A., Rauer, H., Schneider, J., Tulej, M., von Paris, Ph., Wurz, P., 2011. Constraints on the exosphere of CoRoT-7b. *A&A* 525, A24. URL: <https://doi.org/10.1051/0004-6361/201014868>, doi:10.1051/0004-6361/201014868.
- Günther, M.N., Zhan, Z., Seager, S., Rimmer, P.B., Ranjan, S., Stassun, K.G., Oelkers, R.J., Daylan, T., Newton, E., Kristiansen, M.H., Olah, K., Gillen, E., Rappaport, S., Ricker, G.R., Vanderspek, R.K., Latham, D.W., Winn, J.N., Jenkins, J.M., Glidden, A., Fausnaugh, M., Levine, A.M., Dittmann, J.A., Quinn, S.N., Krishnamurthy, A., Ting, E.B., 2020. Stellar Flares from the First TESS Data Release: Exploring a New Sample of M Dwarfs. *AJ* 159, 60. doi:10.3847/1538-3881/ab5d3a, arXiv:1901.00443.
- Guo, J.H., 2019. The Effect of Photoionization on the Loss of Water of the Planet. *ApJ* 872, 99. doi:10.3847/1538-4357/aaffd4.
- Halliday, A.N., 2000. Terrestrial accretion rates and the origin of the Moon. *Earth and Planetary Science Letters* 176, 17–30.
- Hamano, K., Abe, Y., Genda, H., 2013. Emergence of two types of terrestrial planet on solidification of magma ocean. *Nature* 497, 607–610. doi:10.1038/nature12163.
- Hamano, K., Kawahara, H., Abe, Y., Onishi, M., Hashimoto, G.L., 2015. Lifetime and spectral evolution of a magma ocean with a steam atmosphere: its detectability by future direct imaging. *The Astrophysical Journal* 806, 216. URL: <https://doi.org/10.1088/0004-637X/806/2/216>, doi:10.1088/0004-637X/806/2/216.
- Hansen, B.M.S., Zink, J., 2015. On the potentially dramatic history of the super-Earth ρ 55 Cancri e. *MNRAS* 450, 4505–4520. doi:10.1093/mnras/stv916, arXiv:1505.05539.
- Harman, C.E., Felton, R., Hu, R., Domagal-Goldman, S.D., Segura, A., Tian, F., Kasting, J.F., 2018. Abiotic O₂ Levels on Planets around F, G, K, and M Stars: Effects of Lightning-produced Catalysts in Eliminating Oxygen False Positives. *ApJ* 866, 56. doi:10.3847/1538-4357/aadd9b.
- Harris, A.J., Carniel, R., Jones, J., 2005. Identification of variable convec-

- tive regimes at erta ale lava lake. *Journal of Volcanology and Geothermal Research* 142, 207 – 223. URL: <http://www.sciencedirect.com/science/article/pii/S0377027304003737>, doi:<https://doi.org/10.1016/j.jvolgeores.2004.11.011>.
- Harris, A.J.L., 2008. Modeling lava lake heat loss, rheology, and convection. *Geophysical Research Letters* 35, 1–6. doi:[10.1029/2008GL033190](https://doi.org/10.1029/2008GL033190).
- Harris, A.J.L., Flynn, L.P., Rothery, D.A., Oppenheimer, C., Sherman, S.B., 1999. Mass flux measurements at active lava lakes: Implications for magma recycling. *Journal of Geophysical Research: Solid Earth* 104, 7117–7136. URL: <https://agupubs.onlinelibrary.wiley.com/doi/abs/10.1029/98JB02731>, doi:[10.1029/98JB02731](https://doi.org/10.1029/98JB02731), arXiv:<https://agupubs.onlinelibrary.wiley.com/doi/pdf/10.1029/98JB02731>.
- Hartmann, W.K., Davis, D.R., 1975. Satellite-sized planetesimals and lunar origin. *Icarus* 24, 504–515.
- Hatzes, A.P., 2014. The detection of Earth-mass planets around active stars. *A&A* 568, A84. URL: <http://dx.doi.org/10.1051/0004-6361/201424025>, doi:[10.1051/0004-6361/201424025](https://doi.org/10.1051/0004-6361/201424025).
- Hatzes, A.P., Fridlund, M., Nachmani, G., Mazeh, T., Valencia, D., Hébrard, G., Carone, L., Pätzold, M., Udry, S., Bouchy, F., Deleuil, M., Moutou, C., Barge, P., Bordé, P., Deeg, H., Tingley, B., Dvorak, R., Gandolfi, D., Ferraz-Mello, S., Wuchterl, G., Guenther, E., Guilhot, T., Rauer, H., Erikson, A., Cabrera, J., Csizmadia, S., Léger, A., Lammer, H., Weingrill, J., Queloz, D., Alonso, R., Rouan, D., Schneider, J., 2011. The mass of CoRoT-7b. *The Astrophysical Journal* 743, 75. URL: <https://doi.org/10.1088/0004-637x/743/1/75>, doi:[10.1088/0004-637x/743/1/75](https://doi.org/10.1088/0004-637x/743/1/75).
- Hatzes, A. P., Dvorak, R., Wuchterl, G., Guterman, P., Hartmann, M., Fridlund, M., Gandolfi, D., Guenther, E., Pätzold, M., 2010. An investigation into the radial velocity variations of CoRoT-7*. *A&A* 520, A93. URL: <https://doi.org/10.1051/0004-6361/201014795>, doi:[10.1051/0004-6361/201014795](https://doi.org/10.1051/0004-6361/201014795).
- Haus, R., Kappel, D., Tellmann, S., Arnold, G., Piccioni, G., Drossart, P., Häusler, B., 2016. Radiative energy balance of Venus based on improved models of the middle and lower atmosphere. *Icarus* 272, 178–205. doi:[10.1016/j.icarus.2016.02.048](https://doi.org/10.1016/j.icarus.2016.02.048).
- Heap, M.J., Kushnir, A.R., Vasseur, J., Wadsworth, F.B., Harlé, P., Baud, P., Kennedy, B.M., Troll, V.R., Deegan, F.M., 2020. The thermal properties of porous andesite. *Journal of Volcanology and Geothermal Research*, 106901.
- Helfenstein, P., Veverka, J., Hillier, J., 1997. The Lunar Opposition Effect: A Test of Alternative Models. *Icarus* 128, 2–14. doi:[10.1006/icar.1997.5726](https://doi.org/10.1006/icar.1997.5726).
- Henning, W.G., O’Connell, R.J., Sasselov, D.D., 2009. Tidally Heated Terrestrial Exoplanets: Viscoelastic Response Models. *ApJ* 707, 1000–1015. doi:[10.1088/0004-637X/707/2/1000](https://doi.org/10.1088/0004-637X/707/2/1000), arXiv:[0912.1907](https://arxiv.org/abs/0912.1907).
- Hofmeister, A.M., Sehlke, A., Avard, G., Bollasina, A.J., Robert, G., Whittington, A.G., 2016. Transport properties of glassy and molten lavas as a function of temperature and composition. *Journal of Volcanology and Geothermal Research* 327, 330–348.
- Howard, A.W., Sanchis-Ojeda, R., Marcy, G.W., Johnson, J.A., Winn, J.N., Isaacson, H., Fischer, D.A., Fulton, B.J., Sinukoff, E., Fortney, J.J., 2013. A rocky composition for an Earth-sized exoplanet. *Nature* 503, 381–384. URL: <http://dx.doi.org/10.1038/nature12767>, doi:[10.1038/nature12767](https://doi.org/10.1038/nature12767).
- Howe, A.R., Adams, F.C., Meyer, M.R., 2020. Survival of Primordial Planetary Atmospheres: Photodissociation-driven Mass Loss. *ApJ* 894, 130. doi:[10.3847/1538-4357/ab620c](https://doi.org/10.3847/1538-4357/ab620c).
- Hu, R., Demory, B.O., Seager, S., Lewis, N., Showman, A.P., 2015. A Semi-analytical Model of Visible-wavelength Phase Curves of Exoplanets and Applications to Kepler-7b and Kepler-10b. *ApJ* 802, 51. doi:[10.1088/0004-637X/802/1/51](https://doi.org/10.1088/0004-637X/802/1/51).
- Hu, R., Ehlmann, B.L., Seager, S., 2012. Theoretical Spectra of Terrestrial Exoplanet Surfaces. *ApJ* 752, 7. doi:[10.1088/0004-637X/752/1/7](https://doi.org/10.1088/0004-637X/752/1/7), arXiv:[1204.1544](https://arxiv.org/abs/1204.1544).
- Hui, H., Peslier, A.H., Zhang, Y., Neal, C.R., 2013. Water in lunar anorthosites and evidence for a wet early Moon. *Nature Geoscience* 6, 177–180. doi:[10.1038/ngeo1735](https://doi.org/10.1038/ngeo1735).
- Huss, G.R., Meyer, B.S., Srinivasan, G., Goswami, J.N., Sahijpal, S., 2009. Stellar sources of the short-lived radionuclides in the early solar system. *Geochim. Cosmochim. Acta* 73, 4922–4945. doi:[10.1016/j.gca.2009.01.039](https://doi.org/10.1016/j.gca.2009.01.039).
- Hyodo, R., Genda, H., Charnoz, S., Rosenblatt, P., 2017. On the Impact Origin of Phobos and Deimos. I. Thermodynamic and Physical Aspects. *ApJ* 845, 125. doi:[10.3847/1538-4357/aa81c4](https://doi.org/10.3847/1538-4357/aa81c4), arXiv:[1707.06282](https://arxiv.org/abs/1707.06282).
- Ikoma, M., Hori, Y., 2012. In situ accretion of hydrogen-rich atmospheres on short-period super-Earths: implications for the Kepler-11 planets. *The Astrophysical Journal* 753, 66.
- Ingersoll, A.P., 1969. The Runaway Greenhouse: A History of Water on Venus. *Journal of Atmospheric Sciences* 26, 1191–1198. doi:[10.1175/1520-0469\(1969\)026<1191:TRGAHO>2.0.CO;2](https://doi.org/10.1175/1520-0469(1969)026<1191:TRGAHO>2.0.CO;2).
- Jackson, B., Barnes, R., Greenberg, R., 2008. Tidal heating of terrestrial extrasolar planets and implications for their habitability. *MNRAS* 391, 237–245. doi:[10.1111/j.1365-2966.2008.13868.x](https://doi.org/10.1111/j.1365-2966.2008.13868.x), arXiv:[0808.2770](https://arxiv.org/abs/0808.2770).
- Jackson, B., Barnes, R., Greenberg, R., 2008. Tidal heating of terrestrial extrasolar planets and implications for their habitability. *Monthly Notices of the Royal Astronomical Society* 391, 237–245. URL: <https://doi.org/10.1111/j.1365-2966.2008.13868.x>, doi:[10.1111/j.1365-2966.2008.13868.x](https://doi.org/10.1111/j.1365-2966.2008.13868.x).
- Jacobson, S.A., Morbidelli, A., Raymond, S.N., O’Brien, D.P., Walsh, K.J., Rubie, D.C., 2014. Highly siderophile elements in Earth’s mantle as a clock for the Moon-forming impact. *Nature* 508, 84–87. doi:[10.1038/nature13172](https://doi.org/10.1038/nature13172), arXiv:[1504.01421](https://arxiv.org/abs/1504.01421).
- Johnstone, C.P., 2020. Hydrodynamic Escape of Water Vapor Atmospheres near Very Active Stars. *ApJ* 890, 79. doi:[10.3847/1538-4357/ab6224](https://doi.org/10.3847/1538-4357/ab6224), arXiv:[1912.07027](https://arxiv.org/abs/1912.07027).
- Kaib, N.A., Raymond, S.N., Duncan, M.J., 2011. 55 Cancri: A coplanar planetary system that is likely misaligned with its star. *The Astrophysical Journal* 742, L24. URL: <http://dx.doi.org/10.1088/2041-8205/742/2/L24>, doi:[10.1088/2041-8205/742/2/L24](https://doi.org/10.1088/2041-8205/742/2/L24).
- Kaltenegger, L., Traub, W.A., 2009. Transits of Earth-like Planets. *ApJ* 698, 519–527. doi:[10.1088/0004-637X/698/1/519](https://doi.org/10.1088/0004-637X/698/1/519), arXiv:[0903.3371](https://arxiv.org/abs/0903.3371).
- Kasting, J.F., Egger, D.H., Raeburn, S.P., 1993. Mantle redox evolution and the oxidation state of the archaic atmosphere. *The Journal of Geology* 101, 245–257. doi:[10.1086/648219](https://doi.org/10.1086/648219).
- Kawabata, Y., Nagahara, H., 2017. Crystallization and cooling conditions for diogenite formation in the turbulent magma ocean of asteroid 4 Vesta. *Icarus* 281, 379–387.
- Kegerreis, J.A., Eke, V.R., Massey, R.J., Teodoro, L.F.A., 2020. Atmospheric Erosion by Giant Impacts onto Terrestrial Planets. arXiv e-prints, arXiv:[2002.02977](https://arxiv.org/abs/2002.02977) arXiv:[2002.02977](https://arxiv.org/abs/2002.02977).
- Keller, T., Suckale, J., 2019. A continuum model of multi-phase reactive transport in igneous systems. *Geophysical Journal International* 219, 185–222. URL: <https://doi.org/10.1093/gji/ggz287>, doi:[10.1093/gji/ggz287](https://doi.org/10.1093/gji/ggz287), arXiv:<https://academic.oup.com/gji/article-pdf/219/1/185/28932388/ggz287.pdf>.
- Khurana, K.K., Jia, X., Kivelson, M.G., Nimmo, F., Schubert, G., Russell, C.T., 2011. Evidence of a Global Magma Ocean in Io’s Interior. *Science* 332, 1186. doi:[10.1126/science.1201125](https://doi.org/10.1126/science.1201125).
- Kislyakova, K.G., Fossati, L., Johnstone, C.P., Noack, L., Lüftinger, T., Zaitsev, V.V., Lammer, H., 2018. Effective Induction Heating around Strongly Magnetized Stars. *ApJ* 858, 105. doi:[10.3847/1538-4357/aabae4](https://doi.org/10.3847/1538-4357/aabae4), arXiv:[1804.06346](https://arxiv.org/abs/1804.06346).
- Kislyakova, K.G., Noack, L., Johnstone, C.P., Zaitsev, V.V., Fossati, L., Lammer, H., Khodachenko, M.L., Odert, P., Guedel, M., 2017. Magma oceans and enhanced volcanism on TRAPPIST-1 planets due to induction heating. *Nature Astronomy* 1, 878–885. doi:[10.1038/s41550-017-0284-0](https://doi.org/10.1038/s41550-017-0284-0), arXiv:[1710.08761](https://arxiv.org/abs/1710.08761).
- Kite, E.S., Barnett, M.N., 2020. Exoplanet secondary atmosphere loss and revival. *Proceedings of the National Academy of Science* 117, 18264–18271. arXiv:[2006.02589](https://arxiv.org/abs/2006.02589).
- Kite, E.S., Fegley, Jr., B., Schaefer, L., Gaidos, E., 2016. Atmosphere-interior Exchange on Hot, Rocky Exoplanets. *ApJ* 828, 80. doi:[10.3847/0004-637X/828/2/80](https://doi.org/10.3847/0004-637X/828/2/80), arXiv:[1606.06740](https://arxiv.org/abs/1606.06740).
- Kite, E.S., Fegley, Bruce, J., Schaefer, L., Ford, E.B., 2019. Superabundance of Exoplanet Sub-Neptunes Explained by Fugacity Crisis. *ApJ* 887, L33. doi:[10.3847/2041-8213/ab59d9](https://doi.org/10.3847/2041-8213/ab59d9), arXiv:[1912.02701](https://arxiv.org/abs/1912.02701).

- Kite, E.S., Fegley Jr, B., Schaefer, L., Gaidos, E., 2016. Atmosphere-interior exchange on hot, rocky exoplanets. *The Astrophysical Journal* 828, 80.
- de Kleer, K., de Pater, I., 2017. "Io's Loki Patera: Modeling of three brightening events in 2013 – 2016". *Icarus* 289, 181–198.
- Kleine, T., Münker, C., Mezger, K., Palme, H., 2002. Rapid accretion and early core formation on asteroids and the terrestrial planets from Hf–W chronometry. *Nature* 418, 952–955.
- Klima, R.L., Denevi, B.W., Ernst, C.M., Murchie, S.L., Peplowski, P.N., 2018. Global Distribution and Spectral Properties of Low-Reflectance Material on Mercury. *Geophys. Res. Lett.* 45, 2945–2953. doi:10.1002/2018GL077544.
- Koch, D.G., Borucki, W.J., Basri, G., Batalha, N.M., Brown, T.M., Caldwell, D., Christensen-Dalsgaard, J., Cochran, W.D., DeVore, E., Dunham, E.W., et al., 2010. Kepler mission design, realized photometric performance, and early science. *The Astrophysical Journal* 713, L79–L86. URL: <http://dx.doi.org/10.1088/2041-8205/713/2/L79>, doi:10.1088/2041-8205/713/2/L79.
- Koll, D.D.B., Abbot, D.S., 2015. Deciphering Thermal Phase Curves of Dry, Tidally Locked Terrestrial Planets. *ApJ* 802, 21. doi:10.1088/0004-637X/802/1/21, arXiv:1412.8216.
- Komabayasi, M., 1967. Discrete equilibrium temperatures of a hypothetical planet with the atmosphere and the hydrosphere of one component-two phase system under constant solar radiation. *Journal of the Meteorological Society of Japan. Ser. II* 45, 137–139.
- Kreidberg, L., 2018. Exoplanet Atmosphere Measurements from Transmission Spectroscopy and Other Planet Star Combined Light Observations, in: Deeg, H.J., Belmonte, J.A. (Eds.), *Handbook of Exoplanets*, p. 100. doi:10.1007/978-3-319-55333-7_100.
- Kreidberg, L., Loeb, A., 2016. Prospects for Characterizing the Atmosphere of Proxima Centauri b. *ApJ* 832, L12. doi:10.3847/2041-8205/832/1/L12, arXiv:1608.07345.
- Kruijer, T.S., Borg, L.E., Wimpenny, J., Sio, C.K., 2020. Onset of magma ocean solidification on Mars inferred from Mn-Cr chronometry. *Earth and Planetary Science Letters* 542, 116315. doi:10.1016/j.epsl.2020.116315.
- Kruijer, T.S., Kleine, T., Fischer-Gödde, M., Sprung, P., 2015. Lunar tungsten isotopic evidence for the late veneer. *Nature* 520, 534–537. URL: <https://doi.org/10.1038/nature14360>, doi:10.1038/nature14360.
- Kuramoto, K., Kawakatsu, Y., Fujimoto, M., Genda, H., Imamura, T., Kameda, S., Matsumoto, K., Miyamoto, H., Morota, T., Nagaoka, H., Nakamura, T., Ogawa, K., Otake, H., Ozaki, M., Sasaki, S., Senshu, H., Tachibana, S., Terada, N., Usui, T., Wada, K., Watababe, S., MMX Study Team, 2018. Martian Moons Exploration (MMX) Conceptual Study Update, in: *Lunar and Planetary Science Conference*, p. 2143.
- Kurosawa, K., 2015. Impact-driven planetary desiccation: The origin of the dry Venus. *Earth and Planetary Science Letters* 429, 181–190. doi:10.1016/j.epsl.2015.07.061, arXiv:1509.01357.
- Labrosse, S., Hernlund, J.W., Coltice, N., 2007. A crystallizing dense magma ocean at the base of the Earth's mantle. *Nature* 450, 866–869. doi:10.1038/nature06355.
- Labrosse, S., Morison, A., Deguen, R., Alboussière, T., 2018. Rayleigh-Bénard convection in a creeping solid with melting and freezing at either or both its horizontal boundaries. *Journal of Fluid Mechanics* 846, 5–36. doi:10.1017/jfm.2018.258, arXiv:1708.00791.
- Lazzaro, D., Michtchenko, T., Carvano, J.M., Binzel, R.P., Bus, S.J., Burbine, T.H., Mothé-Diniz, T., Florczak, M., Angeli, C.A., Harris, A.W., 2000. Discovery of a Basaltic Asteroid in the Outer Main Belt. *Science* 288, 2033–2035. doi:10.1126/science.288.5473.2033.
- Lebrun, T., Massol, H., Chassefière, E., Davaille, A., Marcq, E., Sarda, P., Leblanc, F., Brandeis, G., 2013. Thermal evolution of an early magma ocean in interaction with the atmosphere. *Journal of Geophysical Research (Planets)* 118, 1155–1176. doi:10.1002/jgre.20068.
- Lee, E.J., Chiang, E., 2015. To Cool is to Accrete: Analytic Scalings for Nebular Accretion of Planetary Atmospheres. *ApJ* 811, 41. doi:10.1088/0004-637X/811/1/41, arXiv:1508.05096.
- Lee, E.J., Chiang, E., 2017. Magnetospheric Truncation, Tidal Inspiral, and the Creation of Short-period and Ultra-short-period Planets. *ApJ* 842, 40. doi:10.3847/1538-4357/aa6fb3, arXiv:1702.08461.
- Leger, A., Grasset, O., Fegley, B., Codron, F., Albarede, A., Barge, P., Barnes, R., Cance, P., Carpy, S., Catalano, F., et al., 2011. The extreme physical properties of the CoRoT-7b super-Earth. *Icarus* 213, 1–11. URL: <http://dx.doi.org/10.1016/j.icarus.2011.02.004>, doi:10.1016/j.icarus.2011.02.004.
- Léger, A., Grasset, O., Fegley, B., Codron, F., Albarede, A.F., Barge, P., Barnes, R., Cance, P., Carpy, S., Catalano, F., Cavarroc, C., Demangeon, O., Ferraz-Mello, S., Gabor, P., Grießmeier, J.M., Leibacher, J., Libourel, G., Maurin, A.S., Raymond, S.N., Rouan, D., Samuel, B., Schaefer, L., Schneider, J., Schuller, P.A., Selsis, F., Sotin, C., 2011. The extreme physical properties of the CoRoT-7b super-Earth. *Icarus* 213, 1–11. doi:10.1016/j.icarus.2011.02.004, arXiv:1102.1629.
- Leitzinger, M., Odert, P., Greimel, R., Vida, K., Kriskovics, L., Guenther, E.W., Korhonen, H., Koller, F., Hanslmeier, A., Kővári, Z., Lammer, H., 2020. A census of coronal mass ejections on solar-like stars. *MNRAS* 493, 4570–4589. doi:10.1093/mnras/staa504, arXiv:2002.04430.
- Leshner, C.E., Spera, F.J., 2015. Chapter 5 - thermodynamic and transport properties of silicate melts and magma, in: Sigurdsson, H. (Ed.), *The Encyclopedia of Volcanoes (Second Edition)*, second edition ed. Academic Press, Amsterdam, pp. 113 – 141. URL: <http://www.sciencedirect.com/science/article/pii/B9780123859389000055>, doi:https://doi.org/10.1016/B978-0-12-385938-9.00005-5.
- Lev, E., Ruprecht, P., Oppenheimer, C., Peters, N., Patrick, M., Hernández, P.A., Spampinato, L., Marlow, J., 2019. A global synthesis of lava lake dynamics. *Journal of Volcanology and Geothermal Research* 381, 16–31.
- Li, H., Zhang, N., Liang, Y., Wu, B., Dygert, N.J., Huang, J., Parmentier, E.M., 2019. Lunar Cumulate Mantle Overturn: A Model Constrained by Ilmenite Rheology. *Journal of Geophysical Research: Planets* 124, 1357–1378. doi:10.1029/2018JE005905.
- Li, J., Agee, C.B., 1996. Geochemistry of mantle-core differentiation at high pressure. *Nature* 381, 686–689.
- Lichtenberg, T., Golabek, G.J., Burn, R., Meyer, M.R., Alibert, Y., Gerya, T.V., Mordasini, C., 2019. A water budget dichotomy of rocky protoplanets from ²⁶Al-heating. *Nature Astronomy* 3, 307–313. doi:10.1038/s41550-018-0688-5, arXiv:1902.04026.
- Lin, Y., Tronche, E.J., Steenstra, E.S., van Westrenen, W., 2017. Evidence for an early wet Moon from experimental crystallization of the lunar magma ocean. *Nature Geoscience* 10, 14–18. URL: <https://doi.org/10.1038/ngeo2845>, doi:10.1038/ngeo2845.
- Lissauer, J.J., 2007. Planets Formed in Habitable Zones of M Dwarf Stars Probably Are Deficient in Volatiles. *ApJ* 660, L149–L152. doi:10.1086/518121, arXiv:astro-ph/0703576.
- Lock, S.J., Stewart, S.T., Petaev, M.I., Leinhardt, Z., Mace, M.T., Jacobsen, S.B., Cuk, M., 2018. The origin of the Moon within a terrestrial synestia. *Journal of Geophysical Research: Planets* 123, 910–951.
- Lopes, R.M.C., Kamp, L.W., Smythe, W.D., Mouginiis-Mark, P., Kargel, J., Radebaugh, J., Turtle, E.P., Perry, J., Williams, D.A., Carlson, R.W., Douté, S., 2004. Lava lakes on Io: Observations of Io's volcanic activity from Galileo NIMS during the 2001 fly-by. *Icarus* 169, 140–174. doi:10.1016/j.icarus.2003.11.013.
- Lopez, E.D., 2017. Born dry in the photoevaporation desert: Kepler's ultra-short-period planets formed water-poor. *Monthly Notices of the Royal Astronomical Society* 472, 245–253. doi:10.1093/mnras/stx1558.
- Lopez, E.D., 2017. Born dry in the photoevaporation desert: Kepler's ultra-short-period planets formed water-poor. *MNRAS* 472, 245–253. doi:10.1093/mnras/stx1558, arXiv:1610.01170.
- López-Morales, M., Triaud, A.H.M.J., Rodler, F., Dumusque, X., Buchhave, L.A., Harutyunyan, A., Hoyer, S., Alonso, R., Gillon, M., Kaib, N.A., Latham, D.W., Lovis, C., Pepe, F., Queloz, D., Raymond, S.N., Ségransan, D., Waldmann, I.P., Udry, S., 2014. Rossiter-McLaughlin Observations of 55 Cnc e. *ApJ* 792, L31. doi:10.1088/2041-8205/792/2/L31, arXiv:1408.2007.
- Lorenz, R.D., 2018. Lightning detection on Venus: a critical review. *Progress in Earth and Planetary Science* 5, 34. doi:10.1186/s40645-018-0181-x.
- Lorenz, R.D., Imai, M., Takahashi, Y., Sato, M., Yamazaki, A., Sato, T.M.,

- Imamura, T., Satoh, T., Nakamura, M., 2019. Constraints on Venus Lightning From Akatsuki's First 3 Years in Orbit. *Geophys. Res. Lett.* 46, 7955–7961. doi:10.1029/2019GL083311.
- Lowe, D.R., Byerly, G.R., 2018. The terrestrial record of Late Heavy Bombardment. *New A Rev.* 81, 39–61. doi:10.1016/j.newar.2018.03.002.
- Lu, Z., Chang, Y.C., Yin, Q.Z., Ng, C.Y., Jackson, W.M., 2014. Evidence for direct molecular oxygen production in CO₂ photodissociation. *Science* 346, 61–64. URL: <https://science.sciencemag.org/content/346/6205/61>, doi:10.1126/science.1257156, arXiv:<https://science.sciencemag.org/content/346/6205/61.full.pdf>.
- Luger, R., Barnes, R., 2015. Extreme Water Loss and Abiotic O₂ Buildup on Planets Throughout the Habitable Zones of M Dwarfs. *Astrobiology* 15, 119–143. doi:10.1089/ast.2014.1231, arXiv:1411.7412.
- Lundin, R., Lammer, H., Ribas, I., 2007. Planetary magnetic fields and solar forcing: implications for atmospheric evolution. *Space Science Reviews* 129, 245–278.
- Lupu, R.E., Zahnle, K., Marley, M.S., Schaefer, L., Fegley, B., Morley, C., Cahoy, K., Freedman, R., Fortney, J.J., 2014. The Atmospheres of Earthlike Planets after Giant Impact Events. *ApJ* 784, 27. doi:10.1088/0004-637X/784/1/27, arXiv:1401.1499.
- Léger, A., Rouan, D., Schneider, J., Barge, P., Fridlund, M., Samuel, B., Ollivier, M., Guenther, E., Deleuil, M., Deeg, H.J., et al., 2009. Transiting exoplanets from the CoRoT space mission. *Astronomy & Astrophysics* 506, 287–302. URL: <http://dx.doi.org/10.1051/0004-6361/200911933>, doi:10.1051/0004-6361/200911933.
- Maas, C., Hansen, U., 2019. Dynamics of a terrestrial magma ocean under planetary rotation: A study in spherical geometry. *Earth and Planetary Science Letters* 513, 81–94.
- MacDonald, R.J., Goyal, J.M., Lewis, N.K., 2020. Why Is it So Cold in Here? Explaining the Cold Temperatures Retrieved from Transmission Spectra of Exoplanet Atmospheres. *ApJ* 893, L43. doi:10.3847/2041-8213/ab8238, arXiv:2003.11548.
- Madden, J.H., Kaltenecker, L., 2018. A Catalog of Spectra, Albedos, and Colors of Solar System Bodies for Exoplanet Comparison. *Astrobiology* 18, 1559–1573. doi:10.1089/ast.2017.1763, arXiv:1807.11442.
- Mader, H., Llewellyn, E., Mueller, S., 2013. The rheology of two-phase magmas: A review and analysis. *Journal of Volcanology and Geothermal Research* 257, 135 – 158. URL: <http://www.sciencedirect.com/science/article/pii/S0377027313000656>, doi:<https://doi.org/10.1016/j.jvolgeores.2013.02.014>.
- Madhusudhan, N., Lee, K.K.M., Mousis, O., 2012. A possible carbon-rich interior in super-Earth 55 Cancri e. *The Astrophysical Journal* 759, L40. URL: <http://dx.doi.org/10.1088/2041-8205/759/2/L40>, doi:10.1088/2041-8205/759/2/L40.
- Malavergne, V., Toplis, M.J., Berthet, S., Jones, J., 2010. Highly reducing conditions during core formation on Mercury: Implications for internal structure and the origin of a magnetic field. *Icarus* 206, 199–209. doi:10.1016/j.icarus.2009.09.001.
- Mallama, A., Krobusek, B., Pavlov, H., 2017. Comprehensive wide-band magnitudes and albedos for the planets, with applications to exoplanets and Planet Nine. *Icarus* 282, 19–33. doi:10.1016/j.icarus.2016.09.023, arXiv:1609.05048.
- Mallonn, M., Köhler, J., Alexoudi, X., von Essen, C., Granzer, T., Poppenhaeger, K., Strassmeier, K.G., 2019. Low albedos of hot to ultra-hot Jupiters in the optical to near-infrared transition regime. *A&A* 624, A62. doi:10.1051/0004-6361/201935079, arXiv:1902.07944.
- Mandler, B.E., Elkins-Tanton, L.T., 2013. The origin of eucrites, diogenites, and olivine diogenites: Magma ocean crystallization and shallow magma chamber processes on Vesta. *Meteoritics & Planetary Science* 48, 2333–2349.
- Manser, C.J., Gänsicke, B.T., Ettl, S., Hollands, M., Izquierdo, P., Koester, D., Landstreet, J.D., Lyra, W., Marsh, T.R., Meru, F., Mustill, A.J., Rodríguez-Gil, P., Toloza, O., Veras, D., Wilson, D.J., Burleigh, M.R., Davies, M.B., Farihi, J., Gentile Fusillo, N., de Martino, D., Parsons, S.G., Quirrenbach, A., Raddi, R., Reffert, S., Del Santo, M., Schreiber, M.R., Silvotti, R., Toonen, S., Villaver, E., Wyatt, M., Xu, S., Portegies Zwart, S., 2019. A planetesimal orbiting within the debris disc around a white dwarf star. *Science* 364, 66–69. doi:10.1126/science.aat5330, arXiv:1904.02163.
- Marchwinski, R.C., Mahadevan, S., Robertson, P., Ramsey, L., Harder, J., 2015. Toward Understanding Stellar Radial Velocity Jitter as a Function of Wavelength: The Sun as a Proxy. *ApJ* 798, 63. doi:10.1088/0004-637X/798/1/63, arXiv:1410.7379.
- Marconi, A., Allende Prieto, C., Amado, P.J., Amate, M., Augusto, S.R., Becerril, S., Bezawada, N., Boisse, I., Bouchy, F., Cabral, A., Chazelas, B., Cirami, R., Coretti, I., Cristiani, S., Cupani, G., de Castro Leão, I., de Medeiros, J.R., de Souza, M.A.F., Di Marcantonio, P., Di Varano, I., D'Odorico, V., Drass, H., Figueira, P., Fragoso, A.B., Fynbo, J.P.U., Genoni, M., González Hernández, J.I., Haehnelt, M., Hughes, I., Huke, P., Kjeldsen, H., Korn, A.J., Landoni, M., Liske, J., Lovis, C., Maiolino, R., Marquart, T., Martins, C.J.A.P., Mason, E., Monteiro, M.A., Morris, T., Murray, G., Niedzielski, A., Oliva, E., Origlia, L., Pallé, E., Parr-Burman, P., Parro, V.C., Pepe, F., Piskunov, N., Rasilila, J.L., Rees, P., Rebolo, R., Riva, M., Rousseau, S., Sanna, N., Santos, N.C., Shen, T.C., Sortino, F., Sosnowska, D., Sousa, S., Stempels, E., Strassmeier, K., Tenegi, F., Tozzi, A., Udry, S., Valenziano, L., Vanzi, L., Weber, M., Woche, M., Xompero, M., Zackrisson, E., 2018. ELT-HIRES, the high resolution spectrograph for the ELT: results from the Phase A study, in: *Ground-based and Airborne Instrumentation for Astronomy VII*, p. 107021Y. doi:10.1117/12.2311664.
- Massol, H., Hamano, K., Tian, F., Ikoma, M., Abe, Y., Chassefière, E., Davaille, A., Genda, H., Güdel, M., Hori, Y., Leblanc, F., Marq, E., Sarda, P., Shematovich, V.I., Stökl, A., Lammer, H., 2016. Formation and Evolution of Protoatmospheres. *Space Sci. Rev.* 205, 153–211. doi:10.1007/s11214-016-0280-1.
- Matson, D.L., Davies, A.G., Veeder, G.J., Rathbun, J.A., Johnson, T.V., Castillo, J.C., 2006. Io: Loki Patera as a magma sea. *Journal of Geophysical Research* 111, 1–21. doi:10.1029/2006JE002703.
- Matsui, T., Abe, Y., 1986. Evolution of an impact-induced atmosphere and magma ocean on the accreting Earth. *Nature* 319, 303–305. doi:10.1038/319303a0.
- Maurice, M., Tosi, N., Schwinger, S., Breuer, D., Kleine, T., 2020. A long-lived magma ocean on a young Moon. *Science Advances* 6. URL: <https://advances.sciencemag.org/content/6/28/eaba8949>, doi:10.1126/sciadv.a8949.
- Mawet, D., Fitzgerald, M., Konopacky, Q., Beichman, C., Jovanovic, N., Dekany, R., Hover, D., Chisholm, E., Ciardi, D., Artigau, É., Banyal, R., Beatty, T., Benneke, B., Blake, G.A., Burgasser, A., Canalizo, G., Chen, G., Do, T., Doppmann, G., Doyon, R., Dressing, C., Fang, M., Greene, T., Hillenbrand, L., Howard, A., Kane, S., Kataria, T., Kempton, E., Knutson, H., Kotani, T., Lafrenière, D., Liu, C., Nishiyama, S., Pandey, G., Plavchan, P., Prato, L., Rajaguru, S.P., Robertson, P., Salyk, C., Sato, B., Schlawin, E., Sengupta, S., Sivarani, T., Skidmore, W., Tamura, M., Terada, H., Vasisth, G., Wang, J., Zhang, H., 2019. High-resolution Infrared Spectrograph for Exoplanet Characterization with the Keck and Thirty Meter Telescopes, in: *Bulletin of the American Astronomical Society*, p. 134. arXiv:1908.03623.
- Mayorga, L.C., Batalha, N.E., Lewis, N.K., Marley, M.S., 2019. Reflected Light Phase Curves in the TESS Era. *AJ* 158, 66. doi:10.3847/1538-3881/ab29fa, arXiv:1905.12662.
- McArthur, B.E., Endl, M., Cochran, W.D., Benedict, G.F., Fischer, D.A., Marcy, G.W., Butler, R.P., Naef, D., Mayor, M., Queloz, D., et al., 2004. Detection of a Neptune-Mass Planet in the ρ_1 Cancri System Using the Hobby-Eberly Telescope. *The Astrophysical Journal* 614, L81–L84. URL: <http://dx.doi.org/10.1086/425561>, doi:10.1086/425561.
- McCord, T.B., Adams, J.B., Johnson, T.V., 1970. Asteroid Vesta: Spectral reflectivity and compositional implications. *Science* 168, 1445–1447.
- McCubbin, F.M., Steele, A., Hauri, E.H., Nekvasil, H., Yamashita, S., Hemley, R.J., 2010. Nominally hydrous magmatism on the Moon. *Proceedings of the National Academy of Sciences* 107, 11223–11228. URL: <https://www.pnas.org/content/107/25/11223>, doi:10.1073/pnas.1006677107, arXiv:<https://www.pnas.org/content/107/25/11223.full1.pdf>.
- McEwen, A.S., IVO Science Team, 2020. Io Volcano Observer (IVO): Does Io Have a Magma Ocean?, in: *Lunar and Planetary Science Conference*, p. 1648.

- McSween Jr, H.Y., 1985. SNC meteorites: Clues to Martian petrologic evolution? *Reviews of Geophysics* 23, 391–416.
- McSween Jr, H.Y., Binzel, R.P., De Sanctis, M.C., Ammannito, E., Prettyman, T.H., Beck, A.W., Reddy, V., Le Corre, L., Gaffey, M.J., McCord, T.B., et al., 2013. Dawn; the Vesta–HED connection; and the geologic context for eucrites, diogenites, and howardites. *Meteoritics & Planetary Science* 48, 2090–2104.
- Meadows, V.S., 2017. Reflections on O₂ as a Biosignature in Exoplanetary Atmospheres. *Astrobiology* 17, 1022–1052. doi:10.1089/ast.2016.1578.
- Meng, H.Y.A., Su, K.Y.L., Rieke, G.H., Stevenson, D.J., Plavchan, P., Rujopakarn, W., Lisse, C.M., Poshyachinda, S., Reichart, D.E., 2014. Large impacts around a solar-analog star in the era of terrestrial planet formation. *Science* 345, 1032–1035. doi:10.1126/science.1255153, arXiv:1503.05609.
- Michioka, H., Sumita, I., 2005. Rayleigh-Taylor instability of a particle packed viscous fluid: Implications for a solidifying magma. *Geophys. Res. Lett.* 32, L03309. doi:10.1029/2004GL021827.
- Milillo, A., Fujimoto, M., Kallio, E., Kameda, S., Leblanc, F., Narita, Y., Cremonese, G., Laakso, H., Laurenza, M., Massetti, S., McKenna-Lawlor, S., Mura, A., Nakamura, R., Omura, Y., Rothery, D.A., Seki, K., Storini, M., Wurz, P., Baumjohann, W., Bunce, E.J., Kasaba, Y., Helbert, J., Sprague, A., Hermean Environment WG members, 2010. The Bepi-Colombo mission: An outstanding tool for investigating the Hermean environment. *Planet. Space Sci.* 58, 40–60. doi:10.1016/j.pss.2008.06.005.
- Miller-Ricci, E., Meyer, M.R., Seager, S., Elkins-Tanton, L., 2009. On the emergent spectra of hot protoplanet collision afterglows. *The Astrophysical Journal* 704, 770–780. URL: <https://doi.org/10.1088%2F0004-637x%2F704%2F1%2F770>, doi:10.1088/0004-637x/704/1/770.
- Miyazaki, Y., Korenaga, J., 2019. On the Timescale of Magma Ocean Solidification and Its Chemical Consequences: 2. Compositional Differentiation Under Crystal Accumulation and Matrix Compaction. *Journal of Geophysical Research (Solid Earth)* 124, 3399–3419. doi:10.1029/2018JB016928.
- Mojzsis, S.J., Brasser, R., Kelly, N.M., Abramov, O., Werner, S.C., 2019. Onset of Giant Planet Migration before 4480 Million Years Ago. *ApJ* 881, 44. doi:10.3847/1538-4357/ab2c03, arXiv:1903.08825.
- Morabito, L., Synnott, S., Kupferman, P., Collins, S.A., 1979. Discovery of currently active extraterrestrial volcanism. *Science* 204, 972–972.
- Morbidelli, A., Lunine, J.I., O'Brien, D.P., Raymond, S.N., Walsh, K.J., 2012. Building Terrestrial Planets. *Annual Review of Earth and Planetary Sciences* 40, 251–275. doi:10.1146/annurev-earth-042711-105319, arXiv:1208.4694.
- Morrison, A.A., Zanetti, M., Hamilton, C.W., Lev, E., Neish, C.D., Whittington, A.G., 2019. Rheological investigation of lunar highland and mare impact melt simulants. *Icarus* 317, 307–323.
- Moskovitz, N., Gaidos, E., 2011. Differentiation of planetesimals and the thermal consequences of melt migration. *Meteoritics and Planetary Science* 46, 903–918. doi:10.1111/j.1945-5100.2011.01201.x, arXiv:1101.4165.
- Moskovitz, N.A., Jedicke, R., Gaidos, E., Willman, M., Nesvorný, D., Fevig, R., Ivezić, Ž., 2008. The distribution of basaltic asteroids in the Main Belt. *Icarus* 198, 77–90. doi:10.1016/j.icarus.2008.07.006, arXiv:0807.3951.
- Mugrauer, M., Neuhäuser, R., Mazeh, T., Guenther, E., Fernández, M., Broeg, C., 2006. A search for wide visual companions of exoplanet host stars: The Calar Alto Survey. *Astronomische Nachrichten* 327, 321–327. URL: <http://dx.doi.org/10.1002/asna.200510528>, doi:10.1002/asna.200510528.
- Muirhead, B.K., Nicholas, A.K., Umland, J., Sutherland, O., Vijendran, S., 2020. Mars Sample Return Campaign Concept Status. *Acta Astronautica* 176, 131–138. doi:10.1016/j.actaastro.2020.06.026.
- Mulders, G.D., Pascucci, I., Apai, D., 2015. A Stellar-mass-dependent Drop in Planet Occurrence Rates. *ApJ* 798, 112. doi:10.1088/0004-637x/798/2/112, arXiv:1406.7356.
- Mura, A., Adriani, A., Tosi, F., Lopes, R.M.C., Sindoni, G., Filacchione, G., Williams, D.A., Davies, A.G., Plainaki, C., Bolton, S., Altieri, F., Cicchetti, A., Grassi, D., Migliorini, A., Moriconi, M.L., Nosciese, R., Olivieri, A., Piccioni, G., Sordini, R., 2020. Infrared observations of Io from Juno. *Icarus* 341, 113607. doi:10.1016/j.icarus.2019.113607.
- Mura, A., Wurz, P., Schneider, J., Lammer, H., Grießmeier, J.M., Khodachenko, M., Weingrill, J., Guenther, E., Cabrera, J., Erikson, A., Fridlund, M., Milillo, A., Rauer, H., [von Paris], P., 2011. Comet-like tail-formation of exospheres of hot rocky exoplanets: Possible implications for corot-7b. *Icarus* 211, 1–9. URL: <http://www.sciencedirect.com/science/article/pii/S0019103510003210>, doi:https://doi.org/10.1016/j.icarus.2010.08.015.
- Nagaoka, H., Takeda, H., Karouji, Y., Ohtake, M., Yamaguchi, A., Yoneda, S., Hasebe, N., 2014. Implications for the origins of pure anorthosites found in the feldspathic lunar meteorites, Dhofar 489 group. *Earth, Planets, and Space* 66, 115. doi:10.1186/1880-5981-66-115.
- Nagel, J.R., 2018. Induced eddy currents in simple conductive geometries: Mathematical formalism describes the excitation of electrical eddy currents in a time-varying magnetic field. *IEEE Antennas and Propagation Magazine* 60, 81–88.
- Nakajima, M., Stevenson, D.J., 2015. Melting and mixing states of the Earth's mantle after the Moon-forming impact. *Earth and Planetary Science Letters* 427, 286–295. doi:10.1016/j.epsl.2015.06.023, arXiv:1506.04853.
- Nelson, B.E., Ford, E.B., Wright, J.T., Fischer, D.A., von Braun, K., Howard, A.W., Payne, M.J., Dindar, S., 2014. The 55 Cancri planetary system: fully self-consistent N-body constraints and a dynamical analysis. *Monthly Notices of the Royal Astronomical Society* 441, 442–451. URL: <http://dx.doi.org/10.1093/mnras/stu450>, doi:10.1093/mnras/stu450.
- Neumann, W., Breuer, D., Spohn, T., 2014. Differentiation of Vesta: Implications for a shallow magma ocean. *Earth and Planetary Science Letters* 395, 267–280.
- Ni, H., Keppler, H., 2013. Carbon in Silicate Melts. *Reviews in Mineralogy and Geochemistry* 75, 251–287. doi:10.2138/rmg.2013.75.9.
- Ni, H., Zhang, L., 2018. A general model of water diffusivity in calc-alkaline silicate melts and glasses. *Chemical Geology* 478, 60–68.
- Nikolaou, A., Katyal, N., Tosi, N., Godolt, M., Grenfell, J.L., Rauer, H., 2019. What Factors Affect the Duration and Outgassing of the Terrestrial Magma Ocean? *ApJ* 875, 11. doi:10.3847/1538-4357/ab08ed, arXiv:1903.07436.
- Nimmo, F., 2009. Energetics of asteroid dynamos and the role of compositional convection. *Geophysical Research Letters* 36. URL: <https://agupubs.onlinelibrary.wiley.com/doi/abs/10.1029/2009GL037997>, doi:10.1029/2009GL037997.
- Nittler, L.R., Starr, R.D., Weider, S.Z., McCoy, T.J., Boynton, W.V., Ebel, D.S., Ernst, C.M., Evans, L.G., Goldsten, J.O., Hamara, D.K., Lawrence, D.J., McNutt, R.L., Schlemm, C.E., Solomon, S.C., Sprague, A.L., 2011. The Major-Element Composition of Mercury's Surface from MESSENGER X-ray Spectrometry. *Science* 333, 1847. doi:10.1126/science.1211567.
- Odert, P., Leitzinger, M., Guenther, E.W., Heinzel, P., 2020. Stellar coronal mass ejections - II. Constraints from spectroscopic observations. *MNRAS* 494, 3766–3783. doi:10.1093/mnras/staa1021, arXiv:2004.04063.
- Ofir, A., Dreizler, S., 2013. An independent planet search in the Kepler dataset. I. One hundred new candidates and revised Kepler objects of interest. *A&A* 555, A58. doi:10.1051/0004-6361/201219877, arXiv:1206.5347.
- Olson, P.L., Sharp, Z.D., 2019. Nebular atmosphere to magma ocean: A model for volatile capture during earth accretion. *Physics of the Earth and Planetary Interiors* 294, 1–18. URL: <http://www.sciencedirect.com/science/article/pii/S0031920119300895>, doi:https://doi.org/10.1016/j.pepi.2019.106294.
- O'Rourke, J.G., 2020. Venus: A Thick Basal Magma Ocean May Exist Today. *Geophysical Research Letters*.
- Oszkiewicz, D.A., Skiff, B.A., Moskovitz, N., Kankiewicz, P., Marciniak, A., Licandro, J., Galiazzo, M.A., Zeilinger, W.W., 2017. Non-Vestoid candidate asteroids in the inner main belt. *A&A* 599, A107. doi:10.1051/0004-6361/201629551, arXiv:1612.07788.
- Owen, J.E., 2019. Atmospheric Escape and the Evolution of Close-In Exoplanets. *Annual Review of Earth and Planetary Sciences* 47, 67–90.

- doi:10.1146/annurev-earth-053018-060246, arXiv:1807.07609.
- Owen, J.E., Wu, Y., 2013. Kepler Planets: A Tale of Evaporation. *ApJ* 775, 105. doi:10.1088/0004-637X/775/2/105, arXiv:1303.3899.
- Oza, A.V., Johnson, R.E., Lellouch, E., Schmidt, C., Schneider, N., Huang, C., Gamborino, D., Gebek, A., Wyttenbach, A., Demory, B.O., Mordasini, C., Saxena, P., Dubois, D., Moullet, A., Thomas, N., 2019. Sodium and Potassium Signatures of Volcanic Satellites Orbiting Close-in Gas Giant Exoplanets. *ApJ* 885, 168. doi:10.3847/1538-4357/ab40cc, arXiv:1908.10732.
- Papike, J., Fowler, G., Shearer, C., 1997. Evolution of the lunar crust: SIMS study of plagioclase from ferroan anorthosites. *Geochimica et Cosmochimica Acta* 61, 2343–2350.
- Papike, J.J., Fowler, G.W., Shearer, C.K., Layne, G.D., 1996. Ion microprobe investigation of plagioclase and orthopyroxene from lunar Mg-suite norites: Implications for calculating parental melt REE concentrations and for assessing postcrystallization REE redistribution. *Geochimica et Cosmochimica Acta* 60, 3967–3978. doi:10.1016/0016-7037(96)00212-8.
- Papoular, R.J., Papoular, R., 2014. Some optical properties of graphite from IR to millimetric wavelengths. *MNRAS* 443, 2974–2982. doi:10.1093/mnras/stu1348, arXiv:1407.1175.
- Park, R.S., de Kleer, K., McEwen, A., Bierson, C.J., Davies, A.G., DellaGiustina, D., Ermakov, A.I., Fuller, J., Hamilton, C., Harris, C., Hay, H., Jacobson, R., Keane, J., Kestay, L., Khurana, K., Kirby, K., Lainey, V., Matsuyama, I., McCarthy, C., Nimmo, F., Panning, M., Pommier, A., Rathbun, J., Steinbrügge, G., Stevenson, D., Tsai, V.C., Turtle, E., 2019. Tidal Heating: Lessons from Io and the Jovian System (Report from the KISS Workshop), in: *Lunar and Planetary Science Conference*, p. 1925.
- Parmentier, V., Crossfield, I.J.M., 2018. Exoplanet Phase Curves: Observations and Theory, in: *Handbook of Exoplanets*, p. 116. doi:10.1007/978-3-319-55333-7_116.
- de Pater, I., de Kleer, K., Davies, A.G., Ádámkóvics, M., 2017. "Three decades of Loki Patera observations". *Icarus* 297, 265–281.
- de Pater, I., Marchis, F., Macintosh, B.A., Roe, H.G., Le Mignant, D., Graham, J.R., Davies, A.G., 2004. Keck AO observations of Io in and out of eclipse. *Icarus* 169, 250–263.
- Patrick, M., Swanson, D., Orr, T., 2019. A review of controls on lava lake level: insights from Halema'uma'u Crater, Kīlauea Volcano. *Bulletin of Volcanology* 81, 13. URL: <https://doi.org/10.1007/s00445-019-1268-y>, doi:10.1007/s00445-019-1268-y.
- Patrick, M.R., Orr, T., Swanson, D.A., Lev, E., 2017. Shallow and deep controls on lava lake surface motion at Kīlauea Volcano. *Journal of Volcanology and Geothermal Research* 328, 247–261. URL: <http://dx.doi.org/10.1016/j.jvolgeores.2016.11.010>, doi:10.1016/j.jvolgeores.2016.11.010.
- Pawley, A.R., Holloway, J.R., McMillan, P.F., 1992. The effect of oxygen fugacity on the solubility of carbon-oxygen fluids in basaltic melt. *Earth and Planetary Science Letters* 110, 213–225. doi:10.1016/0012-821X(92)90049-2.
- Peale, S.J., Cassen, P., 1978. Contribution of tidal dissipation to lunar thermal history. *Icarus* 36, 245–269. doi:10.1016/0019-1035(78)90109-4.
- Pepe, F., Cameron, A.C., Latham, D.W., Molinari, E., Udry, S., Bonomo, A.S., Buchhave, L.A., Charbonneau, D., Cosentino, R., Dressing, C.D., et al., 2013. An Earth-sized planet with an Earth-like density. *Nature* 503, 377–380. URL: <http://dx.doi.org/10.1038/nature12768>, doi:10.1038/nature12768.
- Peplowski, P.N., Klima, R.L., Lawrence, D.J., Ernst, C.M., Denevi, B.W., Frank, E.A., Goldsten, J.O., Murchie, S.L., Nittler, L.R., Solomon, S.C., 2016. Remote sensing evidence for an ancient carbon-bearing crust on Mercury. *Nature Geoscience* 9, 273–276.
- Perez-Becker, D., Chiang, E., 2013. Catastrophic evaporation of rocky planets. *MNRAS* 433, 2294–2309. doi:10.1093/mnras/stt895, arXiv:1302.2147.
- Perez-Becker, D., Chiang, E., 2013. Catastrophic evaporation of rocky planets. *Monthly Notices of the Royal Astronomical Society* 433, 2294–2309. URL: <https://doi.org/10.1093/mnras/stt895>, doi:10.1093/mnras/stt895.
- Pering, T.D., Ilanko, T., Wilkes, T.C., England, R.A., Silcock, S.R., Stanger, L.R., Willmott, J.R., Bryant, R.G., McGonigle, A.J.S., 2019. A Rapidly Convecting Lava Lake at Masaya Volcano, Nicaragua. *Frontiers in Earth Science* 6, 241. URL: <https://www.frontiersin.org/article/10.3389/feart.2018.00241>, doi:10.3389/feart.2018.00241.
- Peron, S., Moreira, M., Putlitz, B., Kurz, M., 2017. Solar wind implantation supplied light volatiles during the first stage of Earth accretion. *Geochemical Perspectives Letters* 3, 151–159.
- Peters, M.A., Turner, E.L., 2013. On the direct imaging of tidally heated exomoons. *The Astrophysical Journal* 769, 98. URL: <http://dx.doi.org/10.1088/0004-637X/769/2/98>, doi:10.1088/0004-637X/769/2/98.
- Peters, N., Oppenheimer, C., Kyle, P., Kingsbury, N., 2014. Decadal persistence of cycles in lava lake motion at Erebus volcano, Antarctica. *Earth and Planetary Science Letters* 395, 1–12. URL: <http://www.sciencedirect.com/science/article/pii/S0012821X14001848>, doi:https://doi.org/10.1016/j.epsl.2014.03.032.
- Petersburg, R.R., Ong, J.M.J., Zhao, L.L., Blackman, R.T., Brewer, J.M., Buchhave, L.A., Cabot, S.H.C., Davis, A.B., Jurgenson, C.A., Leet, C., McCracken, T.M., Sawyer, D., Sharov, M., Trongsgaard, R., Szymkowiak, A.E., Fischer, D.A., 2020. An Extreme-precision Radial-velocity Pipeline: First Radial Velocities from EXPRES. *AJ* 159, 187. doi:10.3847/1538-3881/ab7e31, arXiv:2003.08851.
- Petrovich, C., Deibert, E., Wu, Y., 2019. Ultra-short-period Planets from Secular Chaos. *AJ* 157, 180. doi:10.3847/1538-3881/ab0e0a, arXiv:1804.05065.
- Phillips, R.J., Raubertas, R.F., Arvidson, R.E., Sarkar, I.C., Herrick, R.R., Izenberg, N., Grimm, R.E., 1992. Impact craters and Venus resurfacing history. *Journal of Geophysical Research: Planets* 97, 15923–15948.
- Pierrehumbert, R., Gaidos, E., 2011. Hydrogen Greenhouse Planets Beyond the Habitable Zone. *ApJ* 734, L13. doi:10.1088/2041-8205/734/L13, arXiv:1105.0021.
- Pieters, C.M., Noble, S.K., 2016. Space weathering on airless bodies. *Journal of Geophysical Research (Planets)* 121, 1865–1884. doi:10.1002/2016JE005128.
- Pignatella, F.C., Charnoz, S., Rosenblatt, P., Hyodo, R., Nakamura, T., Genda, H., 2018. On the Impact Origin of Phobos and Deimos. III. Resulting Composition from Different Impactors. *ApJ* 853, 118. doi:10.3847/1538-4357/aaa23e, arXiv:1712.05154.
- Pinkerton, H., Stevenson, R., 1992. Methods of determining the rheological properties of magmas at sub-liquidus temperatures. *Journal of Volcanology and Geothermal Research* 53, 47–66. URL: <http://www.sciencedirect.com/science/article/pii/037702739290073M>, doi:https://doi.org/10.1016/0377-0273(92)90073-M.
- Pluriel, W., Marq, E., Turbet, M., 2019. Modeling the albedo of Earth-like magma ocean planets with H₂O-CO₂ atmospheres. *Icarus* 317, 583–590. doi:10.1016/j.icarus.2018.08.023, arXiv:1809.02036.
- Pommier, A., Gaillard, F., Malki, M., Pichavant, M., 2010. Methodological re-evaluation of the electrical conductivity of silicate melts. *American Mineralogist* 95, 284–291. URL: <https://pubs.geoscienceworld.org/georef/record/6/3179491/Methodological-re-evaluation-of-the-electrical>, doi:10.2138/am.2010.3314.
- Pont, F., Aigrain, S., Zucker, S., 2011. Reassessing the radial-velocity evidence for planets around CoRoT-7. *Monthly Notices of the Royal Astronomical Society* 411, 1953–1962. URL: <https://doi.org/10.1111/j.1365-2966.2010.17823.x>, doi:10.1111/j.1365-2966.2010.17823.x.
- Price, E.M., Rogers, L.A., 2020. Tidally Distorted, Iron-enhanced Exoplanets Closely Orbiting Their Stars. *ApJ* 894, 8. doi:10.3847/1538-4357/ab7c67, arXiv:1901.10666.
- Pu, B., Valencia, D., 2017. Ohmic Dissipation in Mini-Neptunes. *ApJ* 846, 47. doi:10.3847/1538-4357/aa826f, arXiv:1709.01642.
- Qin, L., Dauphas, N., Wadhwa, M., Masarik, J., Janney, P.E., 2008. Rapid accretion and differentiation of iron meteorite parent bodies inferred from ¹⁸²Hf-¹⁸²W chronometry and thermal modeling. *Earth and Planetary Science Letters* 273, 94–104. doi:10.1016/j.epsl.2008.06.018.
- Queloz, D., Bouchy, F., Moutou, C., Hatzes, A., Hébrard, G., Alonso, R., Auvergne, M., Baglin, A., Barbieri, M., Barge, P., Benz, W., Bordé, P., Deeg, H.J., Deleuil, M., Dvorak, R., Erikson, A., Ferraz Mello, S., Fridlund, M., Gandolfi, D., Gillon, M., Guenther, E., Guillot, T., Jorda, L.,

- Hartmann, M., Lammer, H., Léger, A., Llebaria, A., Lovis, C., Magain, P., Mayor, M., Mazeh, T., Olivier, M., Pätzold, M., Pepe, F., Rauer, H., Rouan, D., Schneider, J., Segransan, D., Udry, S., Wuchterl, G., 2009. The CoRoT-7netary system: two orbiting super-Earths. *A&A* 506, 303–319. URL: <https://doi.org/10.1051/0004-6361/200913096>, doi:10.1051/0004-6361/200913096.
- Radebaugh, J., Keszthelyi, L.P., McEwen, A.S., Turtle, E.P., Jaeger, W., Milazzo, M., 2001. Paterae on Io: A new type of volcanic caldera? *Journal of Geophysical Research* 106, 33005–33020.
- Ramirez, R.M., Kaltenecker, L., 2017. A Volcanic Hydrogen Habitable Zone. *ApJ* 837, L4. doi:10.3847/2041-8213/aa60c8, arXiv:1702.08618.
- Rapp, J.F., Draper, D.S., 2018. Fractional crystallization of the lunar magma ocean: Updating the dominant paradigm. *Meteoritics & Planetary Science* 53, 1432–1455. URL: <http://doi.wiley.com/10.1111/maps.13086>, doi:10.1111/maps.13086.
- Rappaport, S., Levine, A., Chiang, E., El Mellah, I., Jenkins, J., Kalomeni, B., Kite, E.S., Kotson, M., Nelson, L., Rousseau-Nepton, L., Tran, K., 2012. Possible Disintegrating Short-period Super-Mercury Orbiting KIC 12557548. *ApJ* 752, 1. doi:10.1088/0004-637X/752/1/1, arXiv:1201.2662.
- Rappaport, S., Sanchis-Ojeda, R., Rogers, L.A., Levine, A., Winn, J.N., 2013. The Roche Limit for Close-orbiting Planets: Minimum Density, Composition Constraints, and Application to the 4.2 hr Planet KOI 1843.03. *ApJ* 773, L15. doi:10.1088/2041-8205/773/1/L15, arXiv:1307.4080.
- Rathbun, J.A., Spencer, J., Davies, A., Howell, R., Wilson, L., 2002. Loki, Io: A periodic volcano. *Geophysical Research Letters* 29, 84–1.
- Rauscher, E., Suri, V., Cowan, N.B., 2018. A More Informative Map: Inverting Thermal Orbital Phase and Eclipse Light Curves of Exoplanets. *AJ* 156, 235. doi:10.3847/1538-3881/aae57f, arXiv:1806.05700.
- Ray, R.D., Egbert, G.D., 2012. Fortnightly Earth rotation, ocean tides and mantle anelasticity. *Geophysical Journal International* 189, 400–413. doi:10.1111/j.1365-246X.2012.05351.x.
- Reddy, V., Dunn, T.L., Thomas, C.A., Moskovitz, N.A., Burbine, T.H., 2015. Mineralogy and Surface Composition of Asteroids. *Asteroids IV* URL: http://dx.doi.org/10.2458/azu_uapress_9780816532131-ch003, doi:10.2458/azu_uapress_9780816532131-ch003.
- Reese, C.C., Orth, C.P., Solomastov, V.S., 2011. Impact megadomes and the origin of the martian crustal dichotomy. *Icarus* 213, 433–442. doi:10.1016/j.icarus.2011.03.028.
- Rengli, C.J., King, P.L., Henley, R.W., Norman, M.D., 2017. Volcanic gas composition, metal dispersion and deposition during explosive volcanic eruptions on the Moon. *Geochim. Cosmochim. Acta* 206, 296–311. doi:10.1016/j.gca.2017.03.012.
- Ricker, G.R., Winn, J.N., Vanderspek, R., Latham, D.W., Bakos, G.Á., Bean, J.L., Berta-Thompson, Z.K., Brown, T.M., Buchhave, L., Butler, N.R., Butler, R.P., Chaplin, W.J., Charbonneau, D., Christensen-Dalsgaard, J., Clampin, M., Deming, D., Doty, J., De Lee, N., Dressing, C., Dunham, E.W., Endl, M., Fressin, F., Ge, J., Henning, T., Holman, M.J., Howard, A.W., Ida, S., Jenkins, J., Jernigan, G., Johnson, J.A., Kaltenecker, L., Kawai, N., Kjeldsen, H., Laughlin, G., Levine, A.M., Lin, D., Lissauer, J.J., MacQueen, P., Marcy, G., McCullough, P.R., Morton, T.D., Narita, N., Paegert, M., Palle, E., Pepe, F., Pepper, J., Quirrenbach, A., Rinehart, S.A., Sasselov, D., Sato, B., Seager, S., Sozzetti, A., Stassun, K.G., Sullivan, P., Szentgyorgyi, A., Torres, G., Udry, S., Villaseñor, J., 2014. Transiting Exoplanet Survey Satellite (TESS), in: *Proc. SPIE*, p. 914320. doi:10.1117/12.2063489, arXiv:1406.0151.
- Ridden-Harper, A.R., Snellen, I.A.G., Keller, C.U., de Kok, R.J., Di Gloria, E., Hoeijmakers, H.J., Brogi, M., Fridlund, M., Vermeersen, B.L.A., van Westrenen, W., 2016. Search for an exosphere in sodium and calcium in the transmission spectrum of exoplanet 55 Cancri e. *Astronomy & Astrophysics* 593, A129. URL: <http://dx.doi.org/10.1051/0004-6361/201628448>, doi:10.1051/0004-6361/201628448.
- Righter, K., Drake, M.J., 1997. A magma ocean on Vesta: Core formation and petrogenesis of eucrites and diogenites. *Meteoritics & Planetary Science* 32, 929–944.
- Rimmer, P.B., Rugheimer, S., 2019. Hydrogen cyanide in nitrogen-rich atmospheres of rocky exoplanets. *Icarus* 329, 124–131. doi:10.1016/j.icarus.2019.02.020, arXiv:1902.08022.
- Ringwood, A.E., 1966. Chemical evolution of the terrestrial planets. *Geochimica et Cosmochimica Acta* 30, 41–104.
- Robinson, T.D., Catling, D.C., 2012. An Analytic Radiative-Convective Model for Planetary Atmospheres. *ApJ* 757, 104. doi:10.1088/0004-637X/757/1/104, arXiv:1209.1833.
- Robinson, T.D., Catling, D.C., 2014. Common 0.1 bar tropopause in thick atmospheres set by pressure-dependent infrared transparency. *Nature Geoscience* 7, 12–15. doi:10.1038/ngeo2020, arXiv:1312.6859.
- Rodríguez Martínez, R., Lopez, L.A., Shappee, B.J., Schmidt, S.J., Jayasinghe, T., Kochanek, C.S., Auchtell, K., Holoiien, T.W.S., 2020. A Catalog of M-dwarf Flares with ASAS-SN. *ApJ* 892, 144. doi:10.3847/1538-4357/ab793a, arXiv:1912.05549.
- Rodríguez-Mozos, J.M., Moya, A., 2019. Erosion of an exoplanetary atmosphere caused by stellar winds. *A&A* 630, A52. doi:10.1051/0004-6361/201935543, arXiv:1908.06695.
- Roig, F., Nesvorný, D., Gil-Hutton, R., Lazzaro, D., 2008. V-type asteroids in the middle main belt. *Icarus* 194, 125–136. doi:10.1016/j.icarus.2007.10.004, arXiv:0707.1012.
- de Ronde, C.E.J., Chadwick, W.W., Ditchburn, R.G., Embley, R.W., Tunnicliffe, V., Baker, E.T., Walker, S.L., Ferrini, V.L., Merle, S.M., 2015. Molten sulfur lakes of intraoceanic arc volcanoes, in: Rouwet, D., Christenson, B., Tassi, F., Vandemeulebrouck, J. (Eds.), *Volcanic Lakes*. Springer Berlin Heidelberg, Berlin, Heidelberg, pp. 261–288. URL: https://doi.org/10.1007/978-3-642-36833-2_11, doi:10.1007/978-3-642-36833-2_11.
- Rothery, D.A., Massironi, M., Alemanno, G., Barraud, O., Besse, S., Bott, N., Brunetto, R., Bunce, E., Byrne, P., Capaccioni, F., Capria, M.T., Carli, C., Charlier, B., Cornet, T., Cremonese, G., D’Amore, M., De Sanctis, M.C., Doressoundiram, A., Ferranti, L.G., Filacchione, G., Galluzzi, V., Giacomini, L., Grande, M., Guzzetta, L.G., Helbert, J., Heyner, D., Hiesinger, H., Hussmann, H., Hyodo, R., Kohout, T., Kozirev, A., Litvak, M., Lucchetti, A., Malakhov, A., Malliband, C., Mancinelli, P., Martikainen, J., Martindale, A., Maturilli, A., Milillo, A., Mitrofanov, I., Mokrousov, M., Morlok, A., Muinonen, K., Namur, O., Owens, A., Nittler, L.R., Oliveira, J.S., Palumbo, P., Pajola, M., Pegg, D.L., Penttilä, A., Politi, R., Quarati, F., Re, C., Sanin, A., Schulz, R., Stangarone, C., Stojic, A., Tretyakov, V., Väisänen, T., Varatharajan, I., Weber, I., Wright, J., Wurz, P., Zambon, F., 2020. Rationale for BepiColombo Studies of Mercury’s Surface and Composition. *Space Sci. Rev.* 216, 66. doi:10.1007/s11214-020-00694-7.
- Rouan, D., Deeg, H.J., Demangeon, O., Samuel, B., Cavarroc, C., Fegley, B., Léger, A., 2011. The Orbital Phases and Secondary Transits of Kepler-10b. A Physical Interpretation Based on the Lava-ocean Planet Model. *ApJ* 741, L30. doi:10.1088/2041-8205/741/2/L30, arXiv:1109.2768.
- Rubie, D., Nimmo, F., Melosh, H., 2007. Formation of earth’s core, in: Schubert, G. (Ed.), *Treatise on Geophysics*. Elsevier, Amsterdam, pp. 51–90. URL: <http://www.sciencedirect.com/science/article/pii/B9780444527486001401>, doi:https://doi.org/10.1016/B978-044452748-6.00140-1.
- Rufu, R., Aharonson, O., Perets, H.B., 2017. A multiple-impact origin for the Moon. *Nature Geoscience* 10, 89–94.
- Sahu, K.C., Casertano, S., Bond, H.E., Valenti, J., Ed Smith, T., Minniti, D., Zoccali, M., Livio, M., Panagia, N., Piskunov, N., et al., 2006. Transiting extrasolar planetary candidates in the Galactic bulge. *Nature* 443, 534–540. URL: <http://dx.doi.org/10.1038/nature05158>, doi:10.1038/nature05158.
- Sanchis-Ojeda, R., Rappaport, S., Pallè, E., Delrez, L., DeVore, J., Gandolfi, D., Fukui, A., Ribas, I., Stassun, K.G., Albrecht, S., Dai, F., Gaidos, E., Gillon, M., Hirano, T., Holman, M., Howard, A.W., Isaacson, H., Jehin, E., Kuzuhara, M., Mann, A.W., Marcy, G.W., Miles-Páez, P.A., Montañés-Rodríguez, P., Murgas, F., Narita, N., Nowak, G., Onitsuka, M., Paegert, M., Van Eylen, V., Winn, J.N., Yu, L., 2015. The K2-ESPRINT Project I: Discovery of the Disintegrating Rocky Planet K2-22b with a Cometary Head and Leading Tail. *ApJ* 812, 112. doi:10.1088/0004-637X/812/2/112, arXiv:1504.04379.

- Sanchis-Ojeda, R., Rappaport, S., Winn, J.N., Kotson, M.C., Levine, A., El Mellah, I., 2014. A Study of the Shortest-period Planets Found with Kepler. *ApJ* 787, 47. doi:10.1088/0004-637X/787/1/47, arXiv:1403.2379.
- Sanchis-Ojeda, R., Rappaport, S., Winn, J.N., Levine, A., Kotson, M.C., Latham, D.W., Buchhave, L.A., 2013. Transits and occultations of an Earth-sized planet in an 8.5 hr orbit. *The Astrophysical Journal* 774, 54. URL: <http://dx.doi.org/10.1088/0004-637X/774/1/54>, doi:10.1088/0004-637X/774/1/54.
- Sarafian, E., Gaetani, G.A., Hauri, E.H., Sarafian, A.R., 2017. Experimental constraints on the damp peridotite solidus and oceanic mantle potential temperature. *Science* 355, 942–945. URL: <https://science.sciencemag.org/content/355/6328/942>, doi:10.1126/science.aaj2165, arXiv:<https://science.sciencemag.org/content/355/6328/942.full.pdf>.
- Schaefer, B.E., Bentley, R.O., Boyajian, T.S., Coker, P.H., Dvorak, S., Dubois, F., Erdelyi, E., Ellis, T., Graham, K., Harris, B.G., Hall, J.E., James, R., Johnston, S.J., Kennedy, G., Logie, L., Nugent, K.M., Oksanen, A., Ott, J.J., Rau, S., Vanaverbeke, S., van Lieshout, R., Wyatt, M., 2018. The KIC 8462852 light curve from 2015.75 to 2018.18 shows a variable secular decline. *MNRAS* 481, 2235–2248. doi:10.1093/mnras/sty1644, arXiv:1806.09911.
- Schaefer, L., Fegley, B., 2007. Outgassing of ordinary chondritic material and some of its implications for the chemistry of asteroids, planets, and satellites. *Icarus* 186, 462–483. doi:10.1016/j.icarus.2006.09.002, arXiv:astro-ph/0606671.
- Schaefer, L., Fegley, B., 2009. Chemistry of Silicate Atmospheres of Evaporating Super-Earths. *ApJ* 703, L113–L117. doi:10.1088/0004-637X/703/2/L113, arXiv:0906.1204.
- Schaefer, L., Fegley, B., 2009. Chemistry of silicate atmospheres of evaporating super-Earths. *The Astrophysical Journal* 703, L113–L117. URL: <https://doi.org/10.1088/0004-637X/703/2/L113>, doi:10.1088/0004-637X/703/2/L113.
- Schaefer, L., Fegley, Bruce, J., 2017. Redox States of Initial Atmospheres Outgassed on Rocky Planets and Planetsimals. *ApJ* 843, 120. doi:10.3847/1538-4357/aa784f.
- Schaefer, L., Wordsworth, R.D., Berta-Thompson, Z., Sasselov, D., 2016. Predictions of the Atmospheric Composition of GJ 1132b. *ApJ* 829, 63. doi:10.3847/0004-637X/829/2/63, arXiv:1607.03906.
- Schiller, M., Baker, J., Creech, J., Paton, C., Millet, M.A., Irving, A., Bizzarro, M., 2011. Rapid Timescales for Magma Ocean Crystallization on the Howardite-Eucrite-Diogenite Parent Body. *ApJ* 740, L22. doi:10.1088/2041-8205/740/1/L22.
- Schiller, M., Connelly, J.N., Bizzarro, M., 2017. Lead and Mg isotopic age constraints on the evolution of the HED parent body. *Meteoritics and Planetary Science* 52, 1233–1243. doi:10.1111/maps.12848.
- Schulz, R., Benkhoff, J., 2006. BepiColombo: Payload and mission updates. *Advances in Space Research* 38, 572–577. doi:10.1016/j.asr.2005.05.084.
- Scora, J., Valencia, D., Morbidelli, A., Jacobson, S., 2020. Chemical diversity of super-Earths as a consequence of formation. *MNRAS* 493, 4910–4924. doi:10.1093/mnras/staa568, arXiv:2002.09042.
- Sehlike, A., Whittington, A., 2020. Rheology of a creep analog magma: Experimental results applied to dike ascent through the lunar crust. *Planetary and Space Science* 187, 104941. URL: <http://www.sciencedirect.com/science/article/pii/S0032063319303745>, doi:<https://doi.org/10.1016/j.pss.2020.104941>.
- Sheets, H.A., Deming, D., 2014. Statistical Eclipses of Close-in Kepler Sub-Saturns. *ApJ* 794, 133. doi:10.1088/0004-637X/794/2/133, arXiv:1408.6234.
- Sematovich, V.I., Marov, M.Y., 2018. Escape of planetary atmospheres: physical processes and numerical models. *Physics-Uspexhi* 61, 217–246. URL: <https://doi.org/10.3367/ufne.2017.09.038212>, doi:10.3367/ufne.2017.09.038212.
- Showman, A.P., Polvani, L.M., 2011. Equatorial Superrotation on Tidally Locked Exoplanets. *ApJ* 738, 71. doi:10.1088/0004-637X/738/1/71, arXiv:1103.3101.
- Shreve, T., Grandin, R., Boichu, M., Garaebiti, E., Moussallam, Y., Ballu, V., Delgado, F., Leclerc, F., Vallée, M., Henriot, N., Ceuvarud, S., Tari, D., Lebellegard, P., Pelletier, B., 2019. From prodigious volcanic degassing to caldera subsidence and quiescence at Ambrym (Vanuatu): the influence of regional tectonics. *Scientific Reports* 9, 18868. URL: <https://doi.org/10.1038/s41598-019-55141-7>, doi:10.1038/s41598-019-55141-7.
- Simonelli, D.P., Dodd, C., Veverka, J., 2001. Regolith variations on Io: Implications for bolometric albedos. *J. Geophys. Res.* 106, 33241–33252. doi:10.1029/2000JE001350.
- Skumanich, A., 1972. Time Scales for CA II Emission Decay, Rotational Braking, and Lithium Depletion. *ApJ* 171, 565. doi:10.1086/151310.
- Smith, J., Anderson, A., Newton, R., Olsen, E., Wyllie, P., Crewe, A., Isaacson, M., Johnson, D., 1970. Petrologic History of the Moon inferred from Petrography, Mineralogy, and Petrogenesis of Apollo 11 Rocks. *Proceedings of the Apollo 11 Lunar Science Conference 1*, 897–925.
- Smrekar, S.E., Davaille, A., Sotin, C., 2018. Venus Interior Structure and Dynamics. *Space Sci. Rev.* 214, 88. doi:10.1007/s11214-018-0518-1.
- Snyder, G.A., Taylor, L.A., Halliday, A.N., 1995. Chronology and petrogenesis of the lunar highlands alkali suite: Cumulates from creep basalt crystallization. *Geochimica et Cosmochimica Acta* 59, 1185–1203. URL: <http://www.sciencedirect.com/science/article/pii/S001670379500034W>, doi:[https://doi.org/10.1016/0016-7037\(95\)00034-W](https://doi.org/10.1016/0016-7037(95)00034-W).
- Solomatov, V., 2015. Magma oceans and primordial mantle differentiation, in: Schubert, G. (Ed.), *Treatise on Geophysics (Second Edition)*. second edition ed. Elsevier, Oxford, pp. 81–104. doi:<https://doi.org/10.1016/B978-0-444-53802-4.00155-X>.
- Solomatova, N., Caracas, R., 2019. Pressure-induced coordination changes in a pyrolytic silicate melt from ab initio molecular dynamics simulations. *Journal of Geophysical Research: Solid Earth* 124, 11232–11250.
- Solomon, S.C., McNutt, R.L., Gold, R.E., Domingue, D.L., 2007. MESSENGER Mission Overview. *Space Sci. Rev.* 131, 3–39. doi:10.1007/s11214-007-9247-6.
- Sonett, C.P., Colburn, D.S., Schwartz, K., 1968. Electrical Heating of Meteorite Parent Bodies and Planets by Dynamo Induction from a Pre-main Sequence T Tauri “Solar Wind”. *Nature* 219, 924–926. doi:10.1038/219924a0.
- Sonett, C.P., Colburn, D.S., Schwartz, K., 1975. Formation of the Lunar Crust: An Electrical Source of Heating. *Icarus* 24, 231–255. doi:10.1016/0019-1035(75)90101-3.
- Soubiran, F., Militzer, B., 2018. Electrical conductivity and magnetic dynamos in magma oceans of super-Earths. *Nature Communications* 9, 3883. URL: <https://doi.org/10.1038/s41467-018-06432-6>, doi:10.1038/s41467-018-06432-6.
- Spampinato, L., Oppenheimer, C., Calvari, S., Cannata, A., Montalto, P., 2008. Lava lake surface characterization by thermal imaging: Erta 'Ale volcano (Ethiopia). *Geochemistry, Geophysics, Geosystems* 9. doi:10.1029/2008GC002164.
- Spinetti, C., Mazarini, F., Casacchia, R., Colini, L., Neri, M., Behncke, B., Salvatori, R., Buongiorno, M.F., Pareschi, M., 2009. Spectral properties of volcanic materials from hyperspectral field and satellite data compared with LiDAR data at Mt. Etna. *International Journal of Applied Earth Observation and Geoinformation* 11, 142–155. doi:10.1016/j.jag.2009.01.001.
- Spohn, T., Sohl, F., Wiczerkowski, K., Conzelmann, V., 2001. The interior structure of Mercury: what we know, what we expect from BepiColombo. *Planet. Space Sci.* 49, 1561–1570. doi:10.1016/S0032-0633(01)00093-9.
- Stassun, K.G., Collins, K.A., Gaudi, B.S., 2017. Accurate Empirical Radii and Masses of Planets and Their Host Stars with Gaia Parallaxes. *The Astronomical Journal* 153, 136. URL: <https://doi.org/10.3847/1538-3881/aa5df3>, doi:10.3847/1538-3881/aa5df3.
- Stern, S.A., 1994. The Detectability of Extrasolar Terrestrial and Giant Planets During Their Luminous Final Accretion. *AJ* 108, 2312. doi:10.1086/117243.
- Stovall, W.K., Houghton, B.F., Harris, A.J.L., Swanson, D.A., 2009. A frozen record of density-driven crustal overturn in lava lakes: the example of Kilauea Iki 1959. *Bulletin of Volcanology* 71, 313–318. URL: <https://doi.org/10.1007/s00445-008-0225-y>, doi:10.1007/s00445-008-0225-y.
- Sulis, S., Dragomir, D., Lendl, M., Bourrier, V., Demory, B.O., Fossati,

- L., Cubillos, P.E., Guenther, D.B., Kane, S.R., Kuschnig, R., Matthews, J.M., Moffat, A.F.J., Rowe, J.F., Sasselov, D., Weiss, W.W., Winn, J.N., 2019. Multi-season optical modulation phased with the orbit of the super-Earth 55 Cancri e. *A&A* 631, A129. doi:10.1051/0004-6361/201936066, arXiv:1910.00383.
- Sweeney, D., Kyle, P.R., Oppenheimer, C., 2008. Sulfur dioxide emissions and degassing behavior of Erebus volcano, Antarctica. *Journal of Volcanology and Geothermal Research* 177, 725–733.
- Sweetser, T., Peterson, C., Nilsen, E., Gershman, B., 2003. Venus sample return missions—a range of science, a range of costs. *Acta Astronautica* 52, 165 – 172. URL: <http://www.sciencedirect.com/science/article/pii/S0094576502001534>, doi:[https://doi.org/10.1016/S0094-5765\(02\)00153-4](https://doi.org/10.1016/S0094-5765(02)00153-4). selected Proceedings of the 4th IAA International conference on Low Cost Planetary Missions.
- Szentgyorgyi, A., Baldwin, D., Barnes, S., Bean, J., Ben-Ami, S., Brennan, P., Budynkiewicz, J., Catropa, D., Chun, M.Y., Conroy, C., Contos, A., Crane, J.D., Durusky, D., Epps, H., Evans, I., Evans, J., Fishman, V., Frebel, A., Gauron, T., Guzman, D., Hare, T., Jang, B.H., Jang, J.G., Jordan, A., Kim, J., Kim, K.M., Kim, Y., Lee, S., Lopez-Morales, M., Mendes de Oliveira, C., McCracken, K., McMuldroy, S., Miller, J., Mueller, M., Oh, J.S., Onyuksel, C., Park, B.G., Park, C., Park, S.J., Paxson, C., Phillips, D., Plummer, D., Podgorski, W., Rubin, A., Seifahrt, A., Stark, D., Steiner, J., Uomoto, A., Walsworth, R., Yu, Y.S., 2018. The GMT-consortium large earth finder (G-CLEF): an optical echelle spectrograph for the Giant Magellan Telescope (GMT), in: *Ground-based and Airborne Instrumentation for Astronomy VII*, p. 107021R. doi:10.1117/12.2313539.
- Tamburo, P., Mandell, A., Deming, D., Garhart, E., 2018. Confirming Variability in the Secondary Eclipse Depth of the Super-Earth 55 Cancri e. *The Astronomical Journal* 155, 221. URL: <http://dx.doi.org/10.3847/1538-3881/aabd84>, doi:10.3847/1538-3881/aabd84.
- Tang, H., Dauphas, N., 2012. Abundance, distribution, and origin of ^{60}Fe in the solar protoplanetary disk. *Earth and Planetary Science Letters* 359, 248–263. doi:10.1016/j.epsl.2012.10.011, arXiv:1212.1490.
- Taylor, G.J., 2013. The bulk composition of Mars. *Geochemistry* 73, 401–420.
- Teske, J.K., Cunha, K., Schuler, S.C., Griffith, C.A., Smith, V.V., 2013. Carbon and oxygen abundances in cool metal-rich exoplanet hosts: A case study of the C/O ratio of 55 Cancri. *The Astrophysical Journal* 778, 132. URL: <http://dx.doi.org/10.1088/0004-637X/778/2/132>, doi:10.1088/0004-637X/778/2/132.
- Thomas, R.J., Rothery, D.A., Conway, S.J., Anand, M., 2014. Long-lived explosive volcanism on Mercury. *Geophysical Research Letters* 41, 6084–6092. URL: <https://agupubs.onlinelibrary.wiley.com/doi/abs/10.1002/2014GL061224>, doi:10.1002/2014GL061224, arXiv:<https://agupubs.onlinelibrary.wiley.com/doi/pdf/10.1002/2014GL061224>.
- Tian, F., 2015. History of water loss and atmospheric O_2 buildup on rocky exoplanets near M dwarfs. *Earth and Planetary Science Letters* 432, 126–132. doi:10.1016/j.epsl.2015.09.051.
- Tian, F., Güdel, M., Johnstone, C.P., Lammer, H., Luger, R., Odert, P., 2018. Water Loss from Young Planets. *Space Sci. Rev.* 214, 65. doi:10.1007/s11214-018-0490-9.
- Tian, F., Toon, O.B., Pavlov, A.A., De Sterck, H., 2005. A Hydrogen-Rich Early Earth Atmosphere. *Science* 308, 1014–1017. doi:10.1126/science.1106983.
- Tilling, R.I., 1987. Fluctuations in surface height of active lava lakes during 1972–1974 Mauna Ulu eruption, Kilauea volcano, Hawaii. *Journal of Geophysical Research: Solid Earth* 92, 13721–13730.
- Tretyakov, V., Mitrofanov, I., Zeleniy, L., 2020. Russian Lunar Landers Luna-25 and Lna-27: goals of the missions and scientific investigations at Moon Polar Regions, in: *EGU General Assembly Conference Abstracts*, p. 6753.
- Tsiasas, A., Rocchetto, M., Waldmann, I.P., Venot, O., Varley, R., Morello, G., Damiano, M., Tinetti, G., Barton, E.J., Yurchenko, S.N., et al., 2016. Detection of an atmosphere around the super-Earth 55 Cancri e. *The Astrophysical Journal* 820, 99. URL: <http://dx.doi.org/10.3847/0004-637X/820/2/99>, doi:10.3847/0004-637X/820/2/99.
- Tu, L., Johnstone, C.P., Güdel, M., Lammer, H., 2015. The extreme ultraviolet and X-ray Sun in Time: High-energy evolutionary tracks of a solar-like star. *A&A* 577, L3. doi:10.1051/0004-6361/201526146, arXiv:1504.04546.
- Turcotte, D.L., Schubert, G., 2002. *Geodynamics - 2nd Edition*. doi:10.2277/0521661862.
- Valade, S., Ripepe, M., Giuffrida, G., Karume, K., Tedesco, D., 2018. Dynamics of mount nyiragongo lava lake inferred from thermal imaging and infrared sound array. *Earth and Planetary Science Letters* 500, 192 – 204. URL: <http://www.sciencedirect.com/science/article/pii/S0012821X18304631>, doi:<https://doi.org/10.1016/j.epsl.2018.08.004>.
- Valencia, D., Ikoma, M., Guillot, T., Nettelmann, N., 2010. Composition and fate of short-period super-Earths. *Astronomy and Astrophysics* 516, A20. URL: <http://dx.doi.org/10.1051/0004-6361/200912839>, doi:10.1051/0004-6361/200912839.
- van Lieshout, R., Min, M., Dominik, C., Brogi, M., de Graaff, T., Hekker, S., Kama, M., Keller, C.U., Ridden-Harper, A., van Werkhoven, T.I.M., 2016. Dusty tails of evaporating exoplanets. II. Physical modelling of the KIC 12557548b light curve. *A&A* 596, A32. doi:10.1051/0004-6361/201629250, arXiv:1609.00275.
- van Summeren, J., Conrad, C.P., Gaidos, E., 2011. Mantle Convection, Plate Tectonics, and Volcanism on Hot Exo-Earths. *ApJ* 736, L15. doi:10.1088/2041-8205/736/1/L15, arXiv:1106.4341.
- Vander Kaaden, K.E., McCubbin, F.M., Byrne, P.K., Chabot, N.L., Ernst, C.M., Johnson, C.L., Thompson, M.S., 2019. Revolutionizing Our Understanding of the Solar System via Sample Return from Mercury. *Space Sci. Rev.* 215, 49. doi:10.1007/s11214-019-0614-x.
- Veeder, G.J., Matson, D.L., Johnson, T.V., Blaney, D.L., Goguen, J.D., 1994. Io's heat flow from infrared radiometry: 1983–1993. *Journal of Geophysical Research: Planets* 99, 17095–17162.
- Veras, D., Wolszczan, A., 2019. Survivability of radio-loud planetary cores orbiting white dwarfs. *MNRAS* 488, 153–163. doi:10.1093/mnras/stz1721, arXiv:1906.08273.
- Vidotto, A.A., Gregory, S.G., Jardine, M., Donati, J.F., Petit, P., Morin, J., Folsom, C.P., Bouvier, J., Cameron, A.C., Hussain, G., Marsden, S., Waite, I.A., Fares, R., Jeffers, S., do Nascimento, J.D., 2014. Stellar magnetism: empirical trends with age and rotation. *MNRAS* 441, 2361–2374. doi:10.1093/mnras/stu728, arXiv:1404.2733.
- Volkov, A.N., Johnson, R.E., Tucker, O.J., Erwin, J.T., 2011. Thermally Driven Atmospheric Escape: Transition from Hydrodynamic to Jeans Escape. *ApJ* 729, L24. doi:10.1088/2041-8205/729/L24, arXiv:1009.5110.
- Wagner, F.W., Tosi, N., Sohl, F., Rauer, H., Spohn, T., 2012. Rocky super-Earth interiors. Structure and internal dynamics of CoRoT-7b and Kepler-10b. *A&A* 541, A103. doi:10.1051/0004-6361/201118441.
- Walker, D., Longhi, J., Hays, J.F., 1975. Differentiation of A Very Thick Magma Body, in: *Lunar and Planetary Science Conference*, p. 838.
- Wallace, P.J., Plank, T., Edmonds, M., Hauri, E.H., 2015. Volatiles in magmas, in: *The encyclopedia of volcanoes*. Elsevier, pp. 163–183.
- Warren, P.H., 1985. The magma ocean concept and lunar evolution. *Annual Review of Earth and Planetary Sciences* 13, 201–240. doi:10.1146/annurev.earth.13.050185.001221.
- Warren, P.H., Wasson, J.T., 1979. The origin of KREEP. *Reviews of Geophysics* 17, 73–88.
- Weiss, L.M., Marcy, G.W., 2014. The Mass-Radius Relation for 65 Exoplanets Smaller than 4 Earth Radii. *ApJ* 783, L6. doi:10.1088/2041-8205/783/1/L6, arXiv:1312.0936.
- Wetzel, D.T., Rutherford, M.J., Jacobsen, S.D., Hauri, E.H., Saal, A.E., 2013. Degassing of reduced carbon from planetary basalts. *Proceedings of the National Academy of Science* 110, 8010–8013. doi:10.1073/pnas.1219266110.
- Widemann, T., Ghail, R.C., Wilson, C.F., Titov, D.V., 2020. EnVision: Europe's Proposed Mission to Venus, in: *Exoplanets in Our Backyard: Solar System and Exoplanet Synergies on Planetary Formation, Evolution, and Habitability*, p. 3024.
- Wiechert, U., Halliday, A.N., Lee, D.C., Snyder, G.A., Taylor, L.A., Rumble, D., 2001. Oxygen isotopes and the Moon-forming giant impact. *Science* 294, 345–348.
- Wildi, F., Blind, N., Reshetov, V., Hernandez, O., Genolet, L., Conod,

- U., Sordet, M., Segovilla, A., Rasilla, J.L., Brousseau, D., Thibault, S., Delabre, B., Bandy, T., Sarajlic, M., Cabral, A., Bovay, S., Vallée, P., Bouchy, F., Doyon, R., Artigau, E., Pepe, F., Hagelberg, J., Melo, C., Delfosse, X., Figueira, P., Santos, N.C., González Hernández, J.I., de Medeiros, J.R., Rebolo, R., Broeg, C., Benz, W., Boisse, I., Malo, L., Käuff, U., Saddlemyer, L., 2017. NIRPS: an adaptive-optics assisted radial velocity spectrograph to chase exoplanets around M-stars, in: Society of Photo-Optical Instrumentation Engineers (SPIE) Conference Series, p. 1040018. doi:10.1117/12.2275660.
- Williams, D.M., Pollard, D., 2002. Earth-like worlds on eccentric orbits: excursions beyond the habitable zone. *International Journal of Astrobiology* 1, 61–69. doi:10.1017/S1473550402001064.
- Williams, P.K.G., Charbonneau, D., Cooper, C.S., Showman, A.P., Fortney, J.J., 2006. Resolving the Surfaces of Extrasolar Planets with Secondary Eclipse Light Curves. *ApJ* 649, 1020–1027. doi:10.1086/506468, arXiv:astro-ph/0601092.
- Wilson, L., Keil, K., 2017. Arguments for the Non-existence of Magma Oceans in Asteroids, in: Elkins-Tanton, L.T., Weiss, B.P. (Eds.), *Planetesimals: Early Differentiation and Consequences for Planets*. Cambridge University Press. Cambridge Planetary Science, p. 159–179. doi:10.1017/9781316339794.008.
- Winn, J.N., Matthews, J.M., Dawson, R.I., Fabrycky, D., Holman, M.J., Kallinger, T., Kuschnig, R., Sasselov, D., Dragomir, D., Guenther, D.B., et al., 2011. A super-Earth transiting a naked-eye star. *The Astrophysical Journal* 737, L18. URL: <http://dx.doi.org/10.1088/2041-8205/737/1/L18>, doi:10.1088/2041-8205/737/1/L18.
- Winn, J.N., Sanchis-Ojeda, R., Rappaport, S., 2018. Kepler-78 and the Ultra-Short-Period planets. *New A Rev.* 83, 37–48. doi:10.1016/j.newar.2019.03.006, arXiv:1803.03303.
- Winn, J.N., Sanchis-Ojeda, R., Rappaport, S., 2018. Kepler-78 and the Ultra-Short-Period planets. *New Astronomy Reviews* 83, 37–48. URL: <http://dx.doi.org/10.1016/j.newar.2019.03.006>, doi:10.1016/j.newar.2019.03.006.
- Witham, F., Llewellyn, E.W., 2006. Stability of lava lakes. *Journal of Volcanology and Geothermal Research* 158, 321–332. doi:10.1016/j.jvolgeores.2006.07.004.
- Witham, F., Woods, A.W., Gladstone, C., 2006. An analogue experimental model of depth fluctuations in lava lakes. *Bulletin of Volcanology* 69, 51–56.
- Witter, J.B., Kress, V.C., Delmelle, P., Stix, J., 2004. Volatile degassing, petrology, and magma dynamics of the villarrica lava lake, southern Chile. *Journal of Volcanology and Geothermal Research* 134, 303–337. URL: <http://www.sciencedirect.com/science/article/pii/S0377027304000630>, doi:https://doi.org/10.1016/j.jvolgeores.2004.03.002.
- Wood, C.A., Ashwal, L.D., 1982. SNC meteorites-Igneous rocks from Mars, in: *Lunar and Planetary Science Conference Proceedings*, pp. 1359–1375.
- Wood, J.A., Dickey, J.S.J., Marvin, U.B., Powell, B.N., 1970. Lunar Anorthosites and a Geophysical Model of the Moon. *Proceedings of the Apollo 11 Lunar Science Conference* 1, 965–988.
- Wordsworth, R.D., Schaefer, L.K., Fischer, R.A., 2018. Redox Evolution via Gravitational Differentiation on Low-mass Planets: Implications for Abiotic Oxygen, Water Loss, and Habitability. *AJ* 155, 195. doi:10.3847/1538-3881/aab608, arXiv:1710.00345.
- Wright, J.T., 2018. Radial Velocities as an Exoplanet Discovery Method. *Handbook of Exoplanets*, 619–631 URL: http://dx.doi.org/10.1007/978-3-319-55333-7_4, doi:10.1007/978-3-319-55333-7_4.
- Wright, J.T., Fakhouri, O., Marcy, G.W., Han, E., Feng, Y., Johnson, J.A., Howard, A.W., Fischer, D.A., Valenti, J.A., Anderson, J., Piskunov, N., 2011. The Exoplanet Orbit Database. *PASP* 123, 412. doi:10.1086/659427, arXiv:1012.5676.
- Yamamoto, S., Nakamura, R., Matsunaga, T., Ogawa, Y., Ishihara, Y., Morota, T., Hirata, N., Ohtake, M., Hiroi, T., Yokota, Y., Haruyama, J., 2012. Massive layer of pure anorthosite on the Moon. *Geophys. Res. Lett.* 39, L13201. doi:10.1029/2012GL052098.
- Yamamoto, S., Watanabe, S., Matsunaga, T., 2018. Space-Weathered Anorthosite as Spectral D-Type Material on the Martian Satellites. *Geophys. Res. Lett.* 45, 1305–1312. doi:10.1002/2017GL076612.
- Yoshioka, T., Nakashima, D., Nakamura, T., Shcheka, S., Keppler, H., 2019. Carbon solubility in silicate melts in equilibrium with a CO₂ gas phase and graphite. *Geochim. Cosmochim. Acta* 259, 129–143. doi:10.1016/j.gca.2019.06.007.
- Young, E.D., Kohl, I.E., Warren, P.H., Rubie, D.C., Jacobson, S.A., Morbidelli, A., 2016. Oxygen isotopic evidence for vigorous mixing during the Moon-forming giant impact. *Science* 351, 493–496. doi:10.1126/science.aad0525, arXiv:1603.04536.
- Young, E.D., Shahar, A., Nimmo, F., Schlichting, H.E., Schauble, E.A., Tang, H., Labidi, J., 2019. Near-equilibrium isotope fractionation during planetesimal evaporation. *Icarus* 323, 1–15. doi:10.1016/j.icarus.2019.01.012, arXiv:1909.05978.
- Yu, S., Tosi, N., Schwinger, S., Maurice, M., Breuer, D., Xiao, L., 2019. Overturn of Ilmenite-Bearing Cumulates in a Rheologically Weak Lunar Mantle. *Journal of Geophysical Research (Planets)* 124, 418–436. doi:10.1029/2018JE005739.
- Zahnle, K., Arndt, N., Cockell, C., Halliday, A., Nisbet, E., Selsis, F., Sleep, N.H., 2007. Emergence of a Habitable Planet. *Space Sci. Rev.* 129, 35–78. doi:10.1007/s11214-007-9225-z.
- Zahnle, K.J., Catling, D.C., Claire, M.W., 2013. The rise of oxygen and the hydrogen hourglass. *Chemical Geology* 362, 26–34. URL: <http://www.sciencedirect.com/science/article/pii/S0009254113003513>, doi:https://doi.org/10.1016/j.chemgeo.2013.08.004. special Issue dedicated to H.D. Holland: Evolution of the atmosphere and ocean through time.
- Zahnle, K.J., Lupu, R., Catling, D.C., Wogan, N., 2020. Creation and Evolution of Impact-generated Reduced Atmospheres of Early Earth. *The Planetary Science Journal* 1, 11. doi:10.3847/PSJ/ab7e2c, arXiv:2001.00095.
- Zeff, G., Williams, Q., 2019a. Fractional Crystallization of Martian Magma Oceans and Formation of a Thermochemical Boundary Layer at the Base of the Mantle. *Geophysical Research Letters* 46, 10997–11007. URL: <https://onlinelibrary.wiley.com/doi/abs/10.1029/2019GL084810>, doi:10.1029/2019GL084810.
- Zeff, G., Williams, Q., 2019b. Fractional crystallization of Martian magma oceans and formation of a thermochemical boundary layer at the base of the mantle. *Geophysical Research Letters* 46, 10997–11007.
- Zellem, R.T., Lewis, N.K., Knutson, H.A., Griffith, C.A., Showman, A.P., Fortney, J.J., Cowan, N.B., Agol, E., Burrows, A., Charbonneau, D., Deming, D., Laughlin, G., Langton, J., 2014. The 4.5 μm Full-orbit Phase Curve of the Hot Jupiter HD 209458b. *ApJ* 790, 53. doi:10.1088/0004-637X/790/1/53, arXiv:1405.5923.
- Zeng, L., Jacobsen, S.B., Sasselov, D.D., Petaev, M.I., Vanderburg, A., Lopez-Morales, M., Perez-Mercader, J., Mattsson, T.R., Li, G., Heising, M.Z., Bonomo, A.S., Damasso, M., Berger, T.A., Cao, H., Levi, A., Wordsworth, R.D., 2019. Growth model interpretation of planet size distribution. *Proceedings of the National Academy of Sciences* 116, 9723–9728. URL: <https://www.pnas.org/content/116/20/9723>, doi:10.1073/pnas.1812905116, arXiv:https://www.pnas.org/content/116/20/9723.full.pdf.
- Zhang, X., Showman, A.P., 2017. Effects of Bulk Composition on the Atmospheric Dynamics on Close-in Exoplanets. *The Astrophysical Journal* 836, 73. URL: <http://dx.doi.org/10.3847/1538-4357/836/1/73>, doi:10.3847/1538-4357/836/1/73.
- Zhang, Y., Ni, H., Chen, Y., 2010. Diffusion data in silicate melts. *Reviews in Mineralogy and Geochemistry* 72, 311–408.
- Zhao, J., Xiao, L., Qiao, L., Glotch, T.D., Huang, Q., 2017. The Mons Rümker volcanic complex of the Moon: A candidate landing site for the Chang'E-5 mission. *Journal of Geophysical Research (Planets)* 122, 1419–1442. doi:10.1002/2016JE005247.
- Zhao, Y., de Vries, J., van den Berg, A., Jacobs, M., van Westrenen, W., 2019. The participation of ilmenite-bearing cumulates in lunar mantle overturn. *Earth and Planetary Science Letters* 511, 1–11. URL: <http://www.sciencedirect.com/science/article/pii/S0012821X1930038X>, doi:https://doi.org/10.1016/j.epsl.2019.01.022.
- Zilinskas, M., Miguel, Y., Mollière, P., Tsai, S.M., 2020. Atmospheric compositions and observability of nitrogen-dominated ultra-short-period super-Earths. *MNRAS* 494, 1490–1506. doi:10.1093/mnras/staa724,

arXiv:2003.05354.

Zolotov, M., 2019. Chemical Weathering on Venus, in: Read, Peter (Ed.), Oxford Research Encyclopedia of Planetary Science. Oxford University Press, p. 146. doi:10.1093/acrefore/9780190647926.013.146.

Zolotov, M.Y., Sprague, A.L., Hauck II, S.A., Nittler, L.R., Solomon, S.C., Weider, S.Z., 2013. The redox state, FeO content, and origin of sulfur-rich magmas on Mercury. *Journal of Geophysical Research: Planets* 118, 138–146. URL: <https://agupubs.onlinelibrary.wiley.com/doi/abs/10.1029/2012JE004274>, doi:10.1029/2012JE004274.

Glossary

achondrites Stony meteorites that have recrystallized and/or melted due heating within a parent body. 5

andesitic Describing magmas or volcanic rocks which are more silicon-rich than basalts; andesitic magmas are also more viscous. 9

anorthosite A relatively low density igneous rock made of 90% by volume Na-, Ca-, and Al-rich plagioclase. 11

bridgmanite A high-pressure phase of magnesian silicate (MgSiO_3), thought to be the first mineral to crystallize from Earth's magma ocean. 21

cation-anion polyhedra The geometric arrangement of atoms in which a cation (e.g. Si^{+4}) is surrounded by and bonds with anions (e.g., O^{-2}) either in regular (in minerals) or transient (in liquids) arrangements. 21

chondritic Referring either to relatively unaltered groups of meteorites that are accumulations of smaller condensates or melted silicates (chondrules), or to elemental abundances that reflect the initial bulk composition of condensable matter in the Solar System. 5

compatible A compatible element prefers the solid phase (as opposed to the liquid) in a crystallizing melt. 12

coordination number The number of atoms or ions that immediately surround a given ion or atom. 21

coronal mass ejection The ejection of plasma and any magnetic field that accompanies it from the corona of the Sun or another star into the solar (stellar) wind. 5

cumulate Igneous rock formed by accumulation of minerals separating from a crystallizing magma. 10

diapirs Regions of upwelling of buoyant material in geologic settings. 9

differentiation Gravitational segregation of silicate and metal phases into the mantle and core of a planetary body during its formation. 5

dissipation quality factor A dimensionless factor Q that is the inverse of the fractional energy dissipated during one cycle of a periodic system. 5

eddy diffusivity A measure of turbulent transport by eddy motion in a fluid, in contrast to, but with the same units of, molecular diffusivity. 7

equilibrium crystallization Crystallization of a silicate melt (magma) when the melt remains in thermodynamic equilibrium with all resulting solids. 13

equilibrium temperature The temperature of a planet if it were radiating as a uniform blackbody. 2

exosphere The outermost part of a planet's atmosphere the density is low enough that the mean free path between collisions is larger than the atmospheric scale height or planetary radius. 19

fractional crystallization Crystallization of silicate melt (magma) when the solids are continuously removed from the melt, e.g. by negative buoyancy, and the chemical composition of the system evolves as a result. 13

geostrophic flow Fluid flow in which the Coriolis force is balanced by a pressure gradient due to buoyancy differences along a temperature gradient. 7

homopause The altitude in an atmosphere above which molecular diffusion dominates over turbulent (eddy) diffusion, and individual gases are not well-mixed and decrease with altitude according to molecular weight. 7

intermediate- and high-mass stars Stars with masses of 3–8 solar masses and > 8 solar masses, respectively. Intermediate mass stars rapidly in red giants and lose their nucleosynthetic element-enriched envelopes as winds into space. The cores of massive stars collapse, ejecting the envelope in a supernova event. 5

Laplace resonance An orbital resonance in which three bodies have orbital periods in the ratio 1:2:4. 10

lock-up temperature Rheology-based temperature below which a magma transitions from a suspension of individual crystals to chains of crystals and the viscosity increases markedly. 7

Love number One of a set of three dimensionless numbers that describe the response of a body to an imposed tidal potential, in this case k , which parameterizes the change in the potential due the tide. 5

mare The lunar mare are dark, volcanic plains, predominantly on the near side, that are ~ 1 Gyr younger than the surrounding crust. 12

olivine An iron-magnesium silicate mineral that is abundant in Earth's crust and upper mantle. 20, 45

- oxygen fugacity** Chemical potential of oxygen in an environment, or the tendency of substances in chemical equilibrium to be oxidized or reduced, expressed as a partial pressure, although often not representing an actual gas phase. 13, 45
- pallasites** Stony-iron meteorites consisting of large olivine crystals in iron-nickel matrix thought to originate from a disrupted, differentiated parent body. 5
- partial melting** Melting in which only some solid phases melt, which can occur when rising material in a silicate mantle undergoing subsolidus convection experiences lower pressures and ambient conditions that cross the solidus in a pressure-temperature diagram. 14
- peridotite** An iron-magnesium-rich rock, primarily composed of olivine and pyroxene minerals, that makes up most of Earth's upper mantle. 3
- phase angle** The angle subtended by lines between the illumination source (star), the reflecting/emitting object (planet) and the observer. 17
- phonolitic** Describing magmas or volcanic rocks which are both more silicon-rich and alkali element-rich than basalts. 9
- plagioclase** A series of Na-, Ca-, and Al-rich silicate minerals in the feldspar group and a major component of planetary crusts. Anorthite is a plagioclase. 44
- planetesimals** ~1-100 km-size bodies that are a hypothetical intermediate step in planet formation and could be related to comets or the parent bodies of asteroids. 24
- plastic yield strength** An applied stress above which a material will become ductile or flow. 11
- primitive melt** Silicate melt that has not experienced the removal or segregation of any its liquid or crystalline components. 12
- pyroxene** A series of (usually) Mg- and Fe-rich silicate minerals common in igneous rocks and the crusts and mantles of planetary bodies. 14, 45
- Rayleigh-Taylor instability** An instability of the interface between two fluids when a less dense fluid is accelerated into a denser fluid, e.g. by buoyancy. 23
- redox buffer** An assemblage of compounds/minerals that are in chemical equilibrium at a certain oxygen fugacity and thus tend to constrain fO_2 . 14
- refractory** A refractory element typically condenses as a solid above 1500 K, depending on ambient chemistry. 19
- Rossiter-McLaughlin effect** A time-dependent shift in a star's apparent radial velocity during the transit of a stellar or planet companion due to the occultation of different regions of the rotating star. 20
- siderophile** Elements that have an equilibrium affinity for the metallic (iron) phase (as opposed to silicate phases) and which tend to be more abundant in the metallic core of a differentiated body. 12
- silicate perovskite** High pressure phases of silicates with the formula $(Fe,Mg)SiO_3$ or $CaSiO_3$ and a common crystal structure, thought to be a dominant constituent of Earth's deep mantle. 14
- smooth particle hydrodynamics** A method of numerical simulation of continuum mechanics in which a fluid is simulated by discrete Lagrangian particles and the properties at any particle location are calculated by summing over neighboring particles weighted by a kernel function. 25
- SNC meteorites** Shergotites, nakhlites, and chassignites, a group of basaltic meteorites demonstrated to be sourced from Mars. 13, 15
- solidus** Temperature at the onset of melting in a geologic material at a given pressure. 2, 45
- spectral type** A system of stellar classification by temperature-sensitive absorption lines in a stellar spectrum, and a proxy for radiative temperature and, for stars fusing hydrogen in their cores, mass. 4
- subsidiary convection** Convection in a solid material, particularly a silicate mantle, due to ductile deformation. 6, 45
- superliquidus** Temperature and pressure conditions where a given silicate composition is completely molten. 10
- T Tauri star** A young (typically less than a few Myr old) approximately solar-mass star with a disk of gas and dust in which planets are expected to form. 18
- volatile** A volatile element is in gaseous form in most planetary settings and condenses as a liquid or solid only at temperatures below a few hundred K, depending on ambient chemistry. 2

CRediT authorship contribution statement

Keng-Hsien Chao: Writing - Original Draft, Visualization. **Rebecca deGraffenried:** Writing - Original Draft, Visualization. **Mackenzie Lach:** Writing - Original Draft, Visualization. **William Nelson:** Writing - Original Draft, Visualization. **Kelly Truax:** Writing - Original Draft, Visualization. **Eric Gaidos:** Conceptualization, Supervision, Writing - Original Draft, Visualization.